



AWRA-L v4.5: Technical description of model algorithms and inputs

[AWRA-L v4.5 technical report]

Neil Viney, Jai Vaze, Russell Crosbie, Biao Wang, Warrick Dawes, Andrew Frost
30 September 2014

A water information R & D alliance between the
Bureau of Meteorology and CSIRO's Land and Water Flagship



Australian Government
Bureau of Meteorology



Water Information
DATA › INFORMATION › INSIGHT

CSIRO Land and Water Flagship

Citation

Viney, N, Vaze J, Crosbie R, Wang B, Dawes W and Frost A (2014) AWRA-L v4.5: technical description of model algorithms and inputs. CSIRO, Australia.

Copyright and disclaimer

© 2014 CSIRO To the extent permitted by law, all rights are reserved and no part of this publication covered by copyright may be reproduced or copied in any form or by any means except with the written permission of CSIRO.

Important disclaimer

CSIRO advises that the information contained in this publication comprises general statements based on scientific research. The reader is advised and needs to be aware that such information may be incomplete or unable to be used in any specific situation. No reliance or actions must therefore be made on that information without seeking prior expert professional, scientific and technical advice. To the extent permitted by law, CSIRO (including its employees and consultants) excludes all liability to any person for any consequences, including but not limited to all losses, damages, costs, expenses and any other compensation, arising directly or indirectly from using this publication (in part or in whole) and any information or material contained in it.

Contents

Acknowledgments	5
Executive summary.....	6
1 Introduction	7
1.1 Background to AWRA.....	7
1.2 History of AWRA development.....	8
1.3 Applicability of AWRA.....	9
2 Model overview	10
2.1 Modelling philosophy	10
2.2 Spatial units.....	11
2.3 Processes modelled	12
3 Model description	14
3.1 Input variables	14
3.2 The water balance.....	26
3.3 The energy balance	33
3.4 Evaporation fluxes	36
3.5 Vegetation phenology.....	40
4 Parameterisation.....	43
4.1 Calibration procedure.....	43
4.2 Parameters available for calibration.....	44
References.....	47
Appendix.....	50
Appendix.....	55

Figures

Figure 1. The AWRA modelling system.....	7
Figure 2. The two hydrological response units of AWRA-L.	12
Figure 3. The AWRA-L model.....	13
Figure 4. Conceptual diagram of AWRA-L showing stores and fluxes. The red arrows represent fluxes of water to the atmosphere, the blue arrows represent fluxes of water into the surface water and the green arrows are internal fluxes of water within the model. Numbers in brackets correspond to equation numbers in the following text.....	14
Figure 5. Continental distribution of the fraction of tree cover within each grid cell.	16
Figure 6. Continental distribution of maximum LAI.	16
Figure 7. Distribution of vegetation height for the deep-rooted HRU.	17
Figure 8. Average slope within a grid cell as derived from 3 second DEM.	18
Figure 9. Continental distribution of reference precipitation.....	18
Figure 10. Distribution of the density of the surface water drainage network. The units are km^{-1}	19
Figure 11. Relative available soil water storage for the surface soil layer (S_{0AWC}).....	21
Figure 12. Relative available soil water storage for the shallow soil layer (S_{sAWC}).	21
Figure 13. Soil saturated hydraulic conductivity for the topsoil ($K_{0satASRIS}$).....	22
Figure 14. Soil saturated hydraulic conductivity for the shallow soil ($K_{ssatASRIS}$).	22
Figure 15. Hydraulic conductivity of the unconfined aquifer.....	24
Figure 16. Effective porosity of the unconfined aquifer.	24
Figure 17. Distribution of the groundwater drainage coefficient (K_g) across the continent.....	25
Figure 18. Arrangement of soil water stores and drainage fluxes.	28
Figure 19. Distribution of calibration and validation catchments.....	43
Figure 20. Soil moisture monitoring sites for (a) OzNet Murrumbidgee (from http://www.oznet.org.au/murrumbidgeesm.html), and (b) SASMAS Goulburn (from http://www.eng.newcastle.edu.au/sasmas/SASMAS/sasdata.html).	56
Figure 21. Cumulative distribution of daily efficiency of streamflow predictions in continental calibration mode for AWRA-L v4.5, Sacramento and GR4J.	58
Figure 22. Cumulative distribution of monthly efficiency of streamflow predictions in continental calibration mode for AWRA-L v4.5, Sacramento and GR4J.....	58
Figure 23. Cumulative distribution of absolute bias of streamflow predictions in continental calibration mode for AWRA-L v4.5, Sacramento and GR4J.	59
Figure 24. Cumulative distribution of F value of streamflow predictions in continental calibration mode for AWRA-L v4.5, Sacramento and GR4J.	59
Figure 25. Cumulative distribution of daily efficiency of streamflow predictions in validation mode for AWRA-L v4.5, Sacramento and GR4J.....	60
Figure 26. Cumulative distribution of monthly efficiency of streamflow predictions in validation mode for AWRA-L v4.5, Sacramento and GR4J.	61
Figure 27. Cumulative distribution of absolute bias of streamflow predictions in validation mode for AWRA-L v4.5, Sacramento and GR4J.....	61

Figure 28. Cumulative distribution of F value of streamflow predictions in validation mode for AWRA-L v4.5, Sacramento and GR4J	62
Figure 29. Cumulative distribution of monthly efficiency of streamflow predictions in calibration mode for AWRA-L v4.5, WaterDyn and CABLE.....	63
Figure 30. Cumulative distribution of absolute bias of streamflow predictions in calibration mode for AWRA-L v4.5, WaterDyn and CABLE.....	63
Figure 31. Cumulative distribution of monthly efficiency of streamflow predictions in validation mode for AWRA-L v4.5, WaterDyn and CABLE.....	64
Figure 32. Cumulative distribution of absolute bias of streamflow predictions in validation mode for AWRA-L v4.5, WaterDyn and CABLE.....	65
Figure 33. Cumulative distribution of daily efficiency of streamflow predictions in continental calibration mode for AWRA-L v4.5, AWRA-L v3.5 and AWRA-L v4.0.	66
Figure 34. Cumulative distribution of monthly efficiency of streamflow predictions in continental calibration mode for AWRA-L v4.5, AWRA-L v3.5 and AWRA-L v4.0.	66
Figure 35. Cumulative distribution of absolute bias of streamflow predictions in continental calibration mode for AWRA-L v4.5, AWRA-L v3.5 and AWRA-L v4.0.	67
Figure 36. Cumulative distribution of F value of streamflow predictions in continental calibration mode for AWRA-L v4.5, AWRA-L v3.5 and AWRA-L v4.0.....	67
Figure 37. Cumulative distribution of daily efficiency of streamflow predictions in validation mode for AWRA-L v4.5, AWRA-L v3.5 and AWRA-L v4.0.	68
Figure 38. Cumulative distribution of monthly efficiency of streamflow predictions in validation mode for AWRA-L v4.5, AWRA-L v3.5 and AWRA-L v4.0.....	69
Figure 39. Cumulative distribution of absolute bias of streamflow predictions in validation mode for AWRA-L v4.5, AWRA-L v3.5 and AWRA-L v4.0.	69
Figure 40. Cumulative distribution of F value of streamflow predictions in validation mode for AWRA-L v4.5, AWRA-L v3.5 and AWRA-L v4.0.	70
Figure 41. Regional calibration zones and summary statistics of AWRA-L v4.5 performance for each region. (The term “objective function” refers to the median of the F value. The term “median bias” refers to the median of the raw bias).....	71
Figure 42. Cumulative distribution of daily efficiency of streamflow predictions for continental and regional implementation of AWRA-L v4.5.....	71
Figure 43. Cumulative distribution of monthly efficiency of streamflow predictions for continental and regional implementation of AWRA-L v4.5.....	72
Figure 44. Cumulative distribution of absolute bias of streamflow predictions for continental and regional implementation of AWRA-L v4.5.....	72
Figure 45. Cumulative distribution of F value of streamflow predictions for continental and regional implementation of AWRA-L v4.5.....	73
Figure 46. Correlation of monthly volumetric soil moisture predictions of models against (a) OzNet and (b) SASMAS probe data over a 90 cm profile.	73
Figure 47. Correlation of model predictions of topsoil moisture content with AMSR-E observations.....	74
Figure 48. Correlation of monthly CMRSET observations with model predictions of ET.....	74

Tables

Table 1. List of initial values for state variables.....	26
Table 2. List of parameters that are currently used for calibration. Parameters that apply only to the deep-rooted HRU are labelled with the suffix _hruDR. Parameters that apply only to the shallow-rooted HRU are labelled with the suffix _hruSR. The allowable range of parameter values is given by Min and Max.	45
Table 3. List of parameters that are currently fixed and not used in calibration. Parameters that apply only to the deep-rooted HRU are labelled with the suffix _hruDR. Parameters that apply only to the shallow-rooted HRU are labelled with the suffix _hruSR. The allowable range of parameter values (were these parameters to be calibrated) is given by Min and Max.....	46
Table 4. List of variable names used in this document and the corresponding variables used in the model code. Units are those given in this document.....	50
Table 5. Median values of various performance metrics in calibration and validation.	60

Acknowledgments

This work is carried out in the Land and Water Flagship, CSIRO and is funded by the WIRADA research alliance between the Bureau of Meteorology and the CSIRO. The authors thank Francis Chiew, Dushmanta Dutta, Jin Teng and Mohsin Hafeez for their comments on the manuscript and Steve Marvanek and Simon Gallant for drafting the figures.

Executive summary

This report describes the algorithms and input parameters for the reconceptualised continental scale water balance model AWRA-L v4.5. AWRA-L has been developed, in part, to provide a modelling tool for the Bureau of meteorology to use in producing the data supporting its National Water Accounts and Water Resources Assessments.

The development of the AWRA modelling system has been guided by several design principles. These include the explicit inclusion of as much observational data as is useful and feasible, the use of a global calibration strategy that yields a single set of model parameters that apply universally, and the implementation of a rigorous benchmark testing scheme to demonstrate that objective improvements flow from any proposed new algorithms, data sets and calibration strategies.

AWRA-L is a grid based distributed water balance model that is conceptualised as a small catchment. It simulates the flow of water through the landscape from the rainfall entering the grid cell through the vegetation and soil and then out of the grid cell through evapotranspiration, surface water flow or lateral flow of groundwater to the neighbouring grid cells (Figure 4). Each grid cell is conceptualised as two separate hydrological response units (HRU), corresponding to deep rooted vegetation (trees) and shallow rooted vegetation (grass). The main difference between these two HRUs is that the shallow rooted vegetation has access to subsurface soil moisture in the two upper soil stores only, while the deep rooted vegetation also has access to moisture in the deep store. The size of a grid cell is assumed to be large enough that hillslope processes are not important but small enough to assume homogeneity of the climate inputs.

AWRA-L v4.5 currently includes descriptions of the following landscape stores, fluxes and processes:

- partitioning of precipitation between interception evaporation and net precipitation,
- partitioning of net precipitation between infiltration, infiltration excess surface runoff, and saturation excess runoff,
- surface topsoil water balance, including infiltration, drainage and soil water evaporation,
- interflow generated at the interface of the soil layers (layer 1/layer 2 & layer 2/layer 3), estimated as a function of the soil stores and physical parameters describing the soil characteristics,
- shallow soil water balance, including incoming and exiting soil drainage and root water uptake,
- deep soil water balance – same as above,
- groundwater dynamics, including recharge, evapotranspiration and discharge, and
- surface water body dynamics, including inflows from runoff and discharge, open water evaporation and catchment water yield.

In addition, the following vegetation processes are described:

- transpiration, as a function of maximum root water uptake and optimum transpiration rate, and
- vegetation cover adjustment, in response to the difference between an actual and a theoretical optimum transpiration, and at a rate corresponding to vegetation cover type.

The groundwater component of the AWRA-L v4.5 system is designed to run at a continental scale but be simple enough that run times are not prohibitive. AWRA-L v4.5 has one (unconfined aquifer) or two (unconfined and confined aquifers) groundwater stores. It includes the following groundwater processes:

- groundwater extraction (pumping, also injection if significant),
- lateral groundwater flow between AWRA-L cells in regional groundwater systems,
- distribution of river losses to groundwater (from AWRA-R),
- recharge from overbank flooding, and
- interactions between deep confined systems and shallow groundwater systems.

1 Introduction

1.1 Background to AWRA

In response to multiple pressures on Australia’s water resources, the Australian Government, through the Commonwealth Water Act 2007, has given the Australian Bureau of Meteorology (hereafter called the Bureau) responsibility for compiling and delivering comprehensive water information across the water sector. To fulfil its legislative responsibilities, the Bureau requires a water balance modelling system developed using state-of-the-art hydrological science and computing technology that quantifies water flux and storage terms and their respective uncertainties (where applicable and possible) using a combination of data sets (on-ground metering, remotely sensed data and model outputs). The system needs to be applicable across the continent and it should be flexible enough to be able to use all available data sources (whether modelling data rich or data limited regions) with the most appropriate modelling techniques and tools to provide nationally consistent and robust estimates. The outputs from the water balance modelling system are used to underpin a range of water information products delivered by the Bureau and thus the system needs to generate all the necessary water flux and storage terms at spatial and temporal scales appropriate for aggregated reporting.

To achieve these objectives, in 2008, the Bureau and CSIRO through the Water for a Healthy Country National Research Flagship agreed to collaborate on research activities in the field of water information, to assist the Bureau develop a number of these new core roles. This collaboration was formalised through the Water Information Research and Development Alliance (WIRADA), which is now in its sixth year of operation.

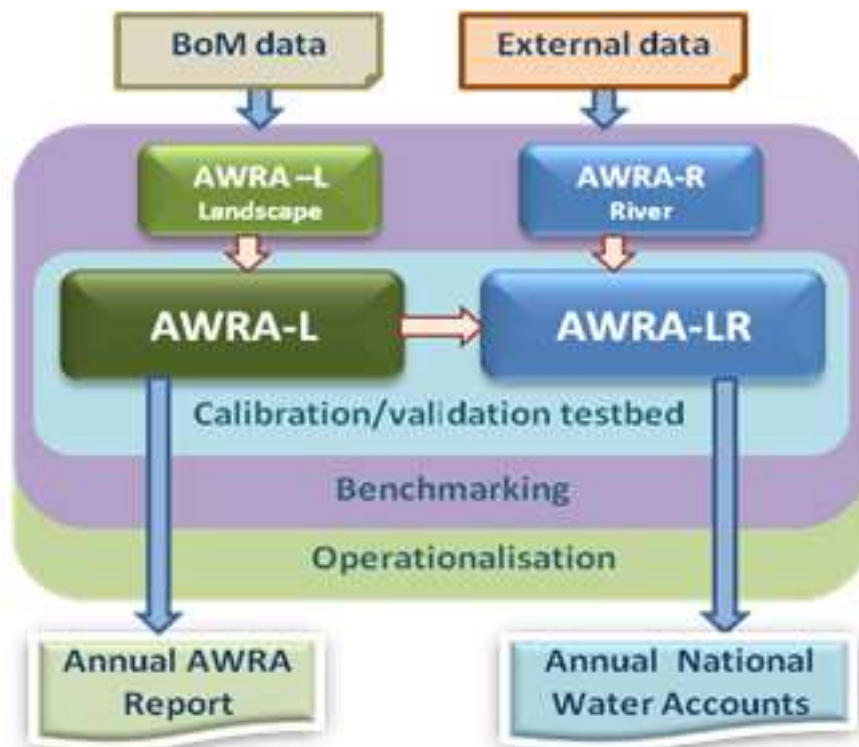


Figure 1. The AWRA modelling system.

A significant research and development effort in WIRADA is directed towards developing improved capability in water resource accounting and assessment. In the first 5 years of WIRADA, the Australian Water Resource Assessment (AWRA) modelling system was developed through three core components, together representing the Australian terrestrial water cycle. The model components (Figure 1) represent processes between the atmosphere, the landscape and the groundwater system (AWRA-L) and in gauged rivers (AWRA-R), including all major water storages and fluxes in and between these components.

Significant effort has been dedicated towards use of observational data wherever possible. The current development is focused on integrating the landscape and groundwater components into a single model (to be called AWRA-L) and integrating this with the river component within a coherent framework (i.e., the AWRA modelling system) such that the integrated research system in CSIRO is readily transferable to, and implemented in, the operational environment at the Bureau (Vaze et al., 2013).

The AWRA system uses available observations and an integrated landscape–groundwater–river water balance model to estimate the stores and fluxes of the water balance required for reporting purposes. This constitutes a unique example of implementing a coupled landscape, groundwater and regulated river system model at a continental scale and rolled out in high priority regions (National Water Account regions). The Bureau has used the AWRA modelling system to undertake water resource assessments across the country and has already published two Water Resource Assessments (2010 and 2012; see www.bom.gov.au/water/awra) and four National Water Accounts (2010–2013; see www.bom.gov.au/water/nwa). There has been a steady and continuous extension and improvement in the AWRA model performance and the Bureau is currently undertaking the next round of the National Water Account (2014) using a recent version of the AWRA system. These early reports provide a clear perspective on current capabilities and operational needs of the AWRA modelling system.

1.2 History of AWRA development

AWRA v0.5 and the technical report describing model conceptualisation and equations were released in 2010 (van Dijk, 2010). Since then, the AWRA modelling suite has undergone continuous revision and refinement. These revisions have included not only changes to the model algorithms, but also changes in calibration methods and strategies. Updated versions of the AWRA-L model were delivered to the Bureau of Meteorology in 2011 (AWRA-L v1.0), 2012 (AWRA-L v2.0) and 2013 (AWRA-L v3.0), but none of these were accompanied by a major revision to the technical documentation.

The current model version (AWRA-L v4.5) introduces a formal coupling of the original landscape and groundwater components of AWRA and was delivered to the Bureau of Meteorology in 2014. This document describes that version of the model.

Among the major changes made to the model structure and algorithms since AWRA-L v0.5 are:

- Numerical values for many model parameters are now calibrated against observations of streamflow. *[In v0.5 all parameters were estimated a priori].* Viney et al. (2011) have shown that calibration leads to a marked increase in streamflow simulation performance.
- Climate input data is now taken from the Australian Water Availability Project (AWAP) data set (Jones et al., 2009). *[Previously, SILO climate data was used for model input].*
- Soil hydraulic properties now come from the Australian Soil Resource Information System (ASRIS). New parameters are introduced to scale the values across the continent). *[In the previous version of AWRA, soil parameters were correlated with functions of climate characteristics].*
- A spatial field of wind speed derived from data supplied by McVicar et al. (2008) is used as input. *[Previously, wind speed was input as a spatially uniform default value].*
- The modelling of runoff components has been revised. In particular the simulation of interflow has been included. Interflow is now generated at the interface of the soil layers and is estimated as a function of the soil stores and physical parameters describing the soil characteristics. *[The initial version of AWRA does not simulate interflow].*
- The saturated fraction of the grid cell is now dependent on the groundwater store and topography, which is defined by hypsometric curves (Peeters et al. (2013). These curves are represented by one

parameter and an *a priori* functional shape calculated from a detailed digital elevation model. *[Previously, saturation fraction was dependent on the groundwater store and a reference threshold parameter which was correlated with climate].*

- A confined groundwater store has been added to represent regional confined aquifers. However default parameters are used across Australia given the lack of groundwater data to parameterise this. *[Previously there was no representation of a confined aquifer in the model].*
- Potential evaporation is now calculated by the Penman equation. *[Previously, the Penman-Monteith potential evaporation formulation was used].*
- Downwelling longwave radiation is now augmented by radiation from the cloud base. [The previous longwave radiation model was appropriate for clear skies only].
- Soil heat flux is no longer included in the energy balance. This is justified on the grounds that over a daily time step, soil heat flux is likely to be near zero. *[The soil heat flux model previously included up to four parameters which no longer need to be specified].*
- The model code has been cleaned up to remove redundant parts (including internal model calls to some redundant components) which has resulted in a more concise and readable code.
- The model has been decoupled from third party software packages (e.g., Trident) and a wrapper has been developed to facilitate model calibration and simulation.

There has been a steady and continuous extension and improvement in the AWRA model performance and this report provides the technical details (model conceptualisation, structure, algorithms and parameters) of the AWRA-L v4.5 model.

1.3 Applicability of AWRA

The impetus for the initialisation and continued development of the AWRA modelling system has been to provide modelling tools for the Bureau to use in its NWA and RWA reports. However, AWRA should not be viewed solely through that prism of applicability. AWRA has applications in general hydrological modelling and has been shown to be an excellent alternative to other hydrological modelling tools (Viney et al., 2013, Viney et al., 2014). AWRA is particularly useful in situations where data from multiple sources—especially multiple streamflow data sets—can be used in calibration.

Furthermore, despite its name, and although its utility in this document is described largely in an Australian context, AWRA should not be thought of as being limited to Australian applications. Its structure and parameterisations make it amenable to use in many other geographical settings. Given the availability of suitable input data, its only general limitation to widespread applicability is its current lack of a snow modelling algorithm.

2 Model overview

2.1 Modelling philosophy

The development of the AWRA modelling system has been guided by several design principles. These principles have arisen in response to Bureau information requirements and to the many workshops and reviews the system has undergone.

2.1.1 MODEL-DATA FUSION

One of the guiding principles behind the development of the AWRA system is that it shouldn't just represent a modelling platform; rather it should incorporate as much observational data as is useful and feasible. Of course, observations are integral to any hydrological modelling exercise. No model can exist in the absence of observational data. Observations are usually required for calibration and always for verification. However, the philosophy behind AWRA is that there is much greater potential use of other observational data than is customary in other similar modelling endeavours.

The on-ground climate and water measurement network is very sparse for most of Australia. The quality of on-ground data is variable and not always well-described. In practice, what observations exist remain difficult to obtain and interpret appropriately while the Bureau is completing its systems to collate, curate, describe, manage and disseminate them. Many terms in the water balance are not measured on the ground, or at least not at the appropriate scale or spatial density; evapotranspiration (ET) being a case in point. Earth observation can address this lack of on-ground observations: remotely-sensed electromagnetic radiation in the visible to passive microwave domain provides valuable information on precipitation, surface temperature, vegetation condition, ET and surface soil moisture content, while unique satellite-derived information on the total amount of water stored in the landscape is now also available. However, remote sensing provides comparatively indirect measurements of the water cycle, requiring retrieval models that have their own assumptions and uncertainties.

This demands caution when integrating satellite products with models. There are also practical operational issues: most current satellite products are derived from research missions whose continuation is not guaranteed; and most products are still in the research domain with potentially unstable supply and often poorly understood errors. Finally, the data volume of satellite imagery at continental scale introduces computational challenges. These challenges have led to an emphasis and investment in the role for satellite data in water balance research. This includes the design and prototyping of operational systems that produce satellite-derived information valuable as input to AWRA (for example precipitation, ET, vegetation cover, inundation) and research to specify uncertainty in data and products, trial alternative assimilation techniques, and design an operationally robust implementation of assimilation techniques in the AWRA system. The first results of this effort are now starting to materialise. In AWRA-L, remotely-sensed soil moisture and leaf area index have been used to constrain parameter estimation (Zhang and Viney, 2012), while efforts are under way to develop methods for adjusting model estimates through model-data assimilation (e.g., Renzullo et al., 2013).

In summary, it might be noted that on-ground observations, while direct are also sparse, gap-prone and not predictive; remotely sensed observations, while having full and frequent coverage, are relatively indirect and not predictive; and biophysical modelling, while having full and continuous coverage and being predictive and directly interpretable, is possibly unhindered by reality. Combining all three gives promise of extracting the best characteristics of each.

2.1.2 GLOBAL CALIBRATION

The spatial variability of hydrological processes throughout a large spatial domain is largely reflective of the spatial variability in precipitation and other climatic factors. Other second-order influences on hydrological variability include land use and vegetation heterogeneity, which is accounted for in AWRA-L through the different proportions of HRUs (see Section 2.2) in each spatial unit. The use of distinct HRUs represents a burden on AWRA-L in that it increases the degree of parameterisation. However, it also confers the great advantage that the model is particularly amenable to global calibration. Global calibration involves the use of observational data from multiple locations (e.g., from multiple streamflow gauges) in calibrating the model to derive a single set of model parameters that is applicable throughout the modelling domain (i.e., globally). In the context of AWRA-L, the global domain is typically the full extent of continental Australia, including Tasmania. Recent research by Viney et al. (2013) has shown that global calibration has significant advantages in predicting streamflow across what is a sparsely-gauged continent.

2.1.3 MODEL IMPROVEMENT STRATEGY

The AWRA modelling system is undergoing continuous development. New model algorithms, data sources and calibration strategies are being regularly proposed, implemented and assessed. Typically, this assessment can only be done after full recalibration of the model for each new development. This has necessitated the development of a rigorous scheme of benchmark testing.

This benchmark testing is distinct from testing the models to ensure that they function correctly, which is more properly termed *verification*. The benchmark testing system refers to a set of (partly or wholly automated) tests designed to assess how well the inputs and the simulations from a modified system version (in comparison to a previous system version, or other models) reproduce a standard set of observations following a standard set of criteria and metrics. This also needs to include ongoing validation of system forcing data where possible. In general, modifications to the modelling system are only accepted in cases where the benchmark testing demonstrates improved modelling performance over the previous version. The current suite of benchmark tests includes comparison against observations of streamflow, soil moisture, evapotranspiration, recharge and vegetation density.

2.2 Spatial units

AWRA-L has a flexible spatial resolution, whose size is usually dictated by the resolution of its input data. For use in Australian Water Resource Assessments and National Water Accounts, AWRA-L is forced by gridded meteorological data (precipitation, solar radiation, air temperature, etc.) from the Bureau of Meteorology. This data has a spatial resolution of 0.5 degrees (about 5 km). It operates at a daily time step.

Each spatial unit (grid cell) in AWRA-L is divided into a number of hydrological response units (HRUs) representing different landscape components (Figure 2). Hydrological processes are modelled separately for each HRU before the resulting fluxes are combined to give cell outputs. The current version of AWRA-L includes two HRUs which notionally represent (i) tall, deep-rooted vegetation (i.e., forest), and (ii) short, shallow-rooted vegetation (i.e., non-forest). Hydrologically, these two HRUs differ in their aerodynamic control of evaporation, in their interception capacities and in their degree of access to different soil layers.

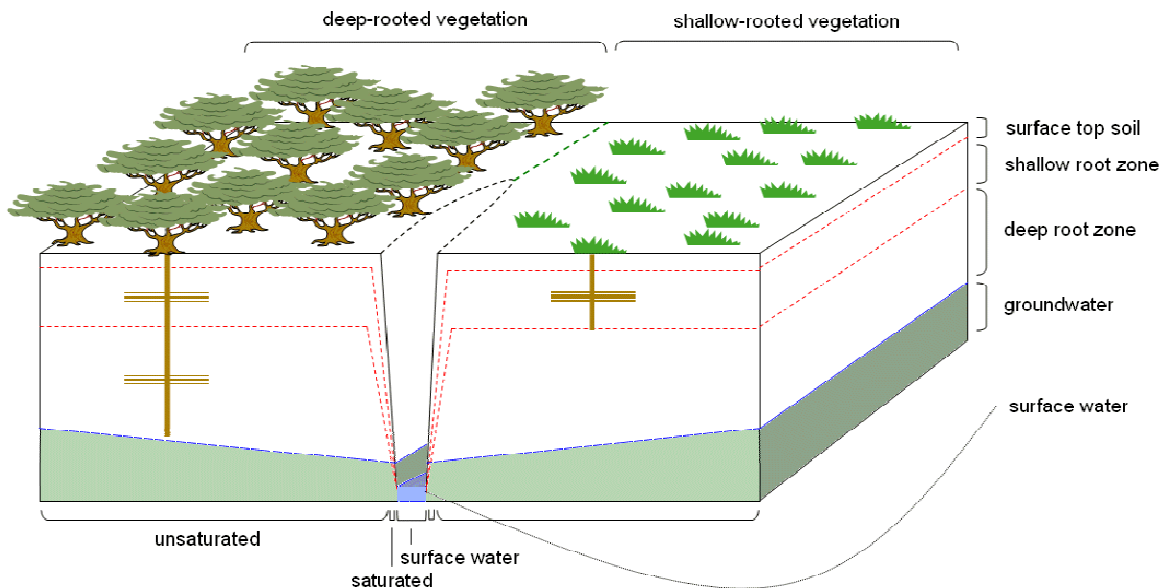


Figure 2. The two hydrological response units of AWRA-L.

2.3 Processes modelled

AWRA-L, which includes landscape and groundwater components of the AWRA system, is a daily grid-based biophysical model of the water balance between the atmosphere, the soil, groundwater and surface water stores. The model aims to produce interpretable water balance component estimates, so that they agree as much as possible with water balance observations, including point gauging data and satellite observations. The model is intended to be parsimonious rather than comprehensive, appropriate to the needs of the AWRA and NWA reporting. AWRA-L v4.5 currently includes descriptions of the following landscape stores, fluxes and processes (Figure 3):

- partitioning of precipitation between interception evaporation and net precipitation,
- partitioning of net precipitation between infiltration, infiltration excess surface runoff, and saturation excess runoff,
- surface topsoil water balance, including infiltration, drainage and soil water evaporation,
- interflow generated at the interface of the soil layers, estimated as a function of the soil stores and physical parameters describing the soil characteristics,
- shallow soil water balance, including incoming and exiting soil drainage and root water uptake,
- deep soil water balance – same as above,
- groundwater dynamics, including recharge, evapotranspiration and discharge, and
- surface water body dynamics, including inflows from runoff and discharge, open water evaporation and catchment water yield.

In addition, the following vegetation processes are described:

- transpiration, as a function of maximum root water uptake and optimum transpiration rate, and
- vegetation cover adjustment, in response to the difference between an actual and a theoretical optimum transpiration, and at a rate corresponding to vegetation cover type.

The groundwater component of the AWRA-L v4.5 system is designed to run at a continental scale but be simple enough that run times are not prohibitive. AWRA-L v4.5 has one (unconfined aquifer) or two (unconfined and confined aquifers) groundwater stores.

The landscape and groundwater components of the AWRA modelling system, AWRA-L and AWRA-G, respectively, were originally developed as separate stand-alone models. In AWRAv4.0, these components have been combined into a single model, AWRA-L. This document represents the first description of the combined model.

The groundwater component of AWRA-L v4.5 has been designed to simulate the groundwater processes to provide exchange of fluxes between AWRA-L and AWRA-R to enable closure of the overall water balance. It shares the water table from the unconfined aquifer with AWRA-R. The groundwater component introduces lateral flow of groundwater between adjacent grid cells along with other potential sources and sinks of water from the AWRA-L groundwater store (Crosbie et al., 2011, Joehnk et al., 2012). AWRA-L v4.5 includes the following groundwater processes:

- groundwater extraction (pumping, also injection if significant),
- lateral groundwater flow between AWRA-L cells in regional groundwater systems,
- distribution of river losses to groundwater (from AWRA-R),
- recharge from overbank flooding (from AWRA-R), and
- interactions between deep confined systems and shallow groundwater systems.

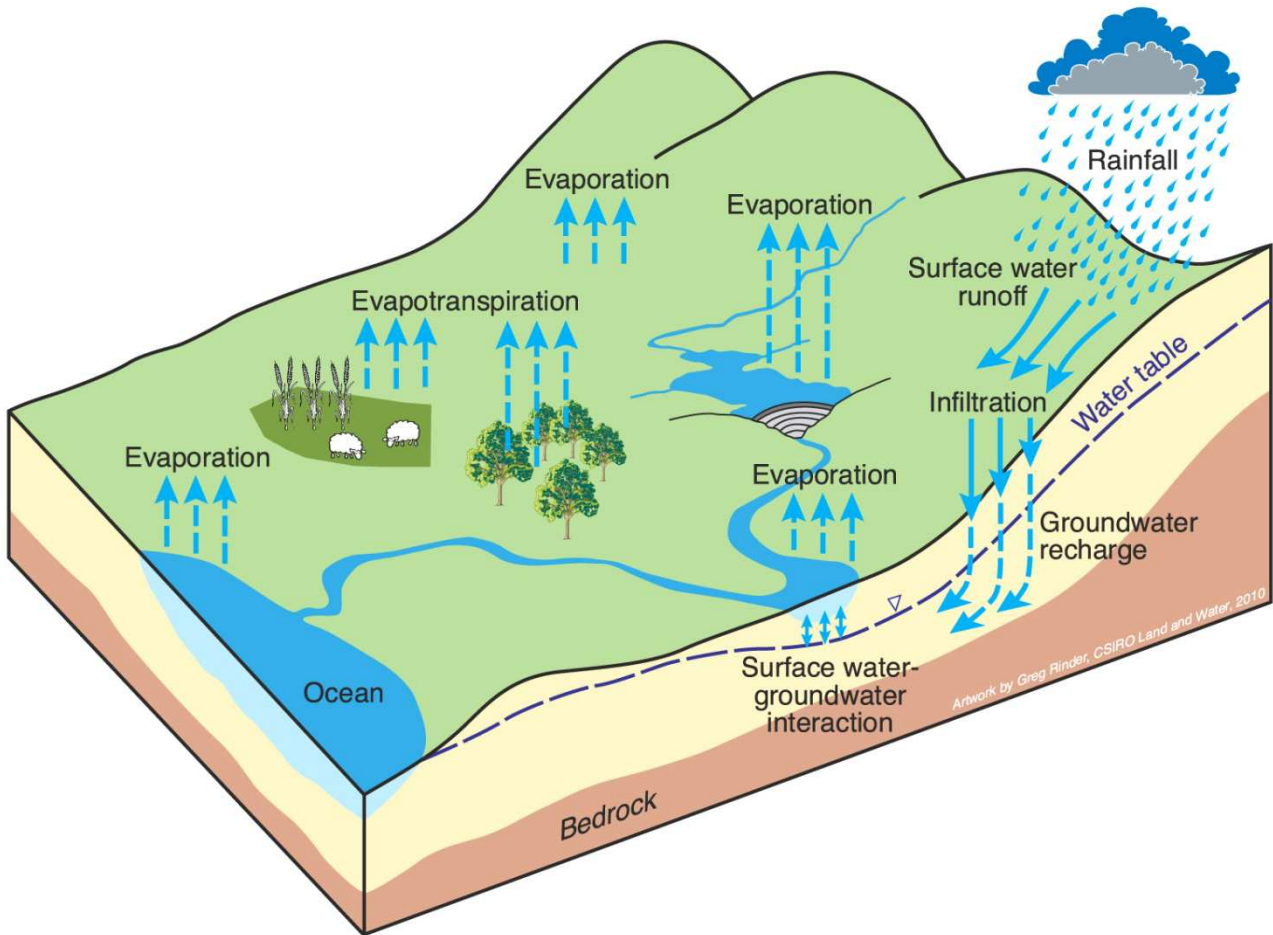


Figure 3. The AWRA-L model

T_{min}	Minimum air temperature (°C)
u_2	Wind speed at 2 m (m s^{-1})

Description

The first four variables are spatially interpolated from observations and are available from the AWAP data set as gridded daily surfaces at 0.05 degree spatial resolution. The data values are assumed to be identical for all hydrological response units within a grid cell.

A fifth meteorological variable, wind speed at 2 m (u_2 , m s^{-1}), is potentially available at the same temporal and spatial resolution. However, in AWRA-L v4.5, wind speed is input as a spatially-gridded long-term average. As such, there is no distinction between individual windy and calm days or between relatively calm and relatively windy seasons.

Future versions of AWRA should consider direct input of gridded daily wind speed and, if available, gridded daily vapour pressure. Availability of the latter would obviate the need to estimate p_e as a function of minimum air temperature (Equation (44), below).

3.1.2 OTHER SPATIAL DATA SETS

In the spirit of incorporating as much ancillary information as possible, some variables used in AWRA-L are input as rasters to have spatially varying properties across the continent. In some cases, where there may be uncertainty over the absolute magnitude of these variables, but not their spatial variability, these values are then calibrated through a single multiplier across the continent. Geographical latitude is given trivially for each grid cell. The remaining spatially varying data sets are described below.

3.1.2.1 Vegetation properties

Variables

f_{tree}	Fraction of tree cover within each grid cell (dimensionless)
Λ	Leaf area index (LAI) (dimensionless)
Λ_{max}	Maximum achievable LAI (dimensionless)
h_v	Vegetation height (m)

Description

The fraction of tree cover within each grid cell is used to apportion the grid cell area to each of the two HRUs. It is based on the Advanced Very High Resolution radiometer (AVHRR) satellite derived fractions of persistent and recurrent photosynthetically active absorbed radiation (fPAR) (Donohue et al., 2008), where persistent vegetation is interpreted to be tree cover (deep rooted) and recurrent vegetation is interpreted to be grass cover (shallow rooted) (Figure 5). The tree fraction is assumed to remain static throughout the simulation.

The maximum achievable LAI, Λ_{max} , is derived from a time series of LAI from the Moderate Resolution Imaging Spectroradiometer (MODIS) satellite (Figure 6). At present, the same values of Λ_{max} are used for both HRUs.

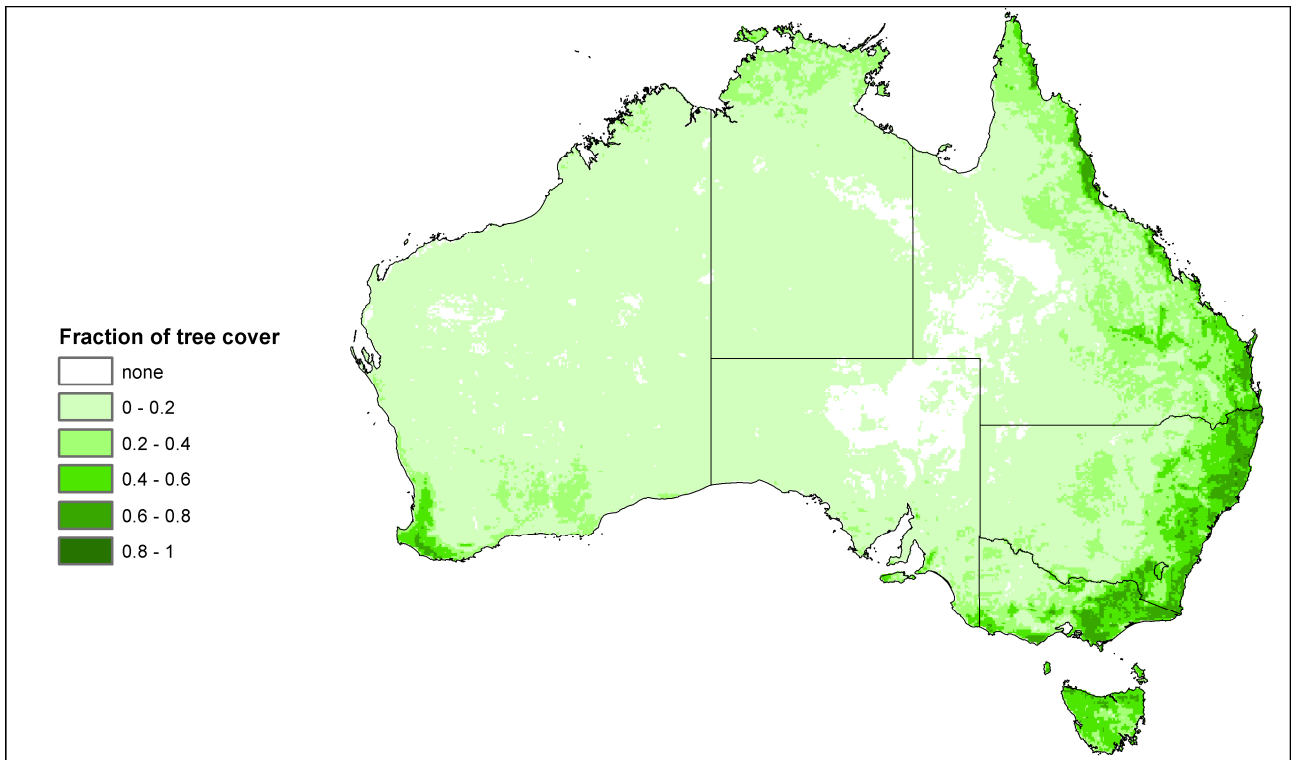


Figure 5. Continental distribution of the fraction of tree cover within each grid cell.

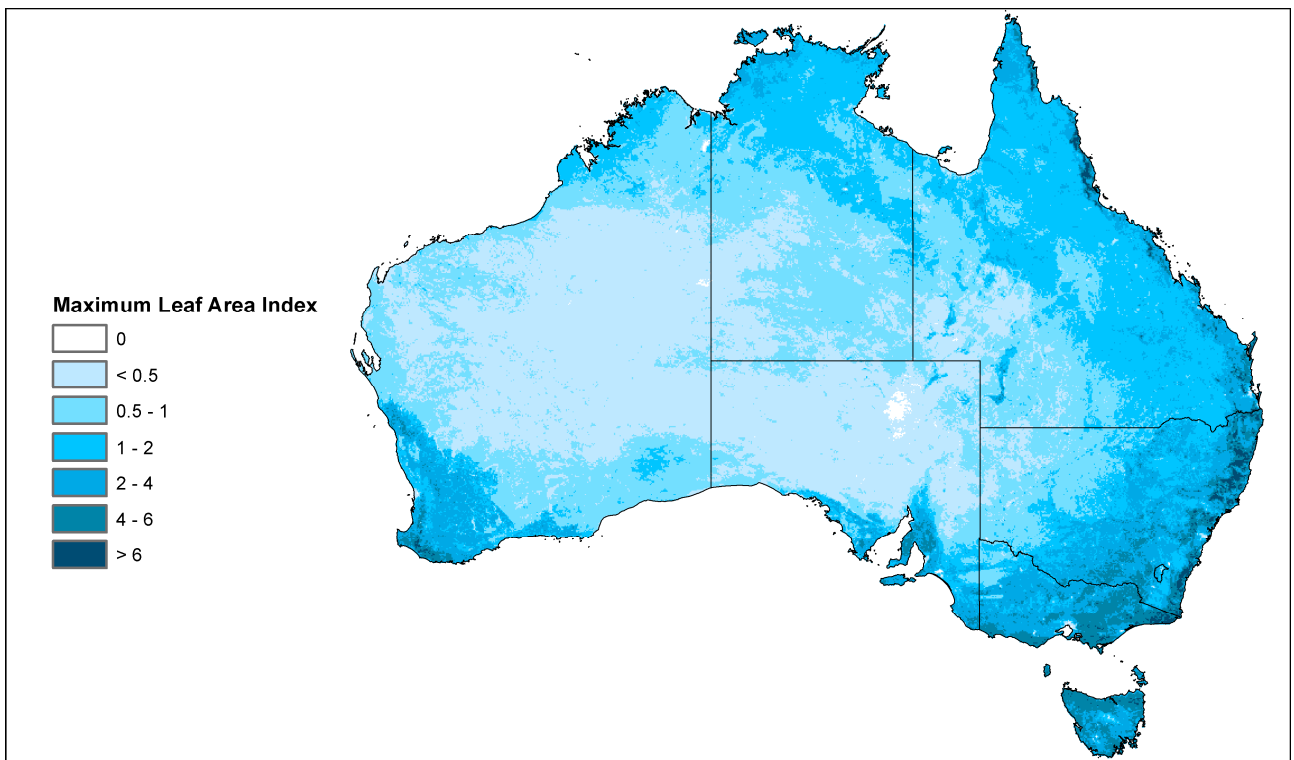


Figure 6. Continental distribution of maximum LAI.

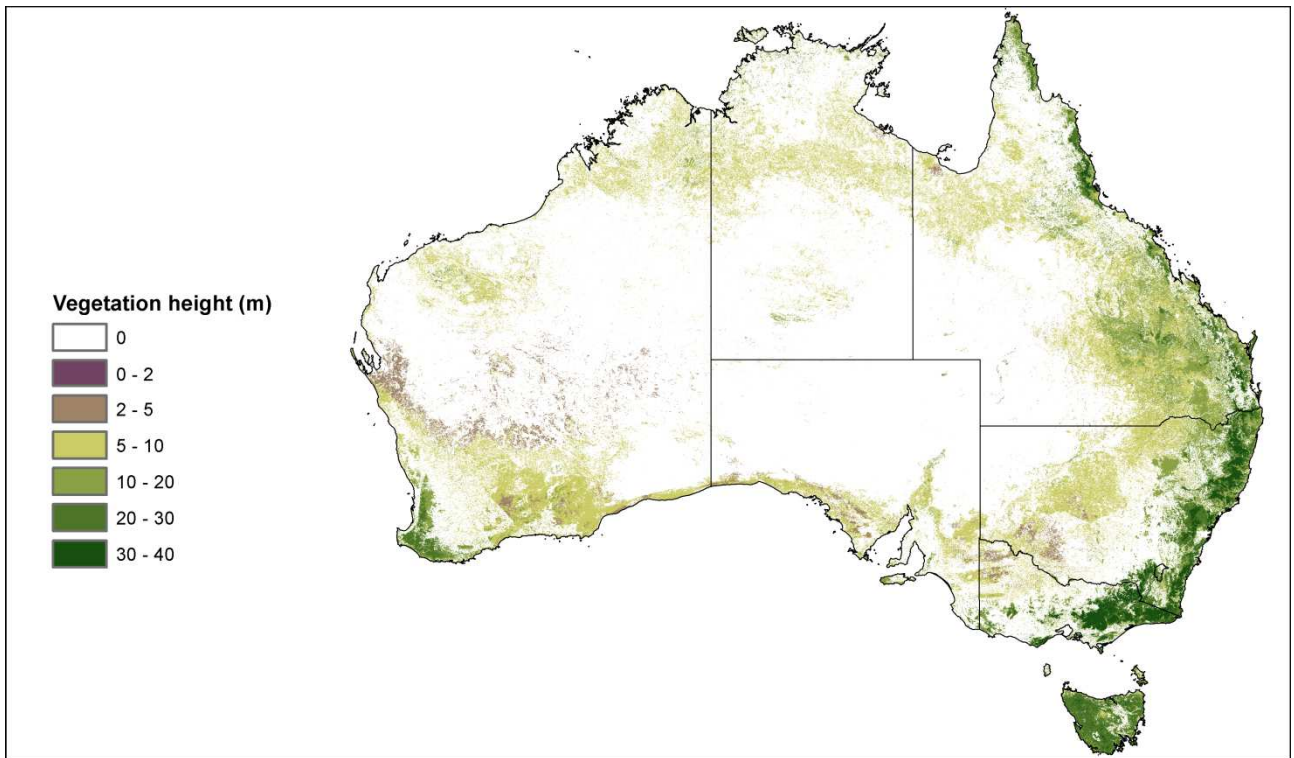


Figure 7. Distribution of vegetation height for the deep-rooted HRU.

The height of the top of the canopy (Figure 7) is derived from the global 1 km lidar estimates of Simard et al. (2011) and is assumed to be appropriate only for the deep-rooted HRU. For the shallow-rooted HRU, the vegetation height is optimisable, but usually assumed to take a fixed value of 0.5 m. Vegetation height is assumed static throughout the simulation.

Leaf area index (LAI) can be input directly from satellite observation. When this is implemented, LAI is allowed to vary daily. However, in AWRA-L v4.5, vegetation density is modelled dynamically (Section 3.5), so no LAI input is required.

3.1.2.2 Surface properties

Variables

β	Average slope within a grid cell (percent)
P_{ref}	Reference precipitation (mm d^{-1})
$P_{refscale}$	Scaling factor for reference precipitation (dimensionless)
K_{0sat}	Saturated hydraulic conductivity of surface soil layer (mm d^{-1})

Equations

$$P_{ref} = 20 P_{refscale} \left(2 + \log \left(\frac{K_{0sat}}{\beta} \right) \right) \quad (1)$$

Optimisable variables

$P_{refscale}$	Scaling factor for reference precipitation (dimensionless)
----------------	--

Description

The average slope within a grid cell is used in the calculation of interflow (Section 3.2.2.4). This is a very simple formulation as we are not simulating hillslope processes. The resulting slope is the average over an

area of about 25 km², and thus represents broad-scale terrain effects only. The slope as used is shown in Figure 8.

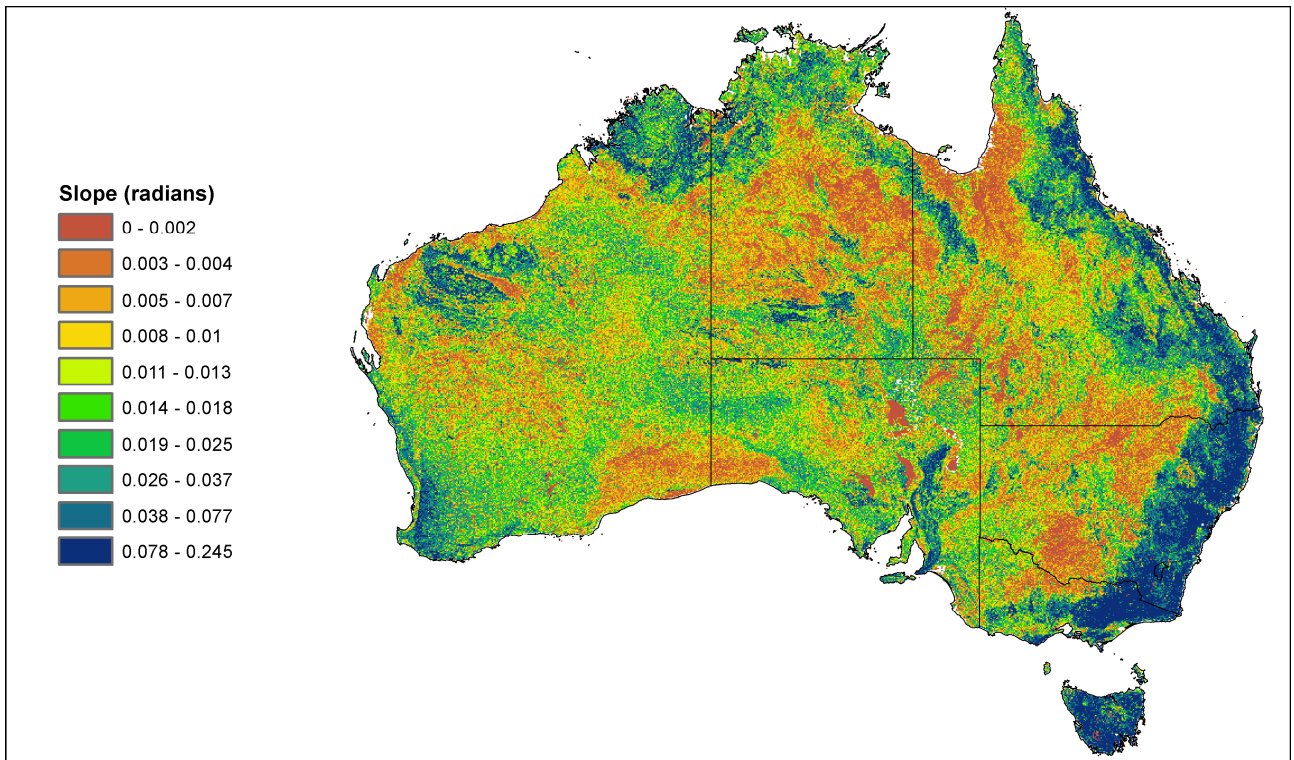


Figure 8. Average slope within a grid cell as derived from 3 second DEM.

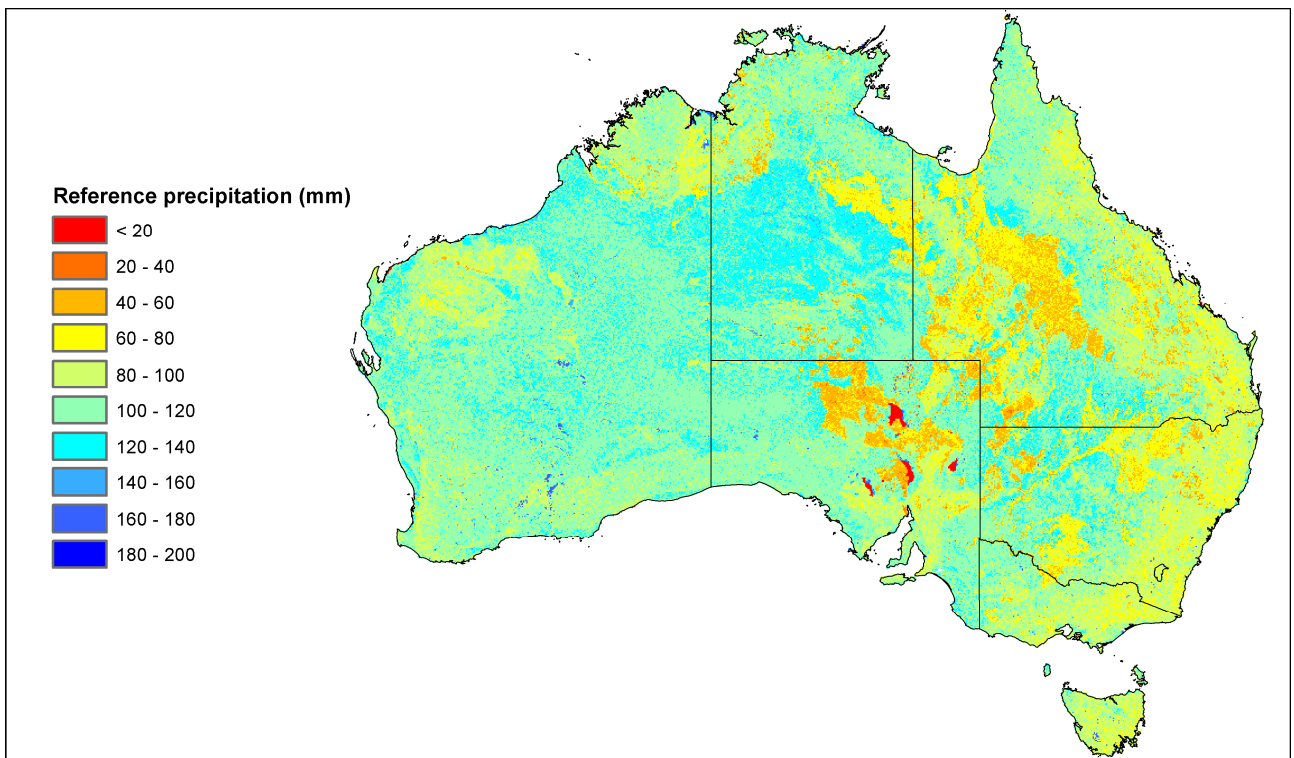


Figure 9. Continental distribution of reference precipitation.

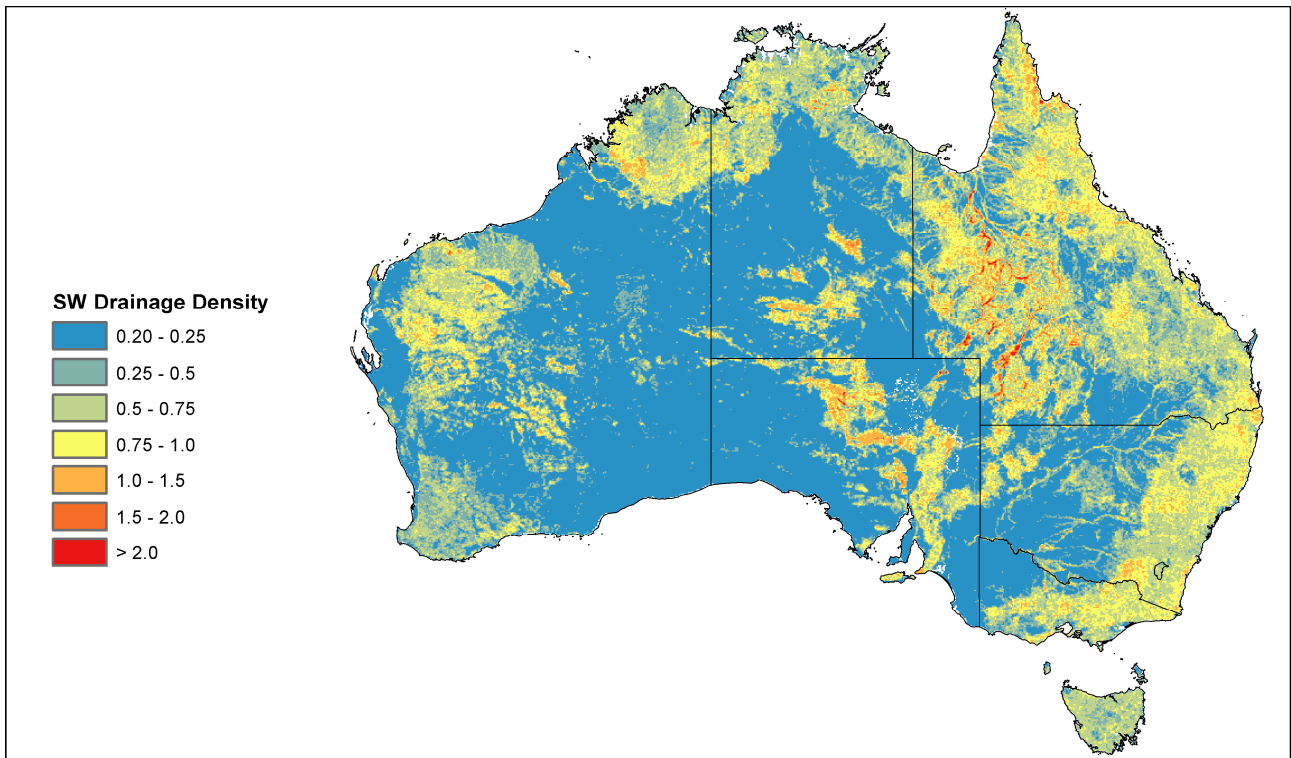


Figure 10. Distribution of the density of the surface water drainage network. The units are km^{-1} .

There has been considerable work looking at infiltration over the past 100 years or so. This mainly comes down to infiltration being controlled by soil properties, hydraulic conductivity in particular. Unfortunately there is no such theoretical development of subsurface storm flow (Bachmair and Weiler, 2011). Mathematically, the variable P_{ref} represents the daily net precipitation amount (i.e., precipitation minus interception) at which approximately 76% of net precipitation becomes infiltration-excess runoff (see Section 3.2.1). This amount, however, is not readily measurable. The generation of a parameterisation for reference precipitation, P_{ref} , therefore requires an empirical approach rather than a theoretical approach.

The resulting relationship for P_{ref} has been developed as a function of the hydraulic conductivity of the topsoil and slope. Higher values of K_{0sat} result in higher P_{ref} and therefore more infiltration, while lower values give rise to more runoff.

The lowest values calculated for P_{ref} are associated with the very low conductivity soils in the interior of the continent (Figure 9). The next lowest grouping is associated with the mountainous regions of the Great Dividing Range. Encouragingly, areas such as Tomago, Fraser Island and the southeast of South Australia, where there should not be any runoff generated, have high values of P_{ref} .

The drainage density (Figure 10) is the total length of stream lines per unit area. It is obtained from the length of mapped streams in a 250k topographic sheet. Drainage density has a lower limit of 0.2 km^{-1} (see Section 3.1.2.4).

3.1.2.3 Soil properties

Variables

S_{0max}	Maximum storage of the surface soil layer (mm)
S_{smax}	Maximum storage of the shallow soil layer (mm)
S_{dmax}	Maximum storage of the deep soil layer (mm)
d_0	Depth of the surface soil layer (mm)
d_s	Depth of the shallow soil layer (mm)
d_d	Depth of the deep soil layer (mm)
S_{0AWC}	Available water holding capacity in the surface soil (dimensionless)
S_{sAWC}	Available water holding capacity in the shallow soil (dimensionless)

$S_{0maxscale}$	Scaling parameter for maximum storage of the surface soil layer (dimensionless)
$S_{smaxscale}$	Scaling parameter for maximum storage of the shallow soil layer (dimensionless)
$S_{dmaxscale}$	Scaling parameter for maximum storage of the deep soil layer (dimensionless)
K_{0sat}	Saturated hydraulic conductivity of surface soil layer (mm d ⁻¹)
K_{ssat}	Saturated hydraulic conductivity of shallow soil layer (mm d ⁻¹)
K_{dsat}	Saturated hydraulic conductivity of deep soil layer (mm d ⁻¹)
$K_{0satscale}$	Scaling factor for hydraulic conductivity of surface soil layer (dimensionless)
$K_{ssatscale}$	Scaling factor for hydraulic conductivity of shallow soil layer (dimensionless)
$K_{dsatscale}$	Scaling factor for hydraulic conductivity of deep soil layer (dimensionless)
$K_{0satASRIS}$	Saturated hydraulic conductivity of surface soil layer provided by ASRIS (mm d ⁻¹)
$K_{ssatASRIS}$	Saturated hydraulic conductivity of shallow soil layer provided by ASRIS (mm d ⁻¹)
$K_{dsatASRIS}$	Saturated hydraulic conductivity of deep soil layer provided by ASRIS (mm d ⁻¹)

Equations

$$S_{0max} = d_0 S_{0AWC} S_{0maxscale} \quad (2)$$

$$S_{smax} = d_s S_{sAWC} S_{smaxscale} \quad (3)$$

$$S_{dmax} = \frac{d_d}{d_s} S_{smax} S_{dmaxscale} \quad (4)$$

$$K_{0sat} = K_{0satscale} K_{0satASRIS} \quad (5)$$

$$K_{ssat} = K_{ssatscale} K_{ssatASRIS} \quad (6)$$

$$K_{dsat} = K_{dsatscale} K_{ssat} \quad (7)$$

Optimisable variables

$S_{0maxscale}$	Scaling parameter for maximum storage of the surface soil layer (dimensionless)
$S_{smaxscale}$	Scaling parameter for maximum storage of the shallow soil layer (dimensionless)
$S_{dmaxscale}$	Scaling parameter for maximum storage of the deep soil layer (dimensionless)
$K_{0satscale}$	Scaling factor for hydraulic conductivity of surface soil layer (dimensionless)
$K_{ssatscale}$	Scaling factor for hydraulic conductivity of shallow soil layer (dimensionless)
$K_{dsatscale}$	Scaling factor for hydraulic conductivity of deep soil layer (dimensionless)

Description

The soil properties that control the storage and flow of water in the unsaturated zone are currently derived from the continental scale mapping within ASRIS Level 4 (Johnston et al., 2003).

The maximum storage within a soil layer is the parameter that the model needs rather than anything stored in ASRIS. This is calculated from the depth of the soil, the relative soil water storage capacity and a calibration parameter. The depths (thicknesses) of the three soil layers (surface, shallow and deep layers) in AWRA-L are notionally taken as 100 mm, 900 mm and 5000 mm, respectively.

The depth of the topsoil is currently fixed across the continent at 0.1 m as a very thin layer that could be used for data assimilation of remotely sensed soil moisture in future and also is the store that is assumed to be the primary source of soil evaporation. The relative available water capacity of the topsoil layer (S_{0AWC}) is derived from the information in ASRIS as the plant available water capacity of a layer divided by its thickness. Its spatial distribution is shown in Figure 11.

The maximum storage capacity of the shallow soil is calculated similarly with the exception of the depth of soil which is currently fixed at 0.9 m across the continent because of an assumption that the rooting depth of the shallow rooted vegetation does not exceed 1 m. Its spatial distribution is shown in Figure 12.

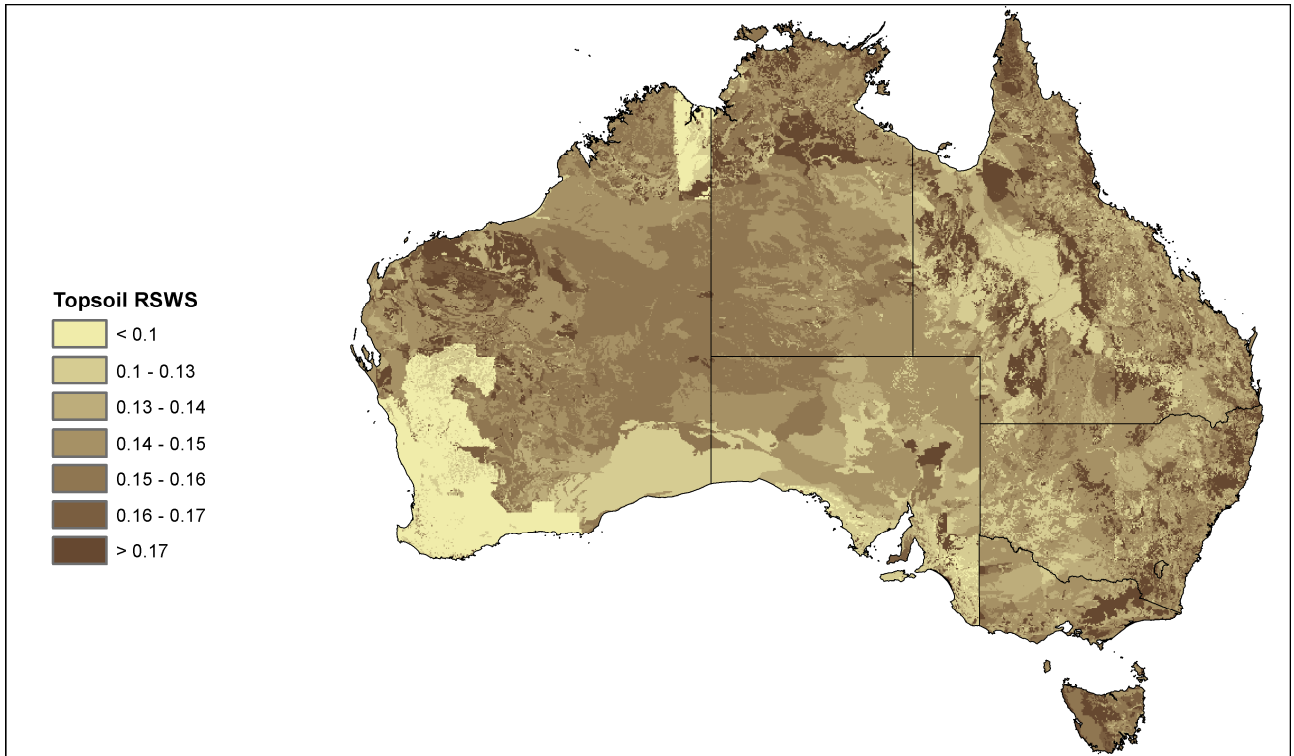


Figure 11. Relative available soil water storage for the surface soil layer (S_{0AWC}).

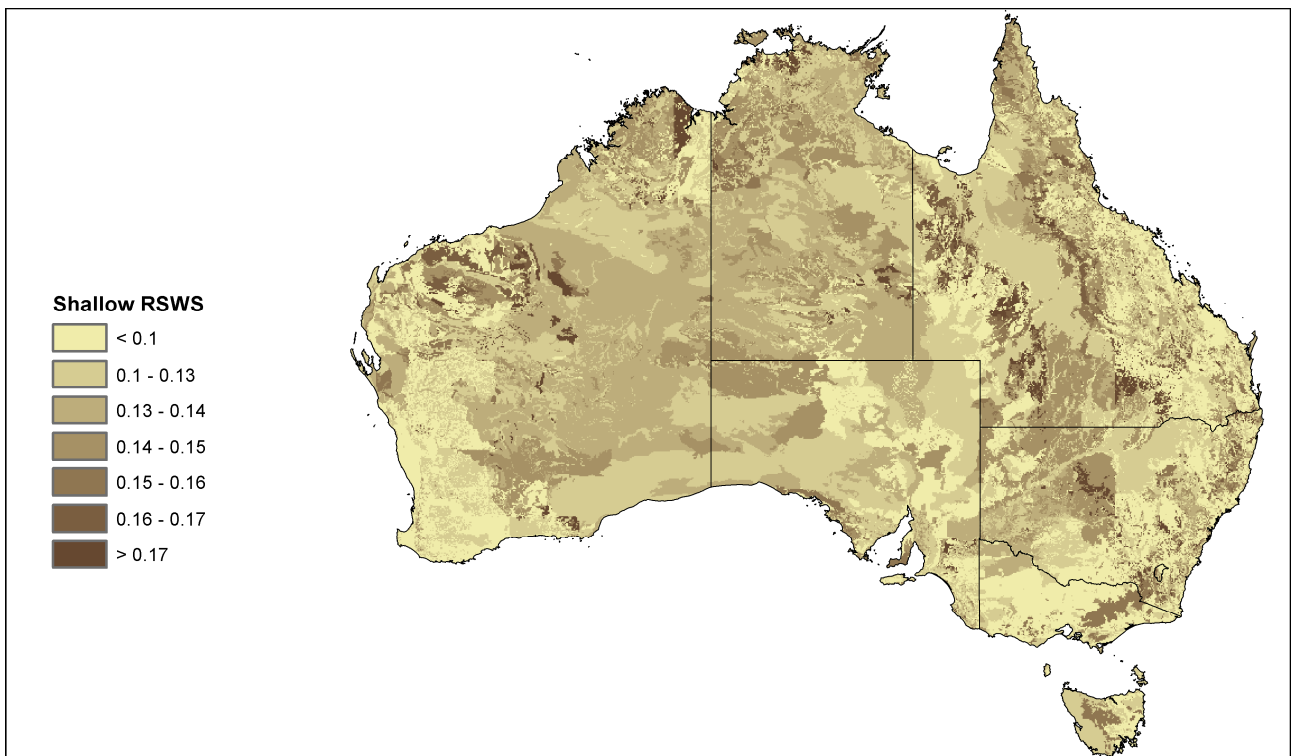


Figure 12. Relative available soil water storage for the shallow soil layer (S_{sAWC}).

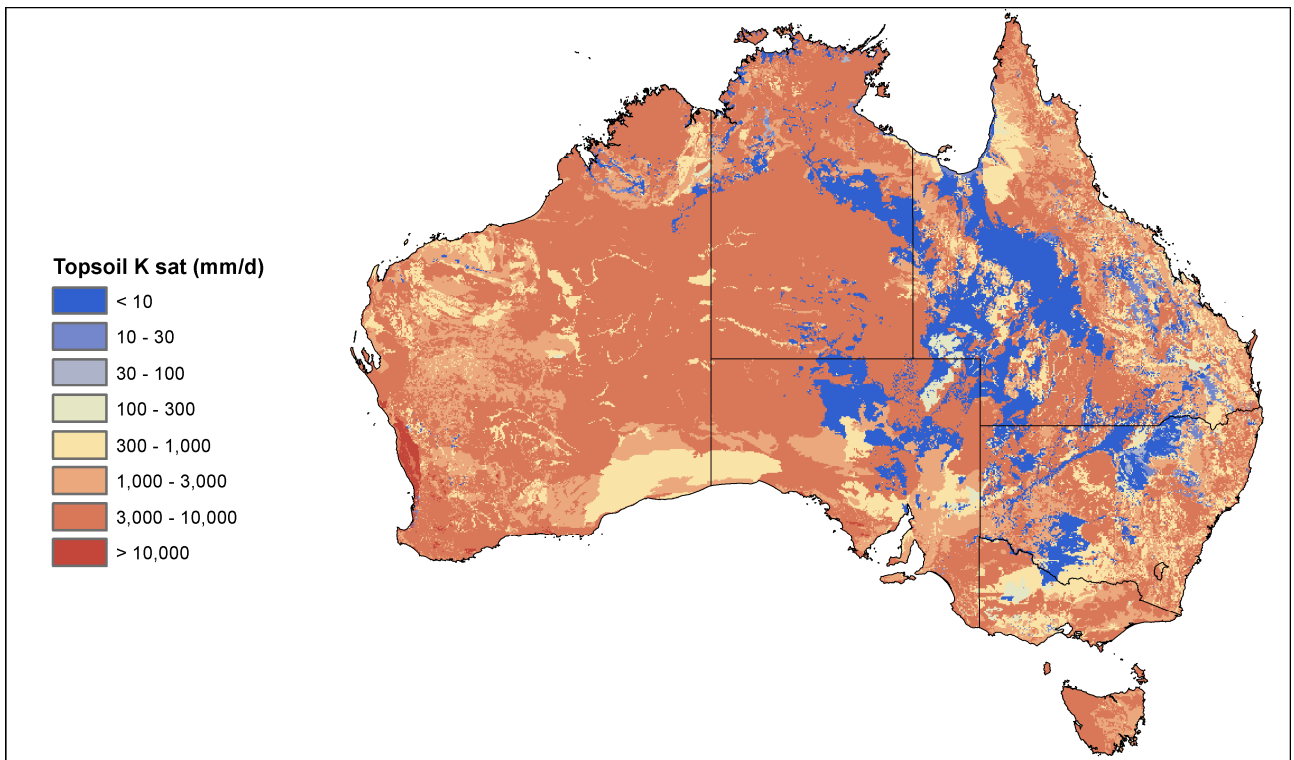


Figure 13. Soil saturated hydraulic conductivity for the topsoil ($K_{0satASRIS}$).

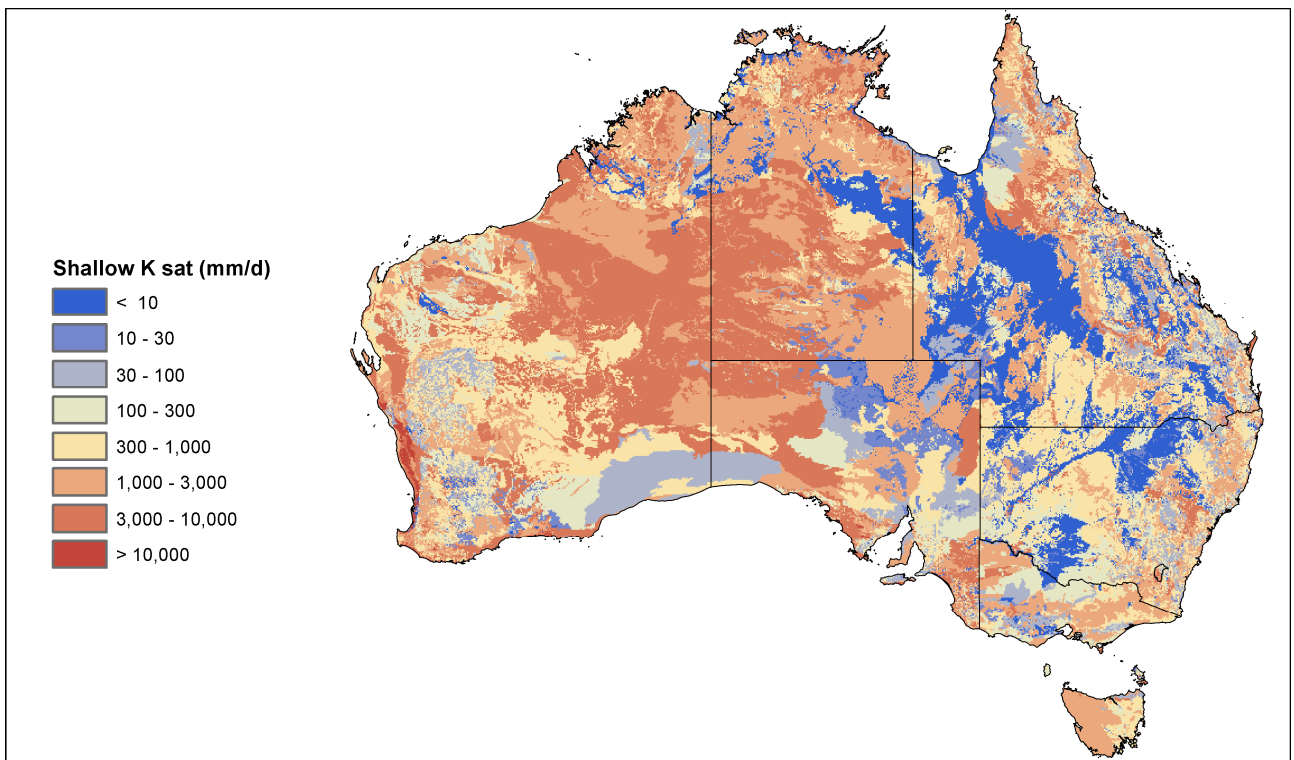


Figure 14. Soil saturated hydraulic conductivity for the shallow soil ($K_{ssatASRIS}$).

The deep soil layer is slightly different because ASRIS Level 4 uses a two layer model across the continent and so we do not have the information available for the deep soil layer. In this case it is assumed that the

bulk density of the deep soil is higher than the shallow soil and so the relative available water capacity will be lower. The relative available water capacity is therefore at most equal to that of the shallow soil but is probably lower and so is calculated as a function of the shallow soil capacity. The depth of the deep soil is assumed to be 5 m across the continent under the assumption that the deep rooted vegetation can access water down to 6 m. The optimisable parameter $S_{dmaxscale}$ is expected to take a value of less than one.

The two layer model of ASRIS level 4 allows the saturated hydraulic conductivity of the surface soil (Figure 13) and shallow soil (Figure 14) to be determined spatially across the continent. A scaling factor is applied to these during calibration.

Note that in the absence of suitable information from ASRIS, the saturated hydraulic conductivity of the deep soil layer is calculated as a function of that of the shallow soil layer.

3.1.2.4 Groundwater properties

Variables

n	Effective porosity (dimensionless)
n_{map}	Effective porosity obtained from continental mapping (dimensionless)
n_{scale}	Scaling factor for effective porosity (dimensionless)
K_g	Groundwater drainage coefficient (d^{-1})
K_{gmap}	Groundwater drainage coefficient obtained from continental mapping (d^{-1})
K_{gscale}	Scaling factor for groundwater drainage coefficient (dimensionless)
k_u	Hydraulic conductivity of the unconfined aquifer ($m\ d^{-1}$)
d_u	Depth of the unconfined aquifer (m)
h_u	Elevation change along the flow path (m)
λ_d	Surface water drainage density (m^{-1})

Equations

$$n = n_{scale} n_{map} \quad (8)$$

$$K_g = K_{gscale} K_{gmap} \quad (9)$$

$$K_{gmap} = \frac{k_u (2\lambda_d)^2 \max\{d_u, h_u\}}{n_{map}} \quad (10)$$

Optimisable variables

n_{scale}	Scaling factor for effective porosity (dimensionless)
K_{gscale}	Scaling factor for groundwater drainage coefficient (dimensionless)

Description

Figure 15 shows the spatial distribution of the hydraulic conductivity of the unconfined layer, k_u . It is used to calculate aquifer transmissivity and the groundwater drainage coefficient.

The modelling of lateral groundwater flow requires the specific yield (effective porosity is used here) and transmissivity of every grid cell in the model domain. This information is currently not available at a continental scale. Instead, these terms are derived from surface geology mapping and a look up table from lithologies. This will be used until better information becomes available. The spatial distribution of effective porosity is shown in Figure 16.

The groundwater drainage coefficient, K_g , controls the rate of groundwater discharge. The linear reservoir used for groundwater in AWRA-L can be derived analytically from the linearised Boussinesq equation (Knight et al., 2005; Walker et al., 2005). The drainage coefficient may be derived from effective porosity, hydraulic conductivity, drainage density and an assumed aquifer depth. Following Dawes et al. (2004),

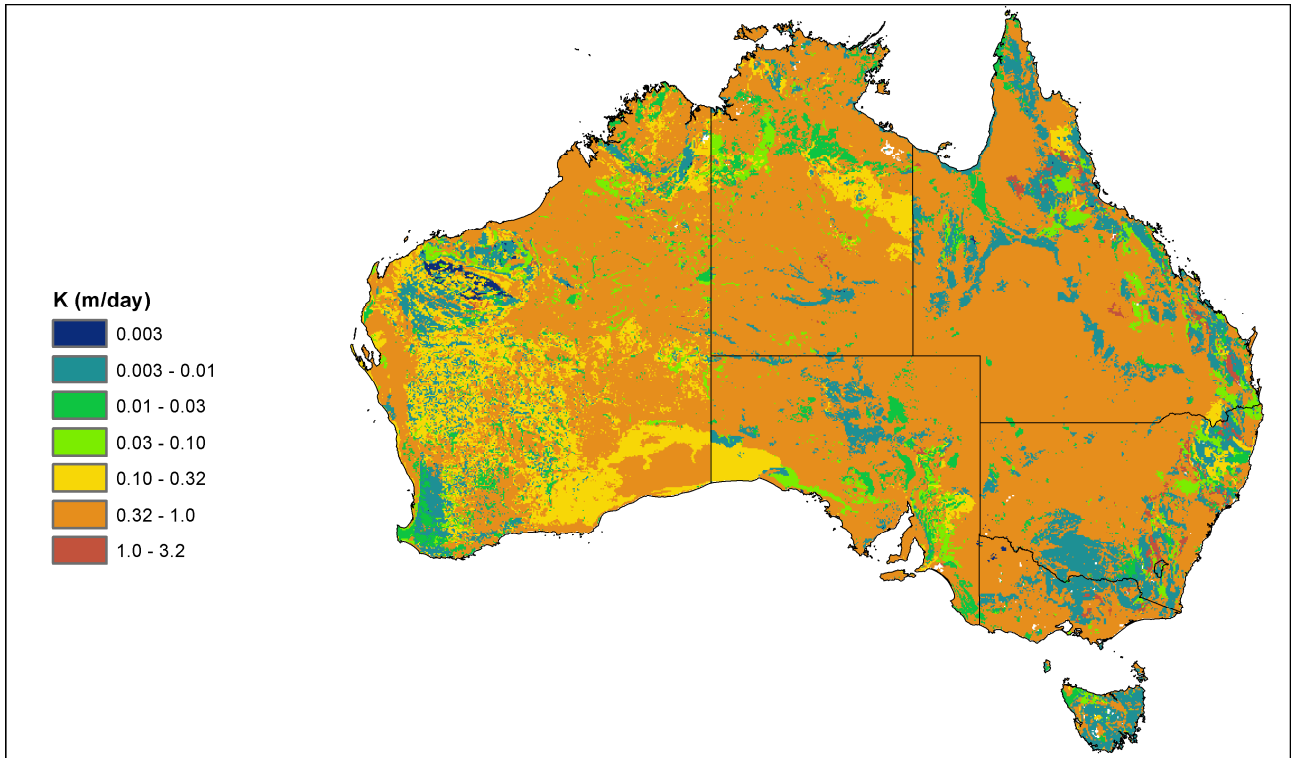


Figure 15. Hydraulic conductivity of the unconfined aquifer.

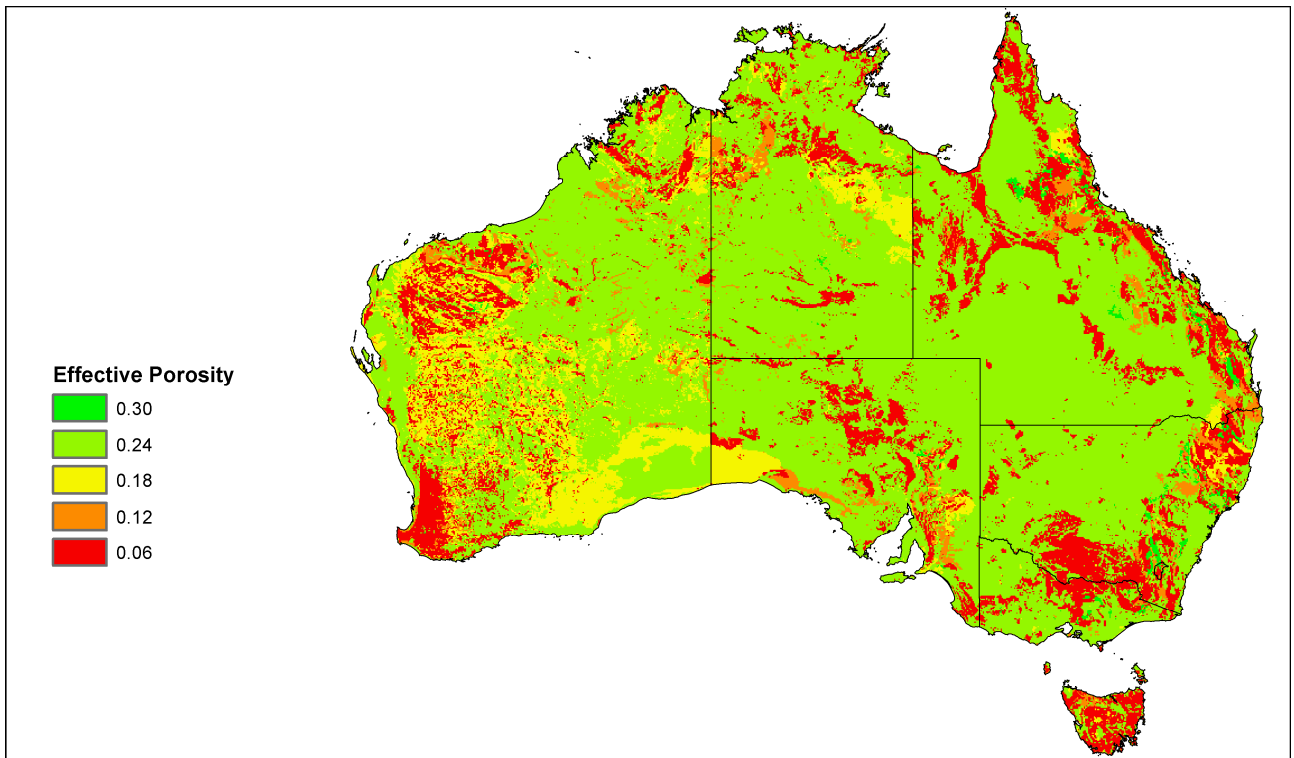


Figure 16. Effective porosity of the unconfined aquifer.

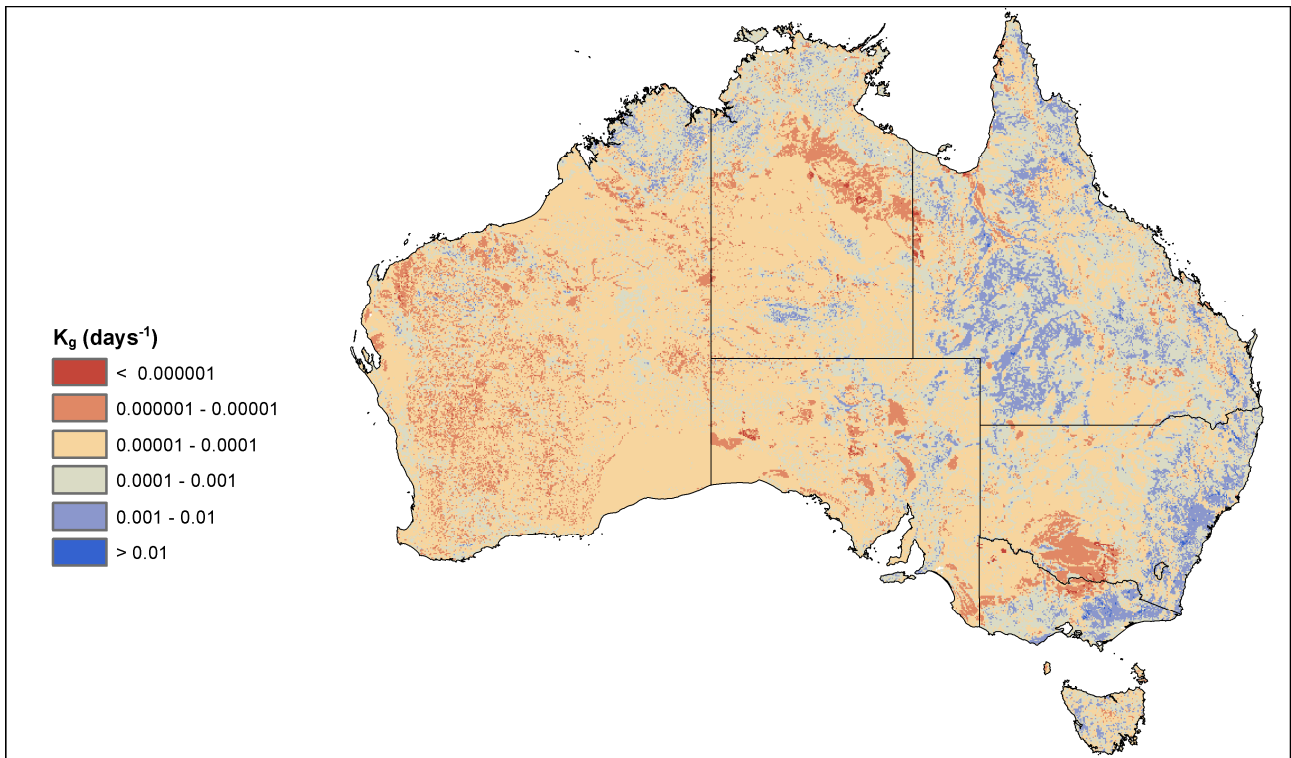


Figure 17. Distribution of the groundwater drainage coefficient (K_g) across the continent.

K_{gmap} is given by Equation (10). The two arguments to the maximum operator, d_u and h_u , are respectively relevant for cases when lateral flow is dominated by a hydraulic gradient (d_u) or by a topographic gradient (h_u). The aquifer depth (d_u) is currently unknown at the continental scale and will hopefully become available in the future. For this initial parameterisation it has been derived from the groundwater flow systems mapping of Coram et al. (2000) by assuming that regional flow systems have a depth of 100 m, intermediate flow systems have a depth of 30 m and local flow systems have a depth of 10 m. The term ($2D_d$) in Equation (10) may be assumed to be the reciprocal of the flow length. The flow length is capped at a maximum of 2500 m, which is half the approximate width of an AWRA-L grid cell. This is equivalent to placing a lower limit of 0.2 km^{-1} on D_d . The spatial distributions of D_d and K_{gmap} are shown in Figure 10 and Figure 17, respectively.

Future versions of AWRA-L might include spatial fields for storativity (Section 3.2.3.2) and time to equilibrium (Section 3.2.3.2), together with a better spatial representation of aquifer depth (d_u). However, for AWRA-L v4.5, these variables have been set to spatially uniform default values.

3.1.3 STATE VARIABLES

The following state variables are included in AWRA-L:

S_0	Top soil water storage (mm)
S_s	Shallow soil water storage (mm)
S_d	Deep soil water storage (mm)
S_g	Unconfined groundwater storage (mm)
S_{gc}	Confined groundwater storage (mm)
S_r	Surface water storage (mm)
M	Leaf biomass (kg m^{-2})

In general, these state variables take on different values for the different HRUs within a grid cell. The exceptions are the groundwater stores which represent the entire grid cell. State variables are updated daily after any additions or subtractions occurring during the day have been accounted for.

3.1.3.1 Initialisation of state variables

The three soil water storage state variables, those describing top soil, shallow soil and deep soil, are constrained by maximum allowable values: S_{0max} , S_{smax} and S_{dmax} , respectively. In the absence of any information about initial values for the three state variables, all three take on initial default values that are half of the value of their respective maximum values (Table 1). The unconfined groundwater storage takes on an initial default value of 100 mm, while surface water storage and the confined groundwater storage are both initialised to 0 mm. Leaf biomass is initialised with reference to specific leaf area, C_s ($m^2 kg^{-1}$), and is given by $M = 2/C_s$. Here the coefficient represents a notional initial LAI value of 2. Values of S_{0max} , S_{smax} , S_{dmax} and C_s are optimised (either directly or indirectly) during calibration.

The surface water, soil water and mass of leaf state variables equilibrate within a short period of time, typically less than a year. However, the groundwater stores can take considerably longer to reach equilibrium, so the specification of initial values for those is much more important. Currently a model spin-up time of seven years is used to allow sufficient time for the groundwater stores to reach equilibrium, but there is scope for developing and adopting a better solution in the future.

Table 1. List of initial values for state variables.

Variable	Description	Initial value
S_0	Surface soil water storage	$S_{0max} / 2$
S_s	Shallow soil water storage	$S_{smax} / 2$
S_d	Deep soil water storage	$S_{dmax} / 2$
S_g	Unconfined groundwater storage	100 mm
S_{gc}	Confined groundwater storage	0 mm
S_r	Surface water storage	0 mm
M	Leaf biomass	$2 / C_s$

3.2 The water balance

3.2.1 SURFACE RUNOFF

Variables

t	Timestep (d)
P	Precipitation (mm)
E_i	Interception (mm)
Q_R	Surface runoff (mm)
I	Infiltration (mm)
P_n	Net precipitation – precipitation minus interception (mm)
Q_h	Infiltration-excess runoff component (mm)
Q_s	Saturation-excess runoff component (mm)
f_s	Fractional saturated area (dimensionless)
P_{ref}	Reference value for precipitation (mm)

Equations

$$P(t) = E_i(t) + I(t) + Q_R(t) \quad (11)$$

$$P_n = \begin{cases} P - E_i, & P > E_i \\ 0, & P \leq E_i \end{cases} \quad (12)$$

$$Q_h = (1 - f_s)(P_n - P_{ref} \tanh \frac{P_n}{P_{ref}}) \quad (13)$$

$$Q_s = f_s P_n \quad (14)$$

$$Q_R = Q_h + Q_s \quad (15)$$

Description

Precipitation is partitioned into interception, surface runoff, and infiltration. The independent variable, time, t (days), indicates that the partitioning is assumed to be completed on the day the precipitation occurs.

Surface runoff, Q_R , is calculated as the sum of an infiltration-excess runoff component, Q_h , and a saturation-excess runoff component, Q_s . In Equation (13), infiltration-excess runoff is assumed to be generated from the unsaturated parts of the landscape at a rate that is modulated by the parameter P_{ref} . In Equation (14), all precipitation falling on the saturated fraction of the landscape is assumed to run off.

The infiltration component, I , is then given by inversion of Equation (11). The calculation of evaporation terms, including interception, E_i , is dealt with in Section 3.4. The calculation of the fractional saturated area is described in the section on the hypsometric curve algorithm (Section 3.2.3.3).

3.2.2 DRAINAGE FLUXES

Variables

t	Timestep (d)
S_0	Water storage in the surface soil layer (mm)
S_s	Water storage in the shallow soil layer (mm)
S_d	Water storage in the deep soil layer (mm)
I	Infiltration (mm)
D_0	Vertical drainage from the bottom of the surface soil layer (mm)
D_s	Vertical drainage from the bottom of the shallow soil layer (mm)
D_d	Vertical drainage from the bottom of the deep soil layer (mm)
Q_{l0}	Interflow draining laterally from the surface soil layer (mm)
Q_{ls}	Interflow draining laterally from the shallow soil layer (mm)
E_0	Evaporation from the surface soil layer (mm)
U_s	Transpiration from the shallow soil layer (mm)
U_d	Transpiration from the deep soil layer (mm)
K_{0sat}	Saturated hydraulic conductivity of surface soil layer (mm d^{-1})
K_{ssat}	Saturated hydraulic conductivity of shallow soil layer (mm d^{-1})
K_{dsat}	Saturated hydraulic conductivity of deep soil layer (mm d^{-1})
S_{0max}	Maximum storage of the surface soil layer (mm)
S_{smax}	Maximum storage of the shallow soil layer (mm)
S_{dmax}	Maximum storage of the deep soil layer (mm)
ρ_0	Partitioning factor for vertical and lateral drainage from the surface soil layer (dimensionless)
ρ_s	Partitioning factor for vertical and lateral drainage from the shallow soil layer (dimensionless)
β	Slope of the land surface (percent)
k_β	Scaling factor for slope (dimensionless)

k_z Scaling factor for ratio of saturated hydraulic conductivity (dimensionless)

3.2.2.1 Water balance of each soil layer

Equations

$$S_0(t) = S_0(t-1) + I(t) - D_0(t) - Q_{I0}(t) - E_0(t) \quad (16)$$

$$S_s(t) = S_s(t-1) + D_0(t) - D_s(t) - Q_{Is}(t) - U_s(t) \quad (17)$$

$$S_d(t) = S_d(t-1) + D_s(t) - D_d(t) - U_d(t) \quad (18)$$

Description

Soil drainage and moisture dynamics are based on simple water balance considerations for each layer, and unsaturated downward movement of water under gravity only. The soil profile is considered in AWRA-L to comprise of three layers with notional thicknesses of 0.1 m, 0.9 m and 5.0 m (Figure 18).

The water storage state variables are updated as a function of their values on the previous day and on any fluxes to and from them. The water balance in this system is described by Equations (16)–(18). In these equations, $S(t-1)$ represents the storage level at the beginning of the current time step and $S(t)$ represents the storage level at the end of the current time step (and also the beginning of the next time step).

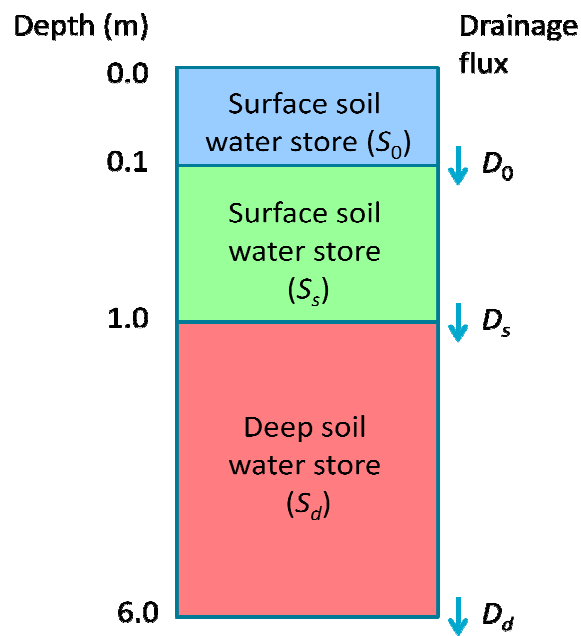


Figure 18. Arrangement of soil water stores and drainage fluxes.

3.2.2.2 Total drainage (vertical and lateral) from each soil layer

Equations

$$D_0(t) + Q_{I0}(t) = \sqrt{K_{0sat}K_{ssat}} \left(\frac{S_0(t)}{S_{0max}} \right)^2 \quad (19)$$

$$D_s(t) + Q_{Is}(t) = \sqrt{K_{ssat}K_{dsat}} \left(\frac{S_s(t)}{S_{smax}} \right)^2 \quad (20)$$

$$D_d(t) = K_{dsat} \left(\frac{S_d(t)}{S_{dmax}} \right)^2 \quad (21)$$

Description

If we make the assumption that, on a daily time step, soil water diffusion is constant, then the total unsaturated drainage (vertical and lateral) from each of the soil layers is given by Equations (19)–(21). There is assumed to be no lateral drainage from the deep soil layer. Drainage from each layer is subject to limits imposed by water availability and hydraulic conductivity. Note that it is assumed that the total drainage depends on the water storage $S(t)$ at the end of the current time step, rather than at the beginning.

3.2.2.3 Updating equations for water balance of each soil layer

Equations

$$S_0(t) = \frac{(S_{0max})^2}{2K_{0sat}} \left(-1 + \sqrt{1 + 4(S_0(t-1) + I(t) - E_0(t)) \frac{K_{0sat}}{(S_{0max})^2}} \right) \quad (22)$$

$$S_s(t) = \frac{(S_{smax})^2}{2K_{ssat}} \left(-1 + \sqrt{1 + 4(S_s(t-1) + D_0(t) - E_s(t)) \frac{K_{ssat}}{(S_{smax})^2}} \right) \quad (23)$$

$$S_d(t) = \frac{(S_{dmax})^2}{2K_{dsat}} \left(-1 + \sqrt{1 + 4(S_d(t-1) + D_s(t) - E_d(t)) \frac{K_{dsat}}{(S_{dmax})^2}} \right) \quad (24)$$

Description

Substitution of Equations (19)–(21) into Equations (16)–(18) yields a quadratic function of $S(t)$ in each layer with coefficients depending on the terms in the right hand side of Equations (16)–(18).

Equations (22)–(24) are, of course, subject to numerical constraints that limit storage levels to the range between zero and the relevant maximum storage for the layer. Any excess water needs to be accounted for in a water balance component like interflow or streamflow.

3.2.2.4 Partitioning of total drainage into vertical and lateral components

Equations

$$D_0(t) = (1 - \rho_0) K_{0sat} \left(\frac{S_0(t)}{S_{0max}} \right)^2 \quad (25)$$

$$D_s(t) = (1 - \rho_s) K_{ssat} \left(\frac{S_s(t)}{S_{smax}} \right)^2 \quad (26)$$

$$Q_{I0}(t) = \rho_0 K_{0sat} \left(\frac{S_0(t)}{S_{0max}} \right)^2 \quad (27)$$

$$Q_{Is}(t) = \rho_s K_{ssat} \left(\frac{S_s(t)}{S_{smax}} \right)^2 \quad (28)$$

$$\rho_0 = \tanh(k_\beta \beta \frac{S_0}{S_{0max}}) \tanh(k_\zeta (\frac{K_{0sat}}{K_{ssat}} - 1) \frac{S_0}{S_{0max}}) \quad (29)$$

$$\rho_s = \tanh(k_\beta \beta \frac{S_s}{S_{smax}}) \tanh(k_\zeta (\frac{K_{ssat}}{K_{dsat}} - 1) \frac{S_s}{S_{smax}}) \quad (30)$$

Optimisable variables

- k_β Scaling factor for slope (dimensionless)
 k_ζ Scaling factor for ratio of saturated hydraulic conductivity (dimensionless)

Description

The total drainage flux from each of the top two layers is partitioned into vertical and lateral component using Equations (25)–(28).

In Equations (29)–(30), the slope of the land surface is taken as a surrogate for the slope of the base of the respective soil layers. The partitioning factors, ρ_0 and ρ_s , increase – and thus so does the proportion of drainage allocated to interflow – with increases in slope, soil moisture and the conductivity difference at the interface of the soil layers.

Drainage from each layer (Equations (26)–(27)) is subject to limits imposed by water availability, maximum soil water capacity and hydraulic conductivity.

3.2.3 GROUNDWATER FLUXES

Variables

- t Timestep (d)
 S_g Groundwater storage in the unconfined aquifer (mm)
 S_{gc} Groundwater storage in the confined aquifer (mm)
 D_d Vertical drainage from the bottom of the deep soil layer (mm)
 Q_g Groundwater discharge to the surface water (mm)
 E_g Evaporation from groundwater where groundwater intersects the surface (mm)
 Y Capillary rise (mm)
 K_g Groundwater drainage coefficient (d^{-1})
 ΔS_{eq} Change in storage between confined and unconfined aquifers (mm)
 S_c Storativity of the confined aquifer (mm)
 n Effective porosity (dimensionless)
 l_{ia} Interaquifer leakage (mm)
 t_{eq} Time to equilibrium (d)
 Q_l Lateral groundwater flow to cell (mm)
 T_{ij} Harmonic mean of the transmissivity between from cell j to cell i ($m^2 d^{-1}$)
 ζ Shape factor that depends on whether cells are direct or diagonal neighbours (dimensionless)
 ΔH_{ij} Difference in head between cells i and j (m)
 H Head in a grid cell (m)
 H_b Drainage base – the lowest topographic point within the grid cell (m)

3.2.3.1 Groundwater balance and groundwater discharge

Equations

$$S_g(t) = S_g(t - 1) + D_d(t) - Q_g(t) - E_g(t) - Y(t) \quad (31)$$

$$Q_g = (S_g + D_d)(1 - e^{-K_g t}) \quad (32)$$

Description

The evaporation and capillary rise terms in the groundwater balance equation are discussed in Section 3.4.

Groundwater discharge to the surface water, or baseflow (Q_g) is conceptualised as a linear reservoir with the discharge being proportional to S_g as determined from a groundwater drainage coefficient, which is derived from a spatially-varying field (Figure 17).

3.2.3.2 Interaquifer leakage

Equations

$$\Delta S_{eq} = \frac{S_{gc}/S_c - S_g/n}{1/S_c + 1/n} \quad (33)$$

$$l_{ia} = \Delta S_{eq}/t_{eq} \quad (34)$$

$$Q_l = \sum_{j=1}^8 T_{ij} \zeta_{ij} \Delta H_{ij} \quad (35)$$

$$H = H_b + 1000 \frac{S_g}{n}, \quad \text{for the unconfined aquifer} \quad (36)$$

$$H = H_b + 1000 \frac{S_{gc}}{S}, \quad \text{for the confined aquifer} \quad (37)$$

Description

The change in storage, ΔS_{eq} , is the amount of water required to be transferred from one aquifer to the other and is computed to equilibrate the heads in each aquifer. The interaquifer leakage, l_{ia} (mm), is then calculated as a fraction of the change in storage as determined by the time to equilibrium.

The lateral groundwater flow (for both unconfined and confined aquifers) to a grid cell from its neighbouring grid cells is calculated using Darcy's Law and summed from eight directions.

The transmissivity used in Equation (35) is the harmonic mean of the transmissivity of the adjoining grid cells. The geometric factor (ζ) describes the proportion of flow between neighbouring cells; it is equal to $\pi/3$ for direct neighbours and $\pi/6$ for diagonal neighbours.

The head, H , in a grid cell is calculated as either the water table elevation in the unconfined layer or the piezometric level in the confined layer.

3.2.3.3 Hypsometric curve algorithm

Variables

S_g	Groundwater storage in the unconfined aquifer (mm)
n	Effective porosity (dimensionless)
h	Elevation of a point on the hypsometric curve (m)
f_s	Fraction of the grid cell that is saturated at the surface (dimensionless)
f_{Eg}	Fraction of the grid cell that is accessible for transpiration from groundwater (dimensionless)
H_b	Drainage base – the lowest topographic point within the grid cell (m)
D_R	Rooting depth (m)

Equations

$$S_g = 1000nh \quad (38)$$

Optimisable variables

D_R Rooting depth (m)

Description

To calculate both f_s and f_{EG} , hypsometric curves are used. The hypsometric curve is the cumulative distribution of elevation within an AWRA grid cell, based on a finer scale DEM. The elevation data, h (in m), are transformed into an equivalent sub-cell storage volume, S_g (in mm). By transforming the hypsometric data into storage volumes, f_s and f_{EG} can be obtained directly for any given groundwater storage S_g .

The saturated fraction of a grid cell (f_s) is determined from the groundwater storage and the topography. This is determined from the water table elevation (Equation (36)) and the hypsometric curve of the grid cell topography as derived from a finer scale DEM (Peeters et al., 2013). The fraction of the grid cell where the water table is above the ground surface is considered to be the saturated area. Thus, f_s (dimensionless) is taken as the fraction on the cumulative curve at which elevation is equal to $1000H_b n + S_g$. In practice, this value is interpolated from lookup tables.

Similarly, the fraction of a grid cell that is accessible for the vegetation to transpire groundwater (f_{EG}) is calculated as the fraction of the grid cell where the water table is above a plane of the rooting depth of the vegetation below the surface elevation. That is, where the elevation is equal to $1000(H_b + D_R)n + S_g$.

The optimisable rooting depth is required to be parameterised separately for each HRU.

3.2.4 STREAMFLOW

Variables

t	Timestep (d)
S_r	Volume of water in the surface water store (mm)
Q_h	Infiltration-excess runoff component (mm)
Q_s	Saturation-excess runoff component (mm)
Q_g	Groundwater discharge to the surface water (mm)
Q_l	Interflow (mm)
Q_t	Total discharge to stream (mm)
K_r	Rate coefficient controlling discharge to stream (dimensionless)
K_{rint}	Intercept coefficient for calculating K_r (dimensionless)
K_{rscale}	Scale coefficient for calculating K_r ($d \text{ mm}^{-1}$)
$\overline{E^*}$	Long term mean daily potential evaporation (mm d^{-1})

Equations

$$S_r(t) = S_r(t - 1) + Q_h(t) + Q_s(t) + Q_g(t) + Q_l(t) - Q_t(t) \quad (39)$$

$$Q_t(t) = (1 - e^{K_r})(S_r(t - 1) + Q_h(t) + Q_s(t) + Q_g(t) + Q_l(t)) \quad (40)$$

$$K_r = K_{rint} + K_{rscale} \overline{E^*} \quad (41)$$

Optimisable variables

K_{rint}	Intercept coefficient for calculating K_r (dimensionless)
K_{rscale}	Scale coefficient for calculating K_r ($d \text{ mm}^{-1}$)

Description

In AWRA, streamflow is sourced from surface runoff, baseflow and interflow. Discharge of water from these sources is routed via a notional surface water store, S_r (mm). The discharge from this surface water store is controlled by a routing delay factor. The water balance in this surface water store is described by Equation (39). Here Q_g and Q_i represent areally weighted averages of baseflow discharge and interflow, respectively, from the two HRUs. For each HRU, the interflow term represents the sum of the total discharge to the stream from the surface and shallow stores.

Note that the formulation of Equations (39) and (40) implies that Q_i depends on a storage level that has already been supplemented by the current time step's baseflow, interflow and surface runoff.

3.3 The energy balance

An estimate of potential evaporation is a key element of the landscape modelling in AWRA-L. Potential evaporation is required to scale, and to provide an upper limit on, evaporation and transpiration processes from the soil and vegetation. Potential evaporation depends on the available energy at the surface, which is given by the net radiation term. This term, in turn, requires estimation of its constituent upward and downward fluxes of shortwave and longwave radiation.

3.3.1 POTENTIAL EVAPORATION

Variables

t	Time step (d)
E^*	Potential evaporation (mm d^{-1})
R_n	Net radiation ($\text{MJ m}^{-2} \text{d}^{-1}$)
p_e	Actual vapour pressure (Pa)
p_{es}	Saturation vapour pressure (Pa)
u_2	Wind speed at a height of 2 m (m s^{-1})
Δ	Slope of the saturation vapour pressure curve (Pa K^{-1})
γ	Psychrometric constant (Pa K^{-1})
λ	Latent heat of vaporisation (MJ kg^{-1})
T_a	Daily mean temperature ($^{\circ}\text{C}$)
T_{min}	Daily minimum temperature ($^{\circ}\text{C}$)
p_a	Air pressure (Pa)

Equations

$$E^* = \frac{\Delta R_n + 6.43\gamma(p_{es} - p_e)(1 + 0.546u_2)}{\lambda(\Delta + \gamma)} \quad (42)$$

$$p_{es} = 610.8 \exp\left(\frac{17.27T_a}{237.3 + T_a}\right) \quad (43)$$

$$p_e = 610.8 \exp\left(\frac{17.27T_{min}}{237.3 + T_{min}}\right) \quad (44)$$

$$\Delta = 4217.457 \frac{p_{es}}{(240.97 + T_a)^2} \quad (45)$$

$$\lambda = 2.501 - 0.002361T_a \quad (46)$$

$$\gamma = 0.000646p_a(1 + 0.000946T_a) \quad (47)$$

Description

Potential evaporation is calculated by the Penman (1948) equation. Since Equation (42) is intended to apply at a daily time step, the soil heat flux is assumed to be negligible in comparison with the net radiation flux, and is therefore ignored.

The daily mean temperature (T_a) and is assumed to be the mean of the daily maximum (T_{max}) and minimum (T_{min}) temperatures. Actual vapour pressure is calculated on the assumption that the air is saturated at night when the air temperature is at its minimum and that this actual vapour pressure remains constant throughout the day.

Air pressure (p_a) is based on an average continental elevation of 330 m and is assumed to be constant at 97500 Pa for all grid cells. Where direct input data is unavailable, the wind speed, u_2 , is taken as 3.5 m s^{-1} for all grid cells.

3.3.2 NET RADIATION

Variables

R_n	Daily net radiation ($\text{MJ m}^{-2} \text{ d}^{-1}$)
K_d	Daily downwelling shortwave (solar) radiation ($\text{MJ m}^{-2} \text{ d}^{-1}$)
K_u	Daily upwelling shortwave radiation ($\text{MJ m}^{-2} \text{ d}^{-1}$)
L_d	Daily downwelling longwave radiation ($\text{MJ m}^{-2} \text{ d}^{-1}$)
L_u	Daily upwelling longwave radiation ($\text{MJ m}^{-2} \text{ d}^{-1}$)
K_{d0}	Expected downwelling shortwave radiation on a cloudless day ($\text{MJ m}^{-2} \text{ d}^{-1}$)
α	Surface albedo (dimensionless)
α_v	Albedo of vegetated surfaces (dimensionless)
α_s	Albedo of soil surface (dimensionless)
f_v	Fractional canopy cover (dimensionless)
V_c	Greenness index per unit canopy cover
α_w	Wet soil albedo (dimensionless)
α_d	Dry soil albedo (dimensionless)
σ	Stefan-Boltzmann constant ($\text{MJ m}^{-2} \text{ d}^{-1} \text{ K}^{-4}$)
T_a	Daily mean temperature ($^{\circ}\text{C}$)
p_e	Actual vapour pressure (Pa)
δ	Solar declination (radians)
Q_0	Function of the day of the year (radians)
d	Day of the year (d)
ω	Sunset hour angle (radians)
φ	Latitude (radians), and is negative in the southern hemisphere
r	Relative distance from earth to sun (dimensionless)
w_0	Relative soil moisture content (S/S_{max}) of the top soil layer (dimensionless)
w_{0ref}	Reference value of w_0 that determines the rate of albedo decrease with wetness (dimensionless)

3.3.2.1 Net radiation balance

Equations

$$R_n = K_d - K_u + L_d - L_u \quad (48)$$

Description

The net radiation balance is given by Equation (48). The incoming (or downwelling) shortwave radiation is available from the forcing data, but the other three terms in the R_n expression must be estimated. Details of how they are estimated are given in the following sections.

3.3.2.2 Upwelling shortwave radiation

Equations

$$K_u = \alpha K_d \quad (49)$$

$$\alpha = f_v \alpha_v + (1 - f_v) \alpha_s \quad (50)$$

$$\alpha_v = 0.452 V_c \quad (51)$$

$$\alpha_s = \alpha_w + (\alpha_d - \alpha_w) \exp\left(-\frac{w_0}{w_{0ref}}\right) \quad (52)$$

Optimisable variables

α_w	Wet soil albedo (dimensionless)
α_d	Dry soil albedo (dimensionless)
V_c	Greenness index per unit canopy cover
w_{0ref}	Reference value of w_0 that determines the rate of albedo decrease with wetness (dimensionless)

Description

The surface albedo, which may be different for different HRUs, is input either through parameter calibration or through satellite observations. If the former, α is estimated as a combination of a vegetation albedo α_v and a soil surface albedo α_s via Equations (50)–(52).

All of the optimisable variables associated with the calculation of albedo are required to be specified separately for each HRU.

3.3.2.3 Upwelling longwave radiation

Equations

$$L_u = \sigma(T_a + 273.15)^4 \quad (53)$$

Description

Upwelling longwave radiation, L_u , is given by the Stefan-Boltzmann Law at the temperature of the air. In Equation (53), it is assumed that T_a is representative of the radiating surface and that the surface emissivity is one.

3.3.2.4 Downwelling longwave radiation

Equations

$$L_d = \sigma(T_a + 273.15)^4 \left(1 - (1 - 0.65 \left(\frac{p_e}{T_a + 273.15}\right)^{0.14}) \left(1.35 \frac{K_d}{K_{d0}} - 0.35\right)\right) \quad (54)$$

$$\begin{aligned} \delta = & 0.006918 - 0.39912 \cos(Q_0) + 0.070257 \sin(Q_0) \\ & - 0.006758 \cos(2Q_0) + 0.000907 \sin(2Q_0) \\ & - 0.002697 \cos(3Q_0) + 0.00148 \sin(3Q_0) \end{aligned} \quad (55)$$

$$Q_0 = 2\pi(d - 1)/365 \quad (56)$$

$$\omega = \cos^{-1}(-\tan \phi \tan \delta) \quad (57)$$

$$r = 1 + 0.033 \cos\left(\frac{2\pi d}{365}\right) \quad (58)$$

$$K_{d0} = \frac{94.5r}{\pi} (\omega \sin \delta \sin \phi + \cos \delta \cos \phi \sin \omega) \quad (59)$$

Description

Downwelling longwave radiation L_d , depends, in a large part, on the amount of cloud in the atmosphere. Cloud amount is calculated from the observed value of downwelling shortwave radiation, K_d , and an estimate of the downwelling shortwave radiation that would be received at the surface on a cloud-free day, K_{d0} (Equation (59)). The steps involved in the calculation of clear sky solar radiation, K_{d0} , are outlined in Equations (55)–(58).

The coefficient in Equation (59) is based on a solar constant of 1367 W m^{-2} and assumes an atmospheric transmissivity of 80 %.

3.4 Evaporation fluxes

3.4.1 TOTAL EVAPOTRANSPIRATION

Variables

E_{tot}	Total evapotranspiration (mm d^{-1})
E_i	Evaporation flux from canopy interception (mm d^{-1})
E_0	Evaporation flux from the surface soil store (mm d^{-1})
E_g	Evaporation flux from the groundwater store (mm d^{-1})
U_s	Root water uptake (transpiration) from the shallow soil store (mm d^{-1})
U_d	Root water uptake (transpiration) from the deep soil store (mm d^{-1})
Y	Root water uptake (transpiration) from the groundwater store via capillary rise (mm d^{-1})

Equations

$$E_{tot} = E_i + E_0 + E_g + U_s + U_d + Y \quad (60)$$

Description

In AWRA-L v4.5, water is evaporated directly from the canopy interception store, the top soil water store and (where it intersects the surface) the groundwater store. In addition water is withdrawn by transpiration from shallow soil water store, the deep water store (for the deep-rooted HRU only) and the groundwater store. The total evapotranspiration flux is therefore given by Equation (60). All fluxes are in units of mm d^{-1} .

3.4.2 ROOT WATER UPTAKE

Variables

U_s	Root water uptake (transpiration) from the shallow soil store (mm d ⁻¹)
U_d	Root water uptake (transpiration) from the deep soil store (mm d ⁻¹)
Y	Root water uptake (transpiration) from the groundwater store via capillary rise (mm d ⁻¹)
E_t	Actual total transpiration flux (mm d ⁻¹)
E_t^*	Potential transpiration rate (mm d ⁻¹)
U^*	Maximum root water uptake (mm d ⁻¹)
E^*	Potential evaporation (mm d ⁻¹)
Δ	Slope of the saturation vapour pressure curve (Pa K ⁻¹)
γ	Psychrometric constant (Pa K ⁻¹)
g_a	Aerodynamic conductance (m s ⁻¹)
g_s	Canopy conductance (m s ⁻¹)
f_v	Fractional canopy cover (dimensionless)
f_s	Fraction of the grid cell that is saturated at the surface (dimensionless)
c_G	Coefficient relating vegetation photosynthetic capacity to maximum stomatal conductance (m s ⁻¹)
V_c	Greenness index per unit canopy cover
u_2	Wind speed at a height of 2 m (m s ⁻¹)
h_v	Vegetation height (m)
U_{smax}	Maximum root water uptake from the shallow soil store at prevailing moisture content (mm d ⁻¹)
U_{dmax}	Maximum root water uptake from the deep soil store at prevailing moisture content (mm d ⁻¹)
U_{s0}	Maximum possible root water uptake from the shallow soil store (mm d ⁻¹)
U_{d0}	Maximum possible root water uptake from the deep soil store (mm d ⁻¹)
w_s	Relative water content (S/S_{max}) of the shallow soil store (dimensionless)
w_d	Relative water content (S/S_{max}) of the deep soil store (dimensionless)
w_{slim}	Water-limiting relative water content of the shallow soil store (dimensionless)
w_{dlim}	Water-limiting relative water content of the deep soil store (dimensionless)
S_s	Water content of the shallow soil store (mm)
S_d	Water content of the deep soil store (mm)
F_{smax}	Soil evaporation scaling factor corresponding to unlimited soil water supply (dimensionless)
f_{Eg}	Fraction of the grid cell that is accessible for transpiration from groundwater (dimensionless)

3.4.2.1 Transpiration from unsaturated soil water stores

Equations

$$E_t = \min (E_t^*, U^*) \quad (61)$$

$$E_t^* = \frac{E^*}{1 + \left(\frac{\gamma}{\gamma + \Delta}\right) \frac{g_a}{g_s}} \quad (62)$$

$$g_s = f_v c_G V_c \quad (63)$$

$$g_a = \frac{0.305 u_2}{\ln\left(\frac{813}{h_v} - 5.45\right) (2.3 + \ln\left(\frac{813}{h_v} - 5.45\right))} \quad (64)$$

$$U_{smax} = U_{s0} \min \left(1, \frac{w_s}{w_{slim}}\right) \quad (65)$$

$$U_{dmax} = U_{d0} \min \left(1, \frac{w_d}{w_{dlim}}\right) \quad (66)$$

$$U^* = \max (U_{smax}, U_{dmax}) \quad (67)$$

$$U_s = \min \left(\frac{U_{smax} E_t}{U_{smax} + U_{dmax}}, S_s \right) \quad (68)$$

$$U_d = \min \left(\frac{U_{dmax} E_t}{U_{smax} + U_{dmax}}, S_d \right) \quad (69)$$

$$E_t = U_s + U_d \quad (70)$$

Optimisable variables

c_G	Coefficient relating vegetation photosynthetic capacity to maximum stomatal conductance ($m s^{-1}$)
V_c	Greenness index per unit canopy cover
h_v	Vegetation height (m)
U_{s0}	Maximum possible root water uptake from the shallow soil store ($mm d^{-1}$)
U_{d0}	Maximum possible root water uptake from the deep soil store ($mm d^{-1}$)
w_{slim}	Water-limiting relative water content of the shallow soil store (dimensionless)
w_{dlim}	Water-limiting relative water content of the deep soil store (dimensionless)

Description

The transpiration fluxes are limited by two factors: a potential transpiration rate and a maximum root water uptake. The actual transpiration is then calculated as the lesser of the two and this amount is distributed among the three potential transpiration water sources. The overall transpiration rate given by Equation (61) is used in the estimation of U_s and U_d . However, since either of U_s and U_d may be limited by available soil water (Equations (68) and (69)), an adjusted total transpiration rate is finally recalculated using Equation (70). This final value of E_t is then used to reduce the energy available for direct evaporation.

The potential transpiration rate, E_t^* , is defined as the transpiration that would occur with unlimited root water supply. It is calculated as a fraction of the potential evaporation rate (Equation (62)). This formulation means that the calculation of E_t^* involves a combination of the Penman equation and the Penman-Monteith equation. This should be of no significant concern since, in Equation (62), the latter is being used merely to partition potential evaporation among transpiring and non-transpiring components.

All of the optimisable variables are required to be specified separately for each HRU. However, h_v is input as a raster layer for the deep-rooted HRU and is only optimisable for the shallow-rooted HRU. Secondly, since the shallow-rooted vegetation cannot access the deep store, the value of U_{d0} for the shallow-rooted HRU is fixed at zero and the value of w_{dlim} for that store can then take on any non-zero value. For mathematical stability, it is still necessary to supply values for these two variables, but they should never be calibrated.

3.4.2.2 Transpiration from groundwater

Equations

$$Y = (f_{Eg} - f_s) F_{smax} (E^* - E_t) \quad (71)$$

Optimisable variables

F_{smax}	Soil evaporation scaling factor corresponding to unlimited soil water supply (dimensionless)
------------	--

Description

Transpiration from the groundwater store is facilitated by a capillary rise term given by Equation (71). As with transpiration from the shallow and deep soil layers, transpiration from capillary rise is only permitted in the deep-rooted HRU.

The optimisable variable, F_{smax} , is required to be specified separately for each HRU.

3.4.3 DIRECT EVAPORATION

Variables

E_i	Evaporation flux from canopy interception (mm d ⁻¹)
E_0	Evaporation flux from the surface soil store (mm d ⁻¹)
E_g	Evaporation flux from the groundwater store (mm d ⁻¹)
E_t	Actual total transpiration flux (mm d ⁻¹)
E^*	Potential evaporation (mm d ⁻¹)
P_w	Reference threshold precipitation amount (mm)
P	Precipitation amount (mm)
s_l	Specific canopy rainfall storage per unit leaf area (mm)
Λ	Leaf area index (LAI) (dimensionless)
f_v	Fractional canopy cover (dimensionless)
f_s	Fraction of the grid cell that is saturated at the surface (dimensionless)
F_{ER}	Ratio of the mean evaporation rate and the mean rainfall intensity during storms (dimensionless)
F_{smax}	Soil evaporation scaling factor corresponding to unlimited soil water supply (dimensionless)
w_0	Relative soil moisture content of the top soil layer (dimensionless)
w_{olim}	Limiting the value of w_0 at which evaporation is reduced (dimensionless)

3.4.3.1 Evaporation of intercepted rainfall

Equations

$$P_w = -\frac{s_l \Lambda}{f_v F_{ER}} \ln(1 - F_{ER}) \quad (72)$$

$$E_i = \begin{cases} f_v (P_w + F_{ER}(P - P_w)) & \text{if } P > P_w \\ f_v P & \text{if } P \leq P_w \end{cases} \quad (73)$$

Optimisable variables

s_l	Specific canopy rainfall storage per unit leaf area (mm)
F_{ER}	Ratio of the mean evaporation rate and the mean rainfall intensity during storms (dimensionless)
F_{smax}	Soil evaporation scaling factor corresponding to unlimited soil water supply (dimensionless)
w_{olim}	Limiting the value of w_0 at which evaporation is reduced (dimensionless)

Description

The algorithm for calculating evaporation of intercepted water uses the event-based approach of Gash (1979). Van Dijk and Bruijnzeel (2001) later modified this approach to allow application to vegetation with a sparse canopy. For small rainfall events where $P < P_w$, all rainfall that falls on the vegetated part of the landscape is assumed to be intercepted.

The energy required for evaporation of intercepted water is assumed independent of potential evaporation. It is further assumed that this energy does not reduce the available energy for the remaining evaporative fluxes.

All of the optimisable variables are required to be specified separately for each HRU. However, F_{ER} is only optimisable for the deep-rooted HRU. For the shallow-rooted HRU, F_{ER} is assumed to take a value that is half of the calibrated value for the deep-rooted HRU.

3.4.3.2 Groundwater evaporation

Equations

$$E_g = f_s F_{smax} (E^* - E_t) \quad (74)$$

Optimisable variables

F_{smax} Soil evaporation scaling factor corresponding to unlimited soil water supply (dimensionless)

Description

Evaporation from groundwater occurs only on those parts of the landscape where the water table intersects the surface. Thus, when the saturated fraction, f_s , is greater than zero, groundwater evaporation is given by Equation (74). The optimisable variable, F_{smax} , is required to be specified separately for each HRU.

3.4.3.3 Soil evaporation

Equations

$$E_o = (1 - f_s) F_{smax} (E^* - E_t) \min\left(1, \frac{w_o}{w_{olim}}\right) \quad (75)$$

Optimisable variables

F_{smax} Soil evaporation scaling factor corresponding to unlimited soil water supply (dimensionless)

w_{olim} Limiting the value of w_o at which evaporation is reduced (dimensionless)

Description

Soil evaporation depends on the moisture content of the surface layer on the unsaturated parts of the landscape. In Equation (75), F_{smax} has the same meaning as for groundwater evaporation (Equation (74)). Both of the optimisable variables are required to be specified separately for each HRU.

3.5 Vegetation phenology

Variables

t	Time step (d)
M	Leaf biomass (kg m^{-2})
M_n	Change in leaf biomass at each time step ($\text{kg m}^{-2} \text{d}^{-1}$)
Δt	Length of the time step (d)
f_{veg}	Equilibrium canopy cover (dimensionless)
U^*	Maximum root water uptake (mm d^{-1})
E^*	Potential evaporation (mm d^{-1})
Δ	Slope of the saturation vapour pressure curve (Pa K^{-1})
γ	Psychrometric constant (Pa K^{-1})
g_a	Aerodynamic conductance (m s^{-1})

c_G	Coefficient relating vegetation photosynthetic capacity to maximum stomatal conductance ($m s^{-1}$)
V_c	Greenness index per unit canopy cover
Λ	Leaf area index (LAI) (dimensionless)
Λ_{max}	Maximum achievable LAI value (dimensionless)
Λ_{ref}	Reference LAI value corresponding to $f_v = 0.63$ (dimensionless)
$FPAR$	Photosynthetically-active radiation (dimensionless)
C_S	Specific leaf area ($m^2 kg^{-1}$)
f_v	Fractional canopy cover (dimensionless)
M_{eq}	Equilibrium leaf biomass ($kg m^{-2}$)
t_g	Characteristic time scale for vegetation growth towards equilibrium (d)
t_s	Characteristic time scale for vegetation senescence towards equilibrium (d)

Equations

$$M(t + 1) = M(t) + \Delta t M_n(t) \quad (76)$$

$$f_{veq} = \min \left\{ \left(\frac{U^*}{E^* - U^*} \right) \left(\frac{\gamma}{\gamma + \Delta} \right) \frac{g_a}{c_G V_c}, \quad 1 - \exp \left(- \frac{\max(\Lambda_{max}, 0.00278)}{\Lambda_{ref}} \right) \right\} \quad (77)$$

$$\Lambda_{ref} = - \frac{\Lambda}{\ln(1 - FPAR)} \quad (78)$$

$$\Lambda = M C_S \quad (79)$$

$$f_v = 1 - \exp \left(- \frac{\Lambda}{\Lambda_{ref}} \right) \quad (80)$$

$$M_{eq} = - \frac{\Lambda_{ref}}{C_S} \ln(1 - f_{veq}) \quad (81)$$

$$M_n = \begin{cases} \frac{M_{eq} - M}{t_g}, & \text{if } M < M_{eq} \\ \frac{M_{eq} - M}{t_s}, & \text{if } M \geq M_{eq} \end{cases} \quad (82)$$

Optimisable variables

c_G	Coefficient relating vegetation photosynthetic capacity to maximum stomatal conductance ($m s^{-1}$)
V_c	Greenness index per unit canopy cover
Λ_{ref}	Reference LAI value corresponding to $f_v = 0.63$ (dimensionless)
t_g	Characteristic time scale for vegetation growth towards equilibrium (d)
t_s	Characteristic time scale for vegetation senescence towards equilibrium (d)

Description

Vegetation density plays a significant role in streamflow generation. Some measure or estimate of vegetation density is therefore crucial for modulating the hydrological processes in AWRA-L. This can be achieved in one of two ways. In the first, vegetation density is directly input into the model as a temporally and spatially varying leaf area index (LAI). In the second, a seasonal vegetation dynamics model is incorporated into AWRA-L to simulate vegetation cover dynamics in response to water availability. This is done under the assumption that the vegetation takes on the maximum density that could be sustained by the available moisture. The seasonal vegetation dynamics model is constrained by the mass balance equation (Equation (76)).

The variable Λ_{ref} is a reference LAI value corresponding to $f_v = 0.63$, which may be derived from MODIS LAI and FPAR products via Equation (78). In AWRA-L v4.0, however, Λ_{ref} is normally calibrated, rather than being calculated as a function of FPAR. Similarly, leaf area index, Λ , can be input directly from remote sensing, or can be estimated from leaf biomass using Equation (79).

The magnitude and direction of the net leaf biomass change in a time step is estimated by comparison of the existing leaf biomass with an equilibrium value, M_{eq} , that depends on water availability and atmospheric demand.

All of the optimisable variables involved in the vegetation phenology calculations are required to be specified separately for each HRU.

4 Parameterisation

4.1 Calibration procedure

As a conceptual model, AWRA-L includes a large number of parameters whose values are not easily prescribed and which may vary between catchments or between different modelling periods. The values of these parameters need to be calibrated. This is done in an automatic procedure by comparing modelled and observed responses and seeking to minimise the differences between them. In AWRA-L v4.5, these response series may include observed streamflow together with remotely sensed leaf area index, surface soil moisture or actual evapotranspiration.

Because some of the optimisable parameters need to be specified separately for each HRU, it is advisable that calibration be done against multiple observed series, particularly multiple observed streamflow series from different locations. This procedure is called regional calibration. If AWRA-L was calibrated against a single streamflow series, it is likely that many of the parameters would not be adequately optimised, since an increase in flow associated with one HRU could be offset by a decrease in flow in the other.

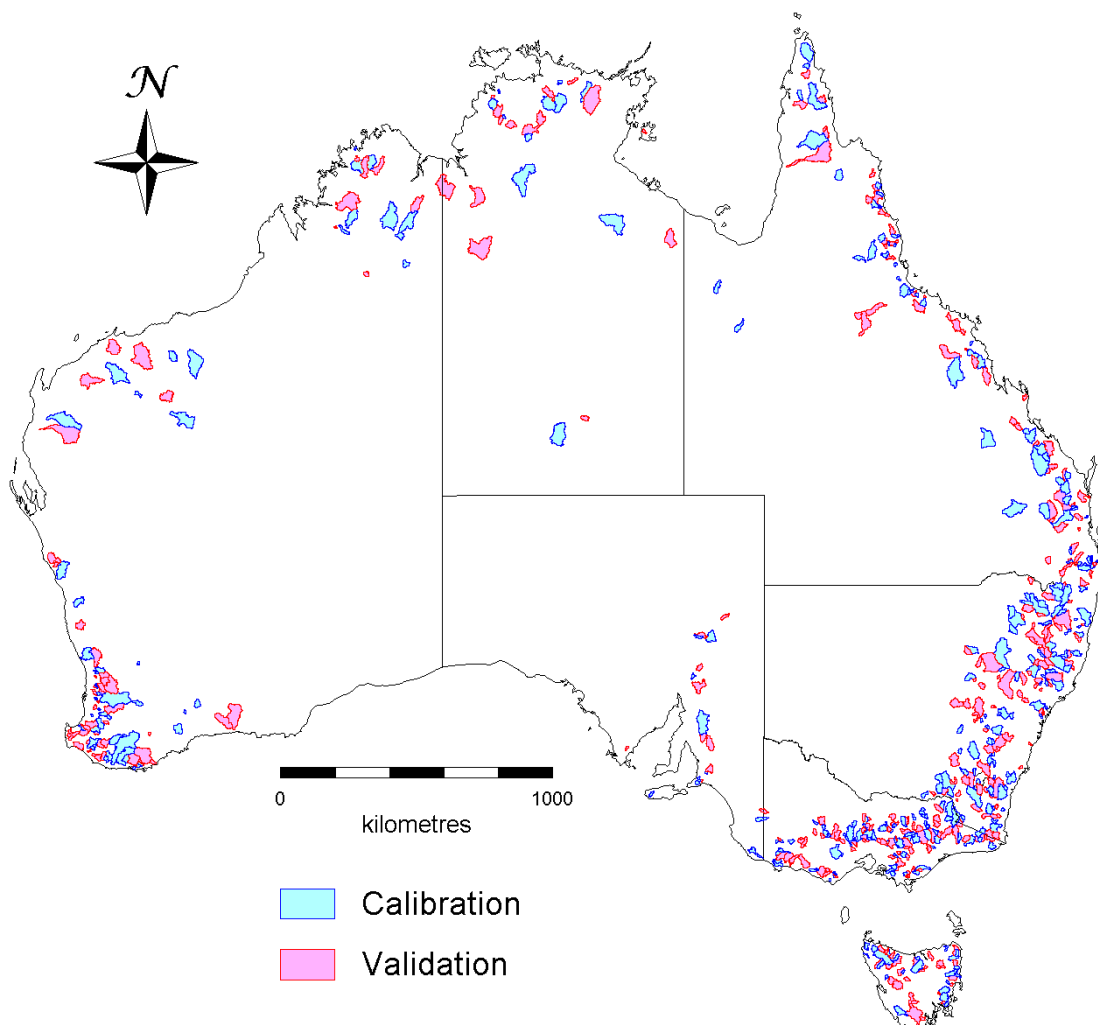


Figure 19. Distribution of calibration and validation catchments.

AWRA-L v4.5 is currently calibrated on a continental domain against streamflow observations from a large number of catchments from around Australia. This yields a single set of model parameters that apply everywhere. Zhang et al. (2013) produced a list of 605 catchments across Australia with streamflow data suitable for calibrating hydrological models. All 605 catchments are non-nested and have catchment areas greater than 50 km². All have unregulated flows and at least 10 years of observed daily streamflow data since 1975. Zhang et al. (2013) divided these catchments into a calibration set of 301 catchments and a validation set of 304 catchments. Continental calibration of AWRA-L is currently done against streamflow data from the calibration data set. Other remotely sensed responses are not currently used in calibration. The locations of the calibration and validation catchments are shown in Figure 19.

The quality of model predictions in each catchment is assessed by using a metric developed by Viney et al. (2009), which combines the Nash-Sutcliffe efficiency of daily and monthly streamflows with a prediction bias term (model error divided by the sum of observed flows). The resulting metric for each catchment is given by

$$F = \frac{(E_d + E_m)}{2} - 5\text{abs}(\ln(1 + B))^{2.5} \quad (83)$$

where E_d and E_m are the daily and monthly Nash-Sutcliffe efficiencies, respectively and B is the bias. The F values range between $-\infty$ and 1. The higher the F value, the better the prediction.

The objective function that is used to assess overall model prediction quality against all calibration catchments involves the mean of a number of percentiles of the 301 F values. Currently, the objective function is given by

$$OF = (F_{25} + F_{50} + F_{75} + F_{100})/4 \quad (84)$$

where F_i represents the i th percentile of the F values. This selection of percentiles makes the objective function robust to the presence of catchments with poor quality observed streamflow. The automatic optimiser seeks to maximise the value of OF .

4.2 Parameters available for calibration

AWRA-L v4.5 contains 49 notionally optimisable parameters. However, not all these parameters are typically calibrated. Sensitivity studies have shown that streamflow and other hydrological and vegetation responses are relatively insensitive to some model parameters. The values of these parameters can therefore be fixed to reasonable prescribed values. The time and computing resources required for calibration are substantially reduced when fewer parameters are calibrated.

In AWRA-L v4.5, 21 of the optimisable parameters are typically calibrated, while the remaining 28 are fixed. Table 2 lists the parameters that are currently used in calibration and Table 3 lists the parameters that are currently fixed and not used in calibration.

Table 2. List of parameters that are currently used for calibration. Parameters that apply only to the deep-rooted HRU are labelled with the suffix *_hruDR*. Parameters that apply only to the shallow-rooted HRU are labelled with the suffix *_hruSR*. The allowable range of parameter values is given by Min and Max.

Parameter	Definition	Status	Unit	Min	Max
c_G _hruDR	Conversion coefficient from vegetation photosynthetic capacity index to maximum stomatal conductance	Free	-	0.02	0.05
c_G _hruSR	Conversion coefficient from vegetation photosynthetic capacity index to maximum stomatal conductance	Free	-	0.02	0.05
f_{ER} _hruDR	Ratio of average evaporation rate over average rainfall intensity during storms per unit canopy cover	Free	-	0.04	0.25
F_{smax} _hruDR	Soil evaporation scaling factor when soil water supply is not limiting evaporation	Free	-	0.2	1
F_{smax} _hruSR	Soil evaporation scaling factor when soil water supply is not limiting evaporation	Free	-	0.2	1
s_l _hruDR	Specific canopy rainfall storage capacity per unit leaf area	Free	mm	0.03	0.8
s_l _hruSR	Specific canopy rainfall storage capacity per unit leaf area	Free	mm	0.03	0.8
U_{d0} _hruDR	Maximum root water uptake rates from deep soil store	Free	mm/d	0.001	10
K_{gscale}	Multiplier on the raster input of K_g	Free	-	0.01	10
$P_{refscale}$	Multiplier on the raster input of P_{ref}	Free	-	0.1	3
K_{rint}	Intercept coefficient for calculating K_r	Free	-	0.05	3
K_{rscale}	Scale coefficient for calculating K_r	Free	-	0.05	3
k_β	Coefficient on the mapped slope for the calculation of interflow	Free	-	0.01	1
k_ζ	Coefficient on the ratio of K_{sat} across soil horizons for the calculation of interflow	Free	-	0.01	1
$S_{0maxscale}$	Scale for maximum water storage in the surface layer	Free	-	0.5	3
$S_{smaxscale}$	Scale for maximum water storage in the shallow layer	Free	-	0.5	3
$S_{dmaxscale}$	Scale for maximum water storage in the deep layer	Free	-	0.5	1
$K_{0satscale}$	Scale for saturated hydraulic conductivity in the surface layer	Free	-	0.1	10
$K_{ssatscale}$	Scale for saturated hydraulic conductivity in the shallow layer	Free	-	0.1	10
$K_{dsatscale}$	Scale for saturated hydraulic conductivity in the deep layer	Free	-	0.1	1
n_{scale}	Scale for effective porosity	Free	-	0.01	1

Table 3. List of parameters that are currently fixed and not used in calibration. Parameters that apply only to the deep-rooted HRU are labelled with the suffix `_hruDR`. Parameters that apply only to the shallow-rooted HRU are labelled with the suffix `_hruSR`. The allowable range of parameter values (were these parameters to be calibrated) is given by Min and Max.

Parameter	Definition	Status	Unit	Min	Max
α_d_hruDR	Dry soil albedo	Fixed	-	0.1	0.5
α_d_hruSR	Dry soil albedo	Fixed	-	0.1	0.5
α_w_hruDR	Wet soil albedo	Fixed	-	0.1	0.5
α_w_hruSR	Wet soil albedo	Fixed	-	0.1	0.5
h_v_hruSR	Height of vegetation canopy	Fixed	m	0.1	50
Λ_{ref}_hruDR	Reference leaf area index (at which $f_v = 0.63$)	Fixed	-	1.3	2.5
Λ_{ref}_hruSR	Reference leaf area index (at which $f_v = 0.63$)	Fixed	-	1.3	2.5
C_s_hruDR	Specific leaf area	Fixed	m ² /kg	0.7	70
C_s_hruSR	Specific leaf area	Fixed	m ² /kg	0.7	70
t_g_hruDR	Characteristic time scale for vegetation growth towards equilibrium	Fixed	d	20	1000
t_g_hruSR	Characteristic time scale for vegetation growth towards equilibrium	Fixed	d	20	1000
t_s_hruDR	Characteristic time scale for vegetation senescence towards equilibrium	Fixed	d	10	200
t_s_hruSR	Characteristic time scale for vegetation senescence towards equilibrium	Fixed	d	10	200
U_{s0}_hruDR	Maximum root water uptake rates from shallow soil store	Fixed	mm/d	1	7
U_{s0}_hruSR	Maximum root water uptake rates from shallow soil store	Fixed	mm/d	1	7
U_{d0}_hruSR	Maximum root water uptake rates from deep soil store	Fixed	mm/d	0	0
V_c_hruDR	Vegetation photosynthetic capacity index per unit canopy cover	Fixed	-	0.05	1
V_c_hruSR	Vegetation photosynthetic capacity index per unit canopy cover	Fixed	-	0.05	1
w_{olim}_hruDR	Relative top soil water content at which evaporation is reduced	Fixed	-	0.6	0.9
w_{olim}_hruSR	Relative top soil water content at which evaporation is reduced	Fixed	-	0.6	0.9
w_{0ref}_hruDR	Reference value of w_0 determining the rate of albedo decrease with wetness	Fixed	-	0.2	0.5
w_{0ref}_hruSR	Reference value of w_0 determining the rate of albedo decrease with wetness	Fixed	-	0.2	0.5
w_{slim}_hruDR	Water-limiting relative water content in shallow soil store	Fixed	-	0.15	0.5
w_{slim}_hruSR	Water-limiting relative water content in shallow soil store	Fixed	-	0.15	0.5
w_{dlim}_hruDR	Water-limiting relative water content in deep soil store	Fixed	-	0.15	0.5
w_{dlim}_hruSR	Water-limiting relative water content in deep soil store	Fixed	-	0.15	0.5
D_R_hruDR	Rooting depth	Fixed	m	3	20
D_R_hruSR	Rooting depth	Fixed	m	0.5	2

References

- Bachmair, S. and Weiler, M., 2011. New dimensions in hillslope hydrology. In D.F. Levia et al. (Eds.), *Forest hydrology and biogeochemistry: Synthesis of past research and future directions*. Springer Science+Business Media B.V.
- Bartalis, Z., Wagner, W., Naeimi, V., Hasenauer, S., Scipal, K., Bonekamp, H., Figa, J. and Anderson, C., 2007. Initial soil moisture retrievals from the METOP-A Advanced Scatterometer (ASCAT). *Geophysical Research Letters*, 34(20): L20401.
- Coram, J.E., Dyson, P.R., Houlder, P.A. and Evans, W.R., 2000. Australian groundwater flow systems contributing to dryland salinity. Project Report for the National Land and Water Resources Audit., Bureau of Rural Sciences, Canberra.
- Crosbie, R.S., Peeters, L., Doble, R.C., Joehnk, K., Carrara, E., Daamen, C. and Frost, A., 2011. AWRA-G: A groundwater component for a continental scale land surface model 19th International Congress on Modelling and Simulation, Perth, Australia.
- Dawes, W.R., Gilfedder, M., Walker, G.R. and Evans, W.R., 2004. Biophysical modelling of catchment-scale surface water and groundwater response to land-use change. *Mathematics and Computers in Simulation*, 64: 3–12.
- Donohue, R.J., Roderick, M.L. and McVicar, T.R., 2008. Deriving consistent long-term vegetation information from AVHRR reflectance data using a cover-triangle-based framework. *Remote Sensing of Environment*, 112: 2938–2949.
- Frost, A.J. and Zhao, F., 2015. Benchmarking of AWRA-L model against observed hydrological data and peer models (WaterDyn and CABLE), Bureau of Meteorology.
- Gash, J.H.C., 1979. An analytical model of rainfall interception by forests. *Quarterly Journal of the Royal Meteorological Society*, 105: 43–55.
- Haverd, V., Raupach, M.R., Briggs, P.R., Canadell, J.G., Isaac, P., Pickett-Heaps, C., Roxburgh, S.H., van Gorsel, E., Viscarra Rossel, R.A. and Wang, Z., 2013. Multiple observation types reduce uncertainty in Australia's terrestrial carbon and water cycles. *Biogeosciences*, 10: 2011–2040.
- Joehnk, K.D., Crosbie, R., Peeters, L. and Doble, R., 2012. AWRA-G: groundwater component of AWRA, CSIRO: Water for a Healthy Country.
- Johnston, R.M., Barry, S.J., Bleys, E., Bui, E.N., Moran, C.J., Simon, D.A.P., Carlile, P., McKenzie, N.J., Henderson, B.L., Chapman, G., Imhoff, M., Maschmedt, D., Howe, D., Grose, C., Schoknecht, N., Powell, B. and Grundy, M., 2003. ASRIS: the database. *Australian Journal of Soil Research*, 41: 1021–1036.
- Jones, D.A., Wang, W. and Fawcett, R., 2009. High-quality spatial climate data-sets for Australia. *Australian Meteorological and Oceanographic Journal*, 58: 233–248.
- King, E.A., Van Niel, T.G., van Dijk, A.I.J.M., Wang, Z., Paget, M.J., Raupach, T., Bastianssen, W.G.M., Guerschman, J., Haverd, V., McVicar, T.R., Miltenburg, I., Raupach, M.R., Renzullo, L.J. and Zhang, Y., 2011. Actual evapotranspiration estimates for Australia: inter-comparison and evaluation, CSIRO: Water for a Healthy Country National Research Flagship.
- Knight, J.H., Gilfedder, M. and Walker, G.R., 2005. Impacts of irrigation and dryland development on groundwater discharge to rivers – a unit response approach to cumulative impacts analysis. *Journal of Hydrology*, 303: 79–91.

- McVicar, T.R., Van Niel, T.G., Li, L.T., Roderick, M.L., Rayner, D.P., Ricciardulli, L. and Donohue, R.J., 2008. Wind speed climatology and trends for Australia, 1975-2006: Capturing the stilling phenomenon and comparison with near-surface reanalysis output. *Geophysical Research Letters*, 35(L20403).
- Peeters, L.J.M., Crosbie, R.S., Doble, R.C. and Van Dijk, A.I.J.M., 2013. Conceptual evaluation of continental land-surface model behaviour. *Environmental Modelling and Software*, 43: 49–59.
- Penman, H.L., 1948. Natural evaporation from open water, bare soil and grass. *Proceedings of the Royal Society of London*, A193: 120–146.
- Raupach, M.R., Briggs, P.R., Haverd, V., King, E.A., Paget, M. and Trudinger, C.M., 2009. Australian Water Availability Project (AWAP) – CSIRO Marine and Atmospheric Research Component: Final Report for Phase 3, CSIRO Marine and Atmospheric Research, Canberra, Australia.
- Renzullo, L., Collins, D., Perraud, J., Henderson, B., Jin, H. and Smith, A., 2013. Improving soil water representation in the Australian Water Resources Assessment landscape model through assimilation of remotely-sensed soil moisture products. *Proceedings of the 20th International Congress on Modelling and Simulation*, Adelaide, Australia.
- Renzullo, L.J., van Dijk, A.I.J.M., Perraud, J.M., Collins, D., Henderson, B., Jin, H., Smith, A.B. and McJannet, D.L., 2014. Continental satellite soil moisture data assimilation improves root-zone moisture analysis for water resources assessment. *Journal of Hydrology*, 519: 2747–2762.
- Rüdiger, C., Hancock, G., Hemakumara, H.M., Jacobs, B., Kalma, J.D., Martinez, C., Thyer, M., Walker, J.P., Wells, T. and Willgoose, G.R., 2007. Goulburn River experimental catchment data set. *Water Resources Research*, 43(10): W10403.
- Rüdiger, C., Western, A.W., Walker, J.P., Smith, A.B., Kalma, J.D. and Willgoose, G.R., 2010. Towards a general equation for frequency domain reflectometers. *Journal of Hydrology*, 383(3–4): 319–329.
- Simard, M., Pinto, N., Fisher, J.B. and Baccini, A., 2011. Mapping forest canopy height globally with spaceborne lidar. *Journal of Geophysical Research: Biogeosciences*, 116(G4): G04021.
- Smith, A.B., Walker, J.P., Western, A.W., Young, R.I., Ellett, K.M., Pipunic, R.C., Grayson, R.B., Siriwardena, L., Chiew, F.H.S. and Richter, H., 2012. The Murrumbidgee soil moisture monitoring network data set. *Water Resources Research*, 48(7): W07701.
- Van Dijk, A.I.J.M., 2010. The Australian Water Resources Assessment System. Technical Report 3. Landscape Model (version 0.5) Technical Description. CSIRO: Water for a Healthy Country National Research Flagship.
- Van Dijk, A. and Bruijnzeel, L.A., 2001. Modelling rainfall interception by vegetation of variable density using an adapted analytical model. Part 1. Model description. *Journal of Hydrology*, 247: 230–238.
- Vaze, J., Viney, N., Stenson, M., Renzullo, L., Van Dijk, A., Dutta, D., Crosbie, R., Lerat, J., Penton, D., Vleeshouwer, J., Peeters, L., Teng, J., Kim, S., Hughes, J., Dawes, W., Zhang, Y., Leighton, B., Perraud, J.M., Joehnk, K., Yang, A., Wang, B., Frost, A., Elmahdi, A., Smith, A., Daamen, C., 2013. The Australian Water Resource Assessment System (AWRA). *Proceedings of the 20th International Congress on Modelling and Simulation*, Adelaide, Australia.
- Viney, N.R., Perraud J. , Vaze, J. and Chiew, F.H.S., 2009. The usefulness of bias constraints in model calibration for regionalisation to ungauged catchments. *Proceedings of the 18th International Congress on Modelling and Simulation*, Cairns, Australia.
- Viney, N.R., Van Dijk, A.I.J.M. and Vaze, J., 2011. Comparison of models and methods for estimating spatial patterns of streamflow across Australia, WIRADA Science Symposium. CSIRO, Melbourne, Australia, p. 30–35.
- Viney, N.R., Vaze, J., Wang, B., Zhang, Y., Yang, A., Vleeshouwer, J., Ramchurn, A. and Frost, A., 2013. Comparison of prediction performance of AWRA-L with other models. CSIRO: Water for a Healthy Country National Research Flagship, 30pp.

- Viney, N.R., Vaze, J., Wang, B., Zhang, Y., Yang, A., Vleeshouwer, J., Ramchurn, A. and Frost, A., 2014. Intercomparison of methods for regionalising rainfall-runoff model predictions over large domains, Hydrology and Water Resources Symposium 2014. Engineers Australia, Perth, p. 970–977.
- Walker, G.R., Gilfedder, M. and Dawes, W.R., 2005. Idealised analogue for predicting groundwater response times from sloping aquifers. Technical Report 14/05, CSIRO Land and Water.
- Zhang, Y. and Viney, N., 2012. Toward optimum multiple objective model calibrations for AWRA-L model. CSIRO: Water for a Healthy Country National Research Flagship.
- Zhang, Y., Viney, N., Frost, A., Oke, A., Brooks, M., Chen, Y. and Campbell, N., 2013. Collation of Australian modeller's streamflow dataset for 780 unregulated Australian catchments. CSIRO: Water for a Healthy Country National Research Flagship, 115pp.

Appendix

A.1 Model variables

Table 4 shows the mapping between the variable names used in this document and those used in the current version of the model code.

Table 4. List of variable names used in this document and the corresponding variables used in the model code. Units are those given in this document.

This document	Model code	Description
α	alb	Surface albedo (dimensionless)
α_d	alb_dry	Dry soil albedo (dimensionless)
α_s	alb_soil	Albedo of soil surface (dimensionless)
α_v	alb_veg	Albedo of vegetated surfaces (dimensionless)
α_w	alb_wet	Wet soil albedo (dimensionless)
β	slope	Slope of the land surface (percent)
γ	gamma	Psychrometric constant (Pa K ⁻¹)
Δ	delta	Slope of the saturation vapour pressure curve (Pa K ⁻¹)
δ	DELTA	Solar declination (radians)
ζ	—	Shape factor that depends on whether cells are direct or diagonal neighbours (dimensionless)
Λ	LAI	Leaf area index (LAI) (dimensionless)
Λ_{max}	LAImax	Maximum achievable LAI value (dimensionless)
Λ_{ref}	LAIref	Reference LAI value corresponding to $f_v = 0.63$ (dimensionless)
λ	lambda	Latent heat of vaporisation (MJ kg ⁻¹)
λ_d	Dd	Surface water drainage density (m ⁻¹)
ρ_0	Rh_0s	Partitioning factor for vertical and lateral drainage from the surface soil layer (dimensionless)
ρ_s	Rh_sd	Partitioning factor for vertical and lateral drainage from the shallow soil layer (dimensionless)
σ	StefBolz	Stefan-Boltzmann constant (MJ m ⁻² d ⁻¹ K ⁻⁴)
φ	latitude	Latitude (radians), and is negative in the southern hemisphere
ω	PI	Sunset hour angle (radians)
C_S	SLA	Specific leaf area (m ² kg ⁻¹)
c_G	cGsmax	Coefficient relating vegetation photosynthetic capacity to maximum stomatal conductance (m s ⁻¹)
D_0	D0	Vertical drainage from the bottom of the surface soil layer (mm)
D_d	Dd	Vertical drainage from the bottom of the deep soil layer (mm)
D_R	RD	Rooting depth (m)

D_s	Ds	Vertical drainage from the bottom of the shallow soil layer (mm)
d	DayOfYear	Day of the year (d)
d_0	—	Depth of the surface soil layer (mm)
d_d	—	Depth of the deep soil layer (mm)
d_s	—	Depth of the shallow soil layer (mm)
d_u	—	Depth of the unconfined aquifer (m)
E^*	E0	Potential evaporation (mm d ⁻¹)
$\overline{E^*}$	meanPET	Long term mean daily potential evaporation (mm d ⁻¹)
E_0	Es	Evaporation flux from the surface soil store (mm d ⁻¹)
E_g	Eg	Evaporation flux from the groundwater store (mm d ⁻¹)
E_i	Ei	Evaporation flux from canopy interception (mm d ⁻¹)
E_t	Et	Actual total transpiration flux (mm d ⁻¹)
E_t^*	Etmax	Potential transpiration rate (mm d ⁻¹)
E_{tot}	Etot	Total evapotranspiration (mm d ⁻¹)
F_{ER}	ER_frac_ref	Ratio of the mean evaporation rate and the mean rainfall intensity during storms (dimensionless)
F_{smax}	FsoilEmax	Soil evaporation scaling factor corresponding to unlimited soil water supply (dimensionless)
f_{Eg}	fEgt	Fraction of the grid cell that is accessible for transpiration from groundwater (dimensionless)
f_s	fsat	Fraction of the grid cell that is saturated at the surface (dimensionless)
f_{tree}	f_tree	Fraction of tree cover within each grid cell (dimensionless)
f_v	fveg	Fractional canopy cover (dimensionless)
f_{veq}	fveq	Equilibrium canopy cover (dimensionless)
$FPAR$	—	Photosynthetically-active radiation (dimensionless)
g_a	ga	Aerodynamic conductance (m s ⁻¹)
g_s	gs	Canopy conductance (m s ⁻¹)
H	—	Head in a grid cell (m)
H_b	—	Drainage base – the lowest topographic point within the grid cell (m)
ΔH_{ij}	—	Difference in head between cells i and j (m)
h	—	Elevation of a point on the hypsometric curve (m)
h_u	—	Elevation change along the flow path (m)
h_v	hveg	Vegetation height (m)
I	I	Infiltration (mm)
K_{0sat}	K0sat	Saturated hydraulic conductivity of surface soil layer (mm d ⁻¹)
$K_{0sat_{scale}}$	K0sat_scale	Scaling factor for hydraulic conductivity of surface soil layer (dimensionless)
$K_{0sat_{ASRIS}}$	K0sat_grid	Saturated hydraulic conductivity of surface soil layer provided by ASRIS (mm d ⁻¹)
K_d	Rgeff	Daily downwelling shortwave (solar) radiation (MJ m ⁻² d ⁻¹)
K_{d0}	RadClearSky	Expected downwelling shortwave radiation on a cloudless day (MJ m ⁻² d ⁻¹)
K_{dsat}	Kdsat	Saturated hydraulic conductivity of deep soil layer (mm d ⁻¹)

$K_{dsatASRIS}$	Kdsat_grid	Saturated hydraulic conductivity of deep soil layer provided by ASRIS (mm d^{-1})
$K_{dsatscale}$	Kdsat_scale	Scaling factor for hydraulic conductivity of deep soil layer (dimensionless)
K_{gmap}	K_gw_grid	Groundwater drainage coefficient obtained from continental mapping (d^{-1})
K_{gscale}	K_gw_scale	Scaling factor for groundwater drainage coefficient (dimensionless)
K_g	K_gw	Groundwater drainage coefficient (d^{-1})
K_r	K_rout	Rate coefficient controlling discharge to stream (dimensionless)
K_{rint}	Krout_int	Intercept coefficient for calculating K_r (dimensionless)
K_{rscale}	K_rout_scale	Scale coefficient for calculating K_r (d mm^{-1})
K_{ssat}	Kssat	Saturated hydraulic conductivity of shallow soil layer (mm d^{-1})
$K_{ssatASRIS}$	Kssat_grid	Saturated hydraulic conductivity of shallow soil layer provided by ASRIS (mm d^{-1})
$K_{ssatscale}$	Kssat_scale	Scaling factor for hydraulic conductivity of shallow soil layer (dimensionless)
K_u	—	Daily upwelling shortwave radiation ($\text{MJ m}^{-2} \text{d}^{-1}$)
k_β	slope_coeff	Scaling factor for slope (dimensionless)
k_u	—	Hydraulic conductivity of the unconfined aquifer (m d^{-1})
k_ζ	Kr_coeff	Scaling factor for ratio of saturated hydraulic conductivity (dimensionless)
L_d	RLin	Daily downwelling longwave radiation ($\text{MJ m}^{-2} \text{d}^{-1}$)
L_u	RLout	Daily upwelling longwave radiation ($\text{MJ m}^{-2} \text{d}^{-1}$)
l_{ia}	IAL	Interaquifer leakage (mm)
M	Mleaf	Leaf biomass (kg m^{-2})
M_{eq}	—	Equilibrium leaf biomass (kg m^{-2})
M_n	Mleafnet	Change in leaf biomass at each time step ($\text{kg m}^{-2} \text{d}^{-1}$)
n	ne	Effective porosity (dimensionless)
n_{map}	—	Effective porosity obtained from continental mapping (dimensionless)
n_{scale}	ne_scale	Scaling factor for effective porosity (dimensionless)
P_w	Pwet	Reference threshold precipitation amount (mm)
P	Pg	Precipitation (mm)
P_n	Pn	Net precipitation – precipitation minus interception (mm)
P_{ref}	PrefR	Reference value for precipitation (mm)
$P_{refscale}$	Pref_gridscale	Scaling factor for reference precipitation (dimensionless)
p_a	pair	Air pressure (Pa)
p_e	pe	Actual vapour pressure (Pa)
p_{es}	pes	Saturation vapour pressure (Pa)
Q_0	Q0	Function of the day of the year (radians)
Q_g	Qg	Groundwater discharge to the surface water (mm)
Q_h	Rhof	Infiltration-excess runoff component (mm)
Q_l	QIF	Interflow (mm)
Q_{l0}	IF0	Interflow draining laterally from the surface soil layer (mm)
Q_{ls}	IFs	Interflow draining laterally from the shallow soil layer (mm)
Q_l	—	Lateral groundwater flow to cell (mm)

Q_R	QR	Surface runoff (mm)
Q_s	Rsof	Saturation-excess runoff component (mm)
Q_t	Qtot	Total discharge to stream (mm)
R_n	Rneff	Daily net radiation ($\text{MJ m}^{-2} \text{d}^{-1}$)
r	DistanceFactor	Relative distance from earth to sun (dimensionless)
S_0	S0	Water storage in the surface soil layer (mm)
S_{0AWC}	S0fracAWC_grid	Available water holding capacity in the surface soil (dimensionless)
S_{0max}	S0max	Maximum storage of the surface soil layer (mm)
$S_{0maxscale}$	S0max_scale	Scaling parameter for maximum storage of the surface soil layer (dimensionless)
S_c	S	Storativity of the confined aquifer (mm)
S_d	Sd	Water content of the deep soil store (mm)
S_{dmax}	Sdmax	Maximum storage of the deep soil layer (mm)
$S_{dmaxscale}$	Sdmax_scale	Scaling parameter for maximum storage of the deep soil layer (dimensionless)
ΔS_{eq}	deltaSeq	Change in storage between confined and unconfined aquifers (mm)
S_g	Sg	Groundwater storage in the unconfined aquifer (mm)
S_{gc}	Sgc	Groundwater storage in the confined aquifer (mm)
S_r	Sr	Volume of water in the surface water store (mm)
S_s	Ss	Water content of the shallow soil store (mm)
S_{sAWC}	SsfracAWC_grid	Available water holding capacity in the shallow soil (dimensionless)
S_{smax}	Ssmax	Maximum storage of the shallow soil layer (mm)
$S_{smaxscale}$	Ssmax_scale	Scaling parameter for maximum storage of the shallow soil layer (dimensionless)
S_l	S_sls	Specific canopy rainfall storage per unit leaf area (mm)
T_a	Ta	Daily mean temperature ($^{\circ}\text{C}$)
T_{ij}	—	Harmonic mean of the transmissivity between from cell j to cell i ($\text{m}^2 \text{d}^{-1}$)
T_{max}	Tmax	Maximum air temperature ($^{\circ}\text{C}$)
T_{min}	Tmin	Minimum air temperature ($^{\circ}\text{C}$)
t	—	Time step (d)
Δt	—	Length of the time step (d)
t_{eq}	Teq	Time to equilibrium (d)
t_g	Tgrow	Characteristic time scale for vegetation growth towards equilibrium (d)
t_s	Tsenc	Characteristic time scale for vegetation senescence towards equilibrium (d)
U^*	U0	Maximum root water uptake (mm d^{-1})
U_d	Ud	Root water uptake (transpiration) from the deep soil store (mm d^{-1})
U_{d0}	Ud0	Maximum possible root water uptake from the deep soil store (mm d^{-1})
U_{dmax}	Udmax	Maximum root water uptake from the deep soil store at prevailing moisture content (mm d^{-1})
U_s	Us	Root water uptake (transpiration) from the shallow soil store (mm d^{-1})
U_{s0}	Us0	Maximum possible root water uptake from the shallow soil store (mm d^{-1})
U_{smax}	Usmax	Maximum root water uptake from the shallow soil store at prevailing moisture content (mm d^{-1})

u_2	u2	Wind speed at a height of 2 m (m s^{-1})
V_c	Vc	Greenness index per unit canopy cover
w_0	w0	Relative soil moisture content of the top soil layer (dimensionless)
w_{0lim}	w0limE	Limiting the value of w_0 at which evaporation is reduced (dimensionless)
w_{0ref}	w0ref_alb	Reference value of w_0 that determines the rate of albedo decrease with wetness (dimensionless)
w_d	wd	Relative water content of the deep soil store (dimensionless)
w_{dlim}	wdlimU	Water-limiting relative water content of the deep soil store (dimensionless)
w_s	ws	Relative water content of the shallow soil store (dimensionless)
w_{slim}	wslimU	Water-limiting relative water content of the shallow soil store (dimensionless)
Y	Y	Root water uptake (transpiration) from the groundwater store via capillary rise (mm d^{-1})

Appendix

A.2 Continental and regional calibration and comparison with peer models

This appendix assesses the ability of the most recent version of the AWRA-L model (version 4.5) to predict streamflow, soil moisture and evapotranspiration across Australia and compares its performance with those of several other models and modelling approaches.

METHODOLOGY

The models

Streamflow predictions of the AWRA-L v4.5 model are compared against those of AWRA-L v3.5 and AWRA-L v4.0 as well as four other peer models. GR4J (Perrin et al., 2003) is a simple lumped rainfall-runoff model. It has been designed with a primary focus on parsimony and has just four optimisable parameters. Sacramento (Burnash et al., 1973) is a more complex model, but remains, at its heart, a lumped rainfall-runoff model. In this study, the calibrations of Sacramento optimise 13 model parameters. WaterDyn (Raupach et al., 2009) and CABLE (Haverd et al., 2013) are both continental scale land surface models which are used here with minimal-calibration (results provided by the Bureau). CABLE has had limited calibration to long term streamflow over 50 unimpaired catchments, along with flux tower ET and gross primary production at six sites across Australia (Haverd et al., 2013). WaterDyn parameterisation is based on parameter sensitivity analysis (and comparison to streamflow) over six catchments within the Murrumbidgee (Raupach et al., 2009). The outputs for CABLE and WaterDyn are available at a monthly time step. For AWRA-L, the same 21 parameters listed in Table 2 are optimised.

In a separate assessment, AWRA-L is individually calibrated in eight climatically similar regions. This yields eight distinct sets of model parameters, as opposed to the single set of parameters obtained from the continental calibration used in all the other comparison tests.

Soil moisture predictions of AWRA-L are assessed against both point-scale terrestrial observations and satellite-based observations.

Input data

Model assessment is conducted using 589 of the 605 catchments shown in Figure 19. Of these, approximately half (295) are used for model calibration, with the remainder (294) being nominated as validation catchments.

The streamflow data used in this study was collated by the Bureau of Meteorology from the collections of the various state agencies. Other input data required by the models and supplied by the Bureau of Meteorology includes daily precipitation, solar radiation and maximum and minimum air temperatures. The non-climatic input data required by AWRA-L includes information on forest cover and soil properties as described elsewhere in this document.

Soil moisture estimates from the models were compared to point scale measurements of soil moisture from the following data sets:

- OzNet: An Australian monitoring network for soil moisture and meteorology, set up and maintained by the University of Melbourne and Monash University (Smith et al., 2012). The measurements used in this study include water content reflectometer measurements of soil moisture at various

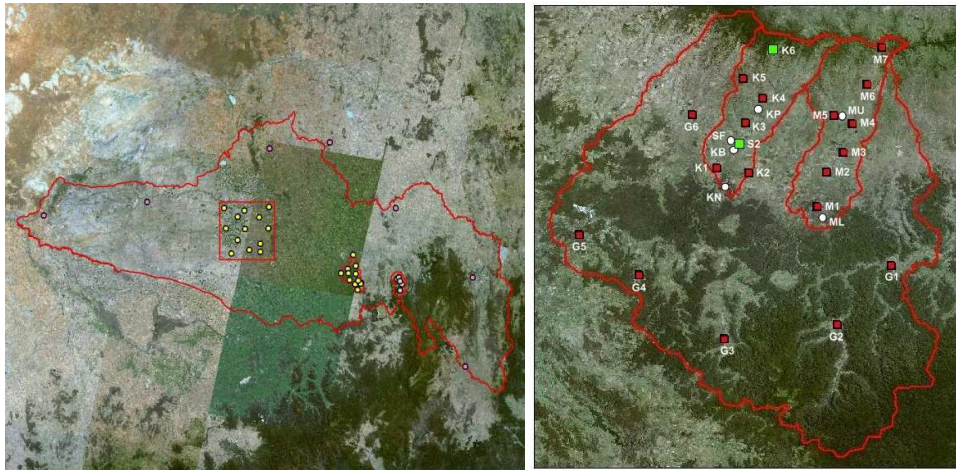


Figure 20. Soil moisture monitoring sites for (a) OzNet Murrumbidgee (from <http://www.oznet.org.au/murrumbidgeesm.html>), and (b) SASMAS Goulburn (from <http://www.eng.newcastle.edu.au/sasmas/SASMAS/sasdata.html>).

depths within the soil profile (0–5 cm, 0–30 cm, 30–60 cm, 60–90 cm) across various locations within the Murrumbidgee River basin, NSW. It is noted that these reflectometers were calibrated according to independent measurements (Rüdiger et al., 2010). The observations available in this study cover the period from September 2001 to May 2011, with varying degrees of missing data at the 38 sites (2–67% days missing) (Figure 20).

- Scaling and Assimilation of Soil Moisture and Streamflow (SASMAS) project monitoring sites (managed by the University of Newcastle): water content reflectometer measurements of soil moisture at various depths within the soil profile (0–5 cm, 0–30 cm, 30–60 cm, 60–90 cm) within the Goulburn River catchment, NSW (Rüdiger et al., 2007). The observations available in this study cover the period from September 2001 to May 2011, with varying degrees of missing data at the 24 sites (5–94% days missing) (Figure 20).

Catchment-averaged AWRA-L predictions of soil moisture are compared to satellite based estimates. The independent soil moisture observations are available as:

- Daily gridded volumetric soil moisture derived from the Advanced Microwave Scanning Radiometer for the Earth Observing System (AMSR-E) covering the period from June 2002 to September 2011 and resampled to the AWRA-L modelling grid of 0.05° resolution for Australia as described in Renzullo et al (2014).
- Derived soil moisture from active Advanced Scatterometer (ASCAT) (Bartalis et al., 2007) covering the period from July 2007 to December 2011. However, based on comparison to the point based data, ASCAT was not used for catchment evaluation.

Each of the model soil moisture estimates are weighted according to the degree of overlap with the 0–90 cm profile sampling depth. It is noted that

- AWRA-L has layers covering 0–10 cm, 10–100 cm and 100–600 cm;
- CABLE has 10 soil layers in this implementation with thicknesses from the surface of 2.2, 5.8, 7, 15, 30, 30, 30, 120, 300, and 450 cm; and
- WaterDyn has two layers of varying thickness with the top layer ranging from 0–70 cm and the lower layer from 50–190 cm in thickness, with a total thickness of no more than 220 cm.

AWRA-L predictions of ET are compared with daily gridded actual ET from CSIRO MODIS reflectance-based scaling ET (CMRSET; Guerschman et al., 2009). CMRSET uses monthly Enhanced Vegetation Index and Global Vegetation Moisture Index derived from MODIS to scale Priestley-Taylor potential evaporation derived from meteorological surfaces. The monthly values were disaggregated to daily according to PET estimates across the month over the period from 2001 to 2010. Monthly statistics are used in the evaluation here.

Calibration procedure

The calibration procedure is as described in Section 4.1, except that 295 calibration catchments are used instead of 301. All the models in this study are calibrated using a consistent methodology and against a consistent set of observational data. The calibration is done simultaneously on all 295 calibration catchments to yield a single set of model parameters that applies in all catchments. For each catchment we calculate the function F (Equation (83)). The function F can take a value between one (for a perfect fit) and minus infinity. The objective function is then taken as the mean of the 25th, 50th, 75th and 100th percentiles of the F values of the 295 calibration catchments (Equation (84)). This objective function value is maximised in calibration. AWRA-L is calibrated solely against streamflow observations. No soil moisture or ET observations are used in calibration.

Evaluation procedure

The evaluation procedure for all the models is same. Streamflow predictions are made for the 295 calibration and 294 validation catchments using the continental (or regional) parameter set. For each catchment we calculate the following metrics:

- daily Nash-Sutcliffe efficiency
- monthly Nash-Sutcliffe efficiency
- absolute bias (absolute value of total prediction error divided by total observed streamflow)
- F value.

The function F is a combination of daily and monthly efficiency and absolute bias. As such, as well as being a good choice for the objective function in calibration, it is also a convenient measure of overall prediction performance in validation.

In the following sections the values of each of these metrics on all 295 calibration catchments or on all 294 validation catchments are combined into a single exceedance curve. At each value of the metric (the y-axis), the x-axis shows the proportion of catchments with a smaller metric value. Better models are shown by higher exceedance curves for the efficiency metrics and for the F value. For bias, the better models have absolute bias curves that are closer to zero.

Soil moisture and ET predictions are compared using the Pearson's correlation coefficient, r . In the boxplots of model performance the box represents the interquartile range of r . Pearson's correlation coefficient is a good indicator for variables where the bias (and absolute value) of the variable is not as important as matching the temporal variability.

COMPARISON WITH CONVENTIONAL RAINFALL-RUNOFF MODELS

Calibration performance

This section assesses the performances of continentally calibrated versions of AWRA-L, GR4J and Sacramento. Calibration performances are shown in Figures Figure 21–Figure 24. All the three models have similar daily efficiencies for the best 40% of catchments after which the GR4J model has slightly lower efficiencies compared to AWRA-L and Sacramento (Figure 21). Both AWRA-L and Sacramento have better monthly efficiencies than GR4J with AWRA-L performing slightly better than Sacramento for most of the catchments (Figure 22). On the bias metric, AWRA-L performs slightly better than Sacramento with both AWRA-L and Sacramento performing better than GR4J (Figure 23). When the daily and monthly efficiencies are combined with bias to yield a combined F metric (Figure 24), AWRA-L performs best followed by Sacramento with GR4J showing the poorest performance. Overall, AWRA-L performs better than the two conventional rainfall-runoff models in the poorly-modelled catchments.

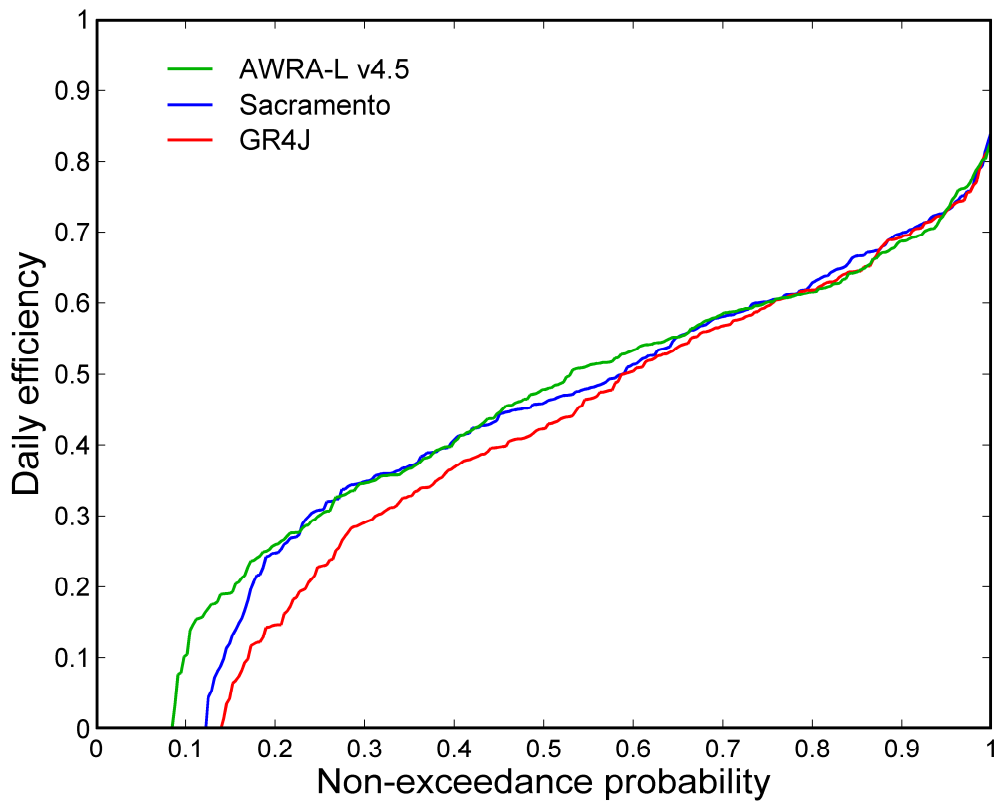


Figure 21. Cumulative distribution of daily efficiency of streamflow predictions in continental calibration mode for AWRA-L v4.5, Sacramento and GR4J.

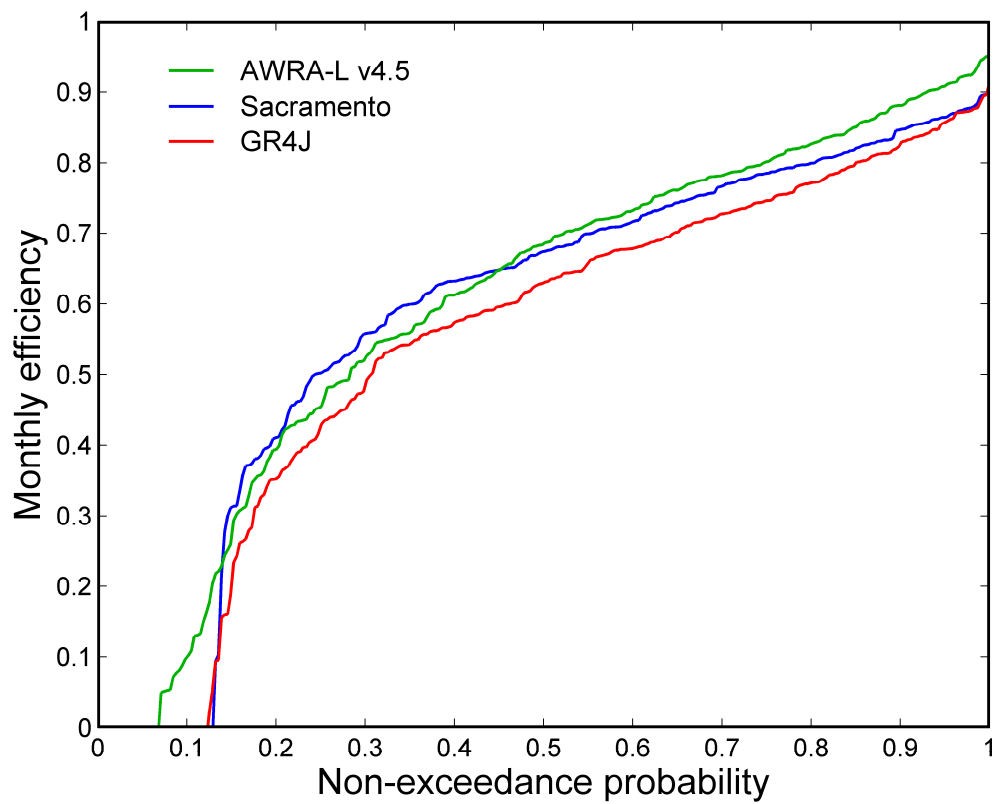


Figure 22. Cumulative distribution of monthly efficiency of streamflow predictions in continental calibration mode for AWRA-L v4.5, Sacramento and GR4J.

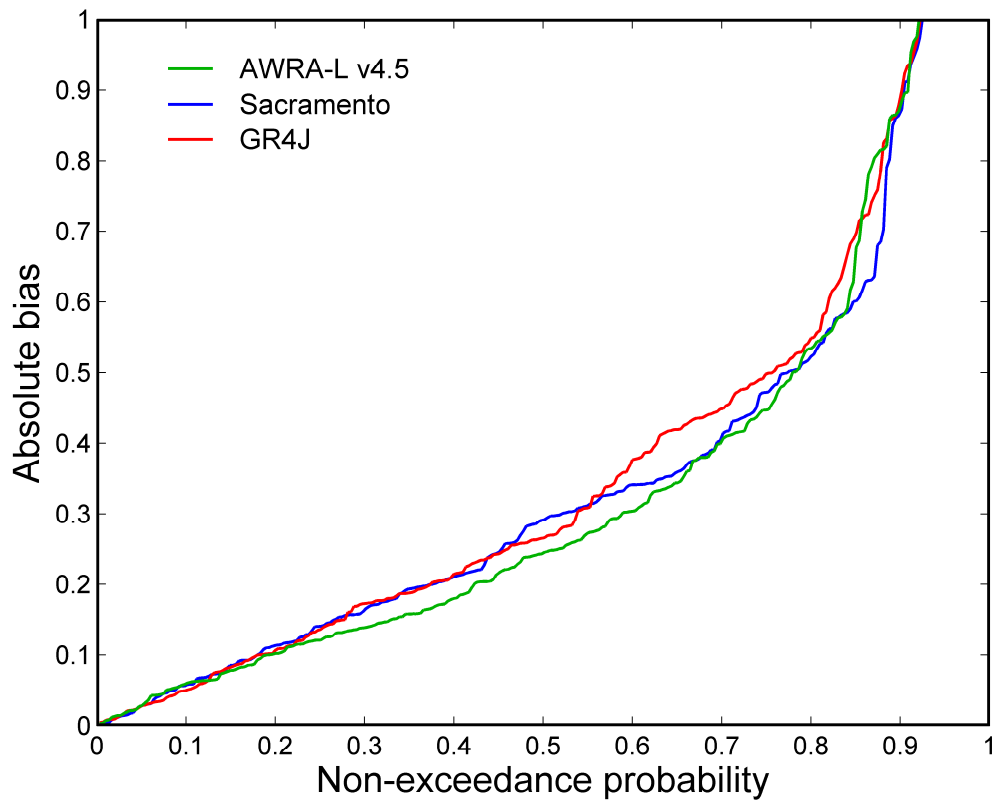


Figure 23. Cumulative distribution of absolute bias of streamflow predictions in continental calibration mode for AWRA-L v4.5, Sacramento and GR4J.

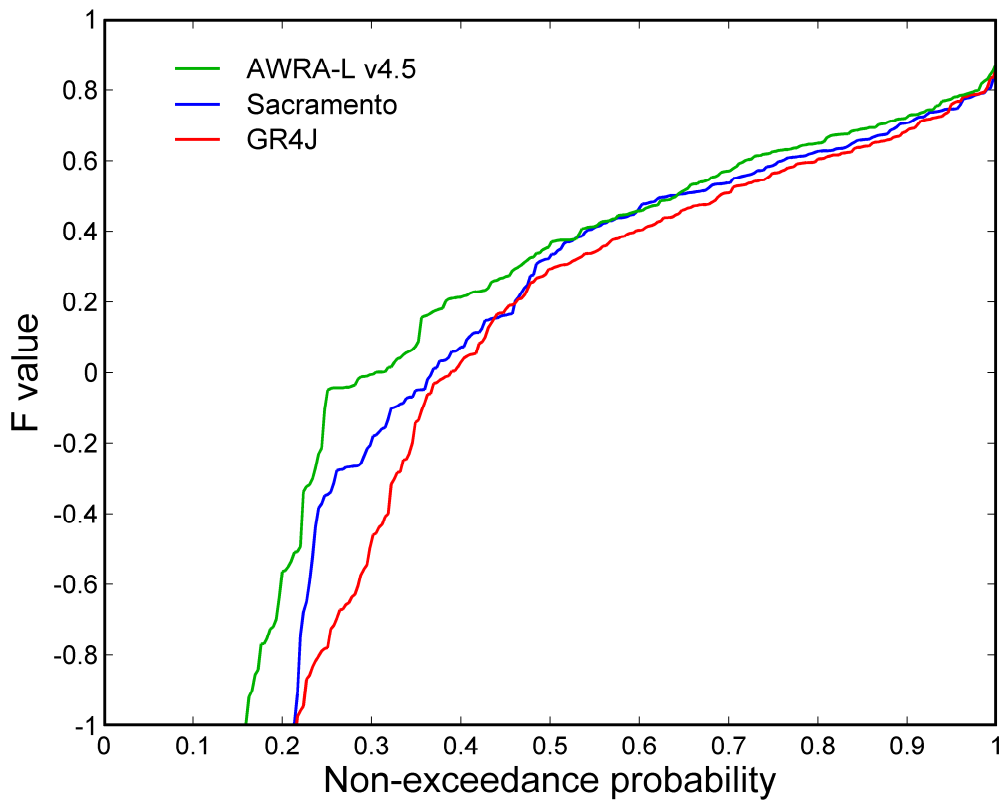


Figure 24. Cumulative distribution of F value of streamflow predictions in continental calibration mode for AWRA-L v4.5, Sacramento and GR4J.

Validation performance

When the parameter values calibrated for the continentally-calibrated models are applied in the validation catchments, there is little, if any deterioration in model performance (Figures Figure 25Figure 28, Table 5). For example, from calibration to validation, median values of daily and monthly efficiencies are approximately identical and bias and F value worsen slightly for all the three models. This is partly due to poorer performance in the poorly-modelled catchments. For example the 25th, 50th, 75th and 100th percentile *F* values for AWRA-L in calibration are -0.05 , 0.37 , 0.63 and 0.88 , respectively, and in validation are -0.45 , 0.37 , 0.64 and 0.86 , respectively.

Table 5. Median values of various performance metrics in calibration and validation.

	Calibration			Validation		
	AWRA-L v4.5	Sacramento	GR4J	AWRA-L v4.5	Sacramento	GR4J
Daily NSE	0.48	0.46	0.42	0.48	0.47	0.44
Monthly NSE	0.69	0.67	0.63	0.67	0.68	0.62
Absolute bias	0.25	0.29	0.27	0.22	0.26	0.30
F value	0.37	0.33	0.29	0.37	0.39	0.27

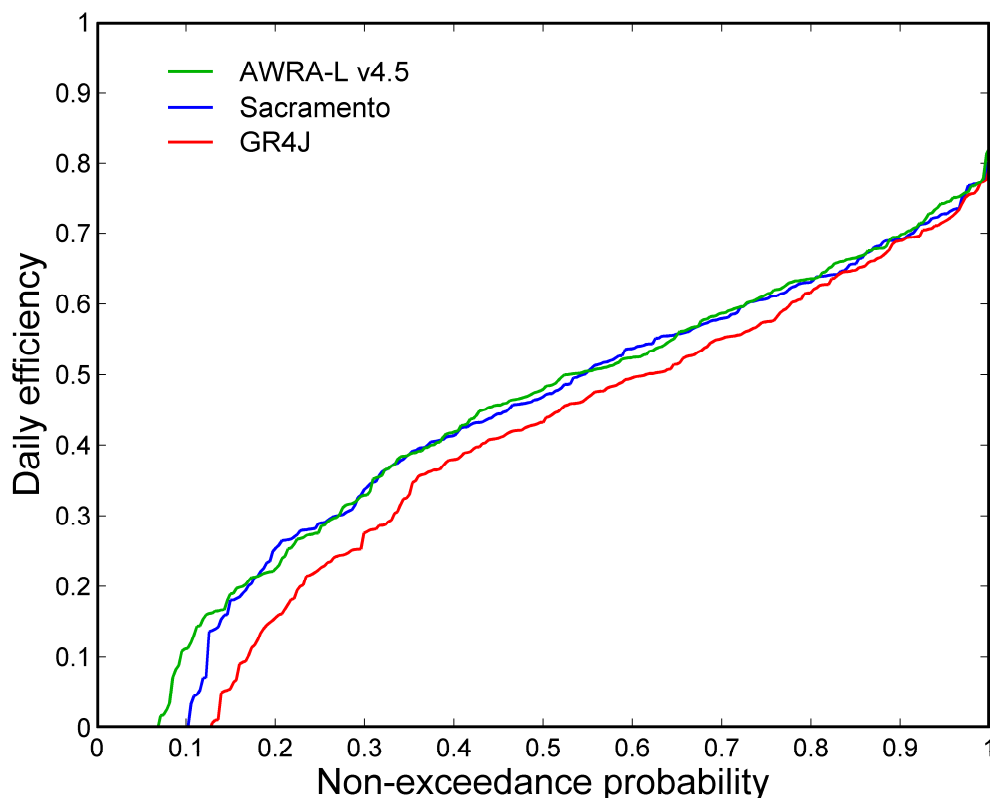


Figure 25. Cumulative distribution of daily efficiency of streamflow predictions in validation mode for AWRA-L v4.5, Sacramento and GR4J.

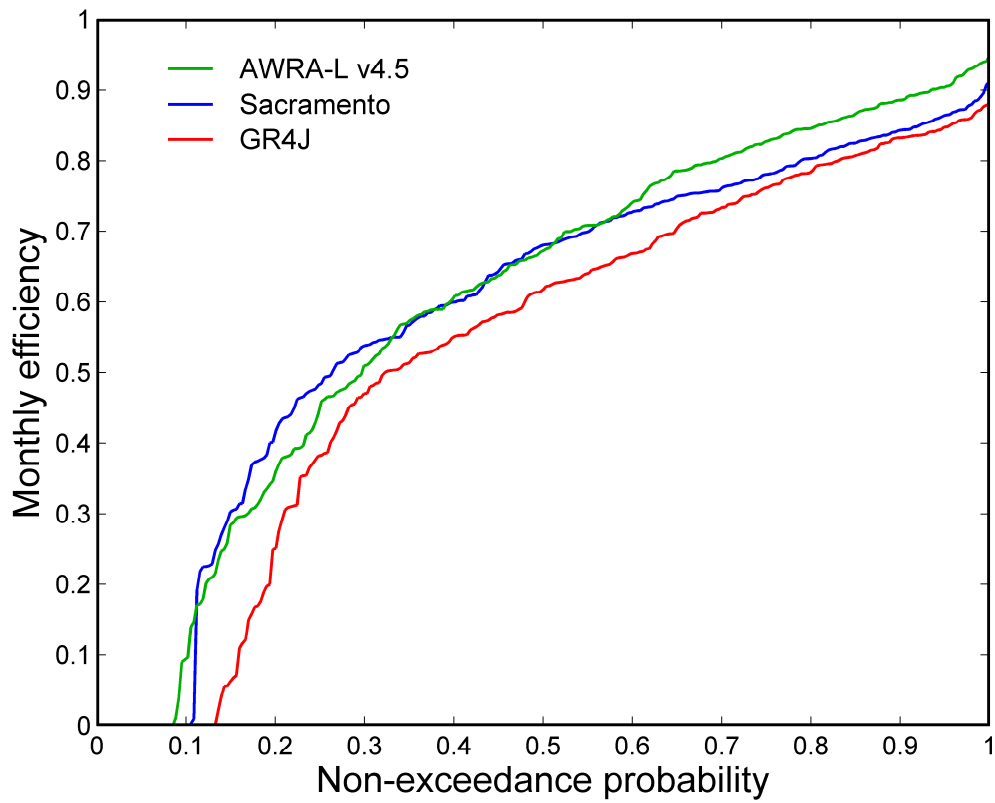


Figure 26. Cumulative distribution of monthly efficiency of streamflow predictions in validation mode for AWRA-L v4.5, Sacramento and GR4J.

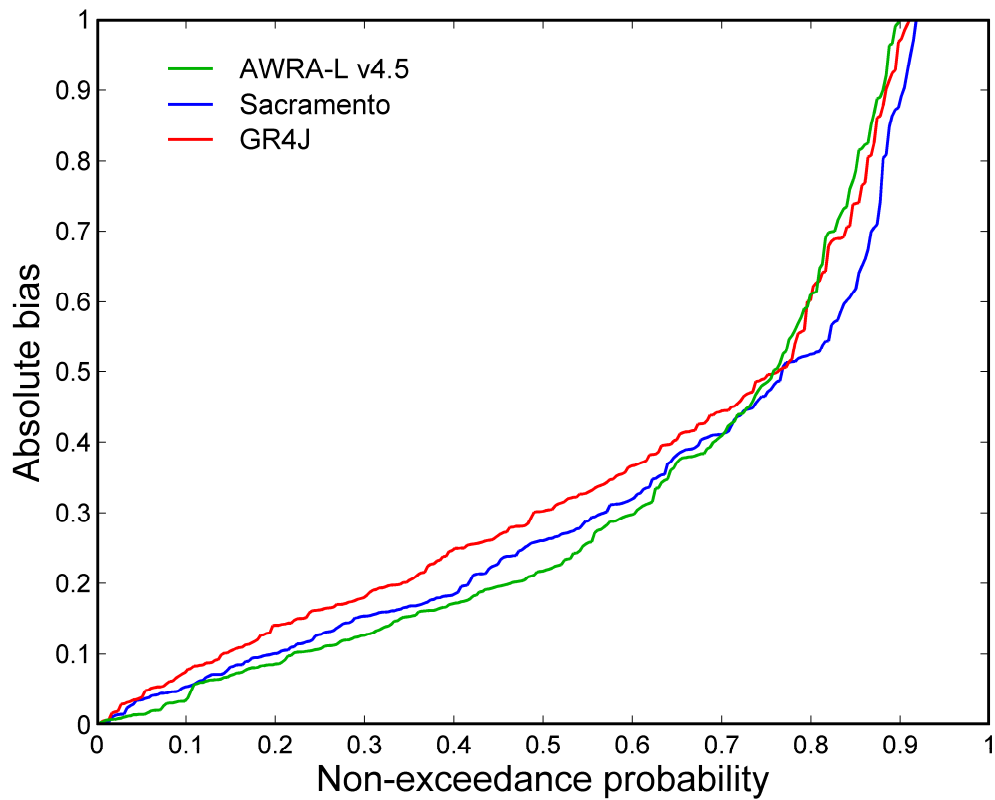


Figure 27. Cumulative distribution of absolute bias of streamflow predictions in validation mode for AWRA-L v4.5, Sacramento and GR4J.

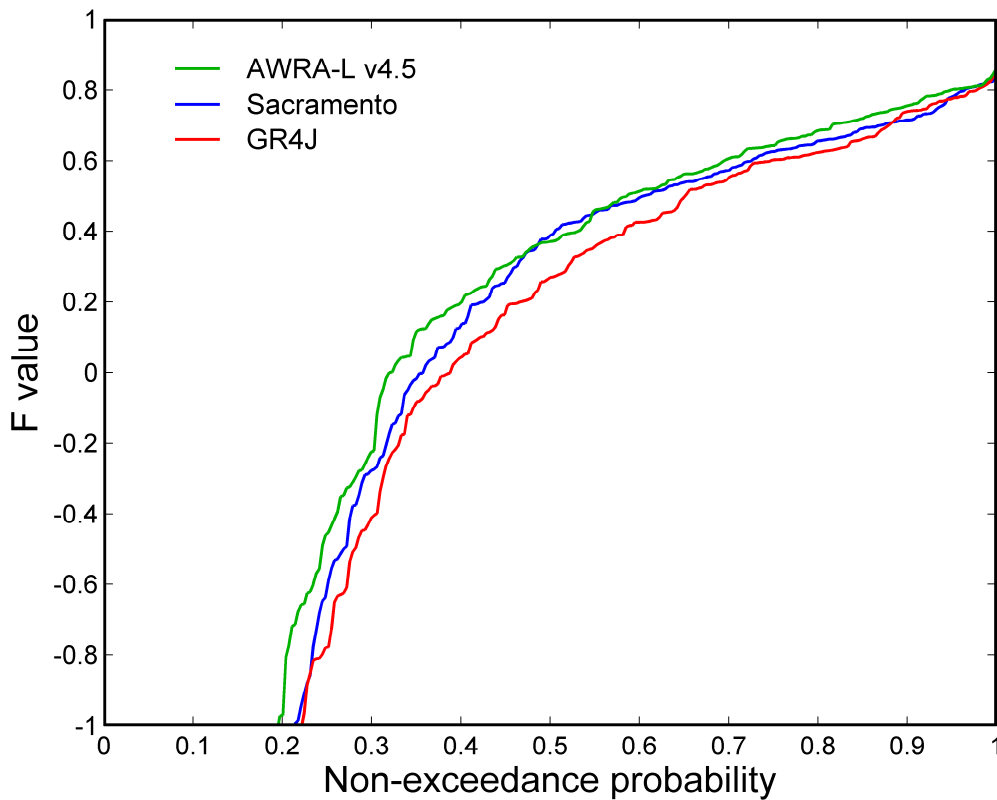


Figure 28. Cumulative distribution of F value of streamflow predictions in validation mode for AWRA-L v4.5, Sacramento and GR4J.

COMPARISON WITH LAND SURFACE MODELS

4.2.1.1 Calibration performance

In this section the continentally-calibrated AWRA-L is compared with continental implementation (with minimal calibration) of WaterDyn and CABLE (results provided by the Bureau). The performances of the three models are shown in Figures Figure 29Figure 30. The curves for AWRA-L in Figures Figure 29Figure 30 are the same as those shown in Figures Figure 22Figure 23.

The monthly efficiencies for the AWRA-L model are substantially better than WaterDyn and CABLE (Figure 29). WaterDyn performs better than CABLE partly because some of the AWRA-L calibration catchments are used to calibrate WaterDyn whereas CABLE is parameterised to match energy fluxes and long term water balance. On the bias metric, AWRA-L performs significantly better than the other two models.

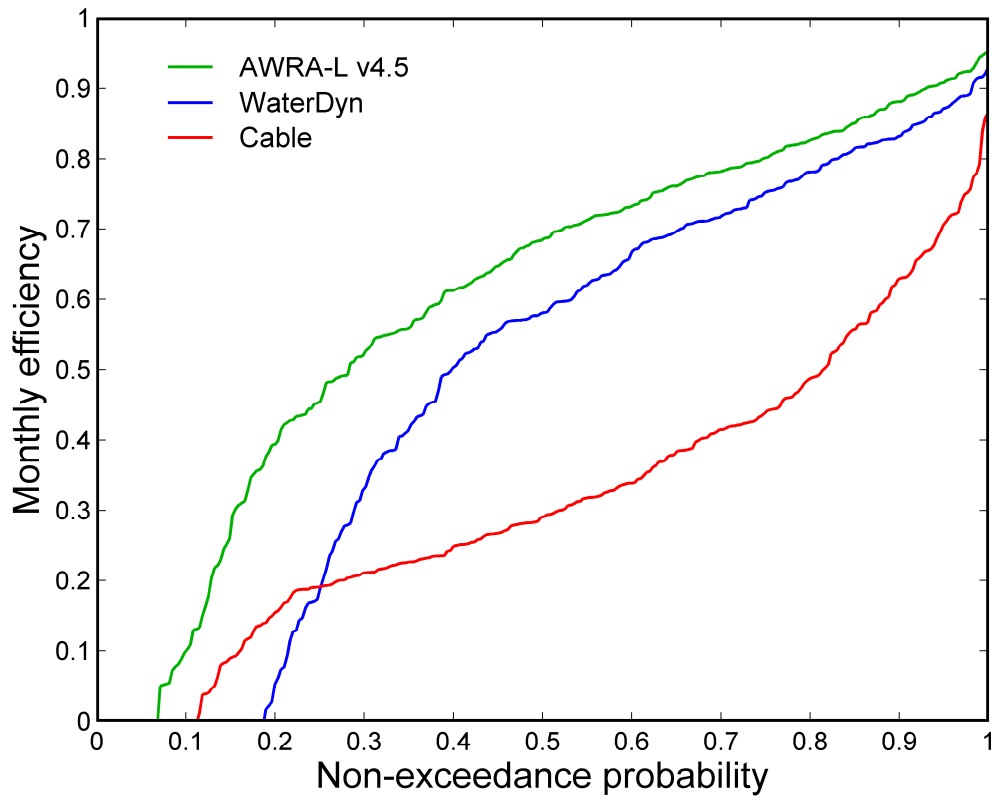


Figure 29. Cumulative distribution of monthly efficiency of streamflow predictions in calibration mode for AWRA-L v4.5, WaterDyn and CABLE.

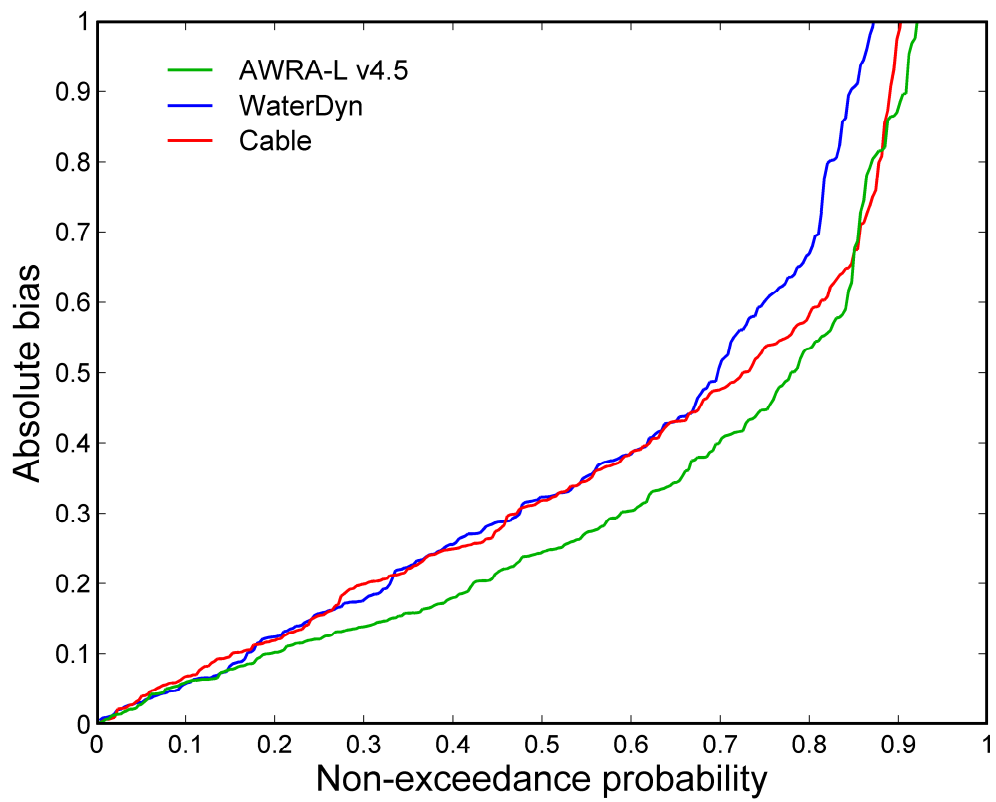


Figure 30. Cumulative distribution of absolute bias of streamflow predictions in calibration mode for AWRA-L v4.5, WaterDyn and CABLE.

Validation performance

The validation results for the three models are almost identical to the calibration results with AWRA-L performing substantially better than the other two models for monthly efficiencies (Figure 31) and for absolute bias (Figure 32).

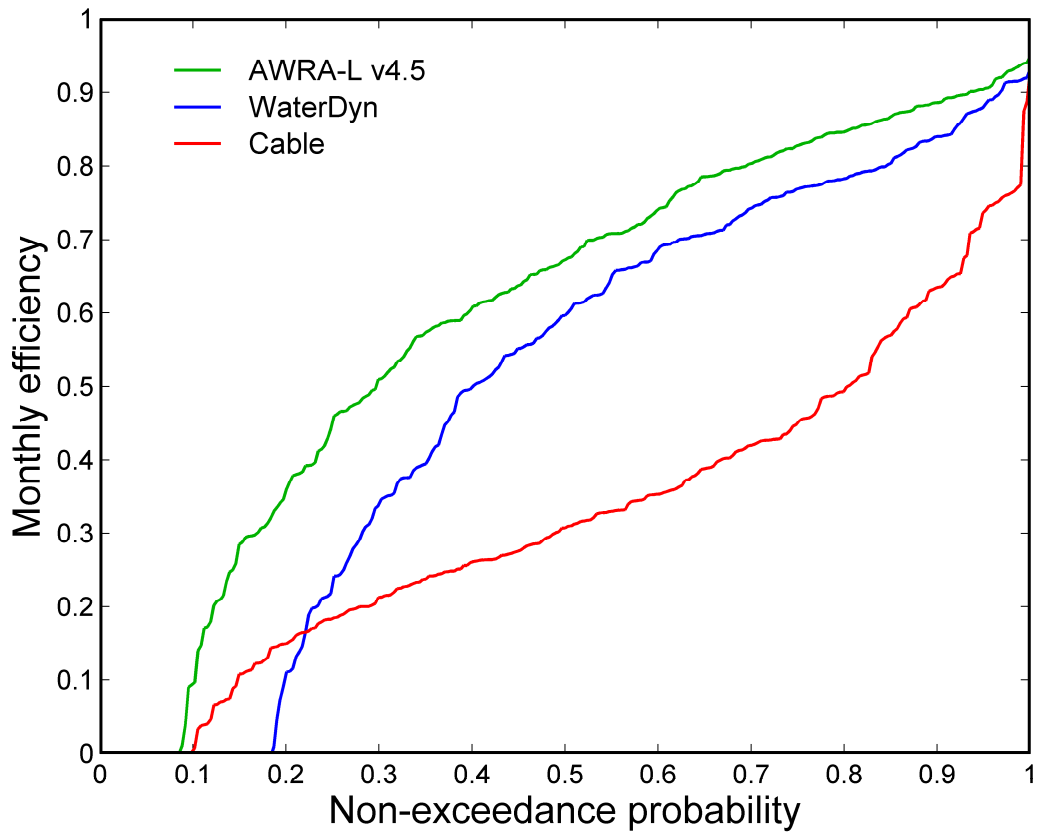


Figure 31. Cumulative distribution of monthly efficiency of streamflow predictions in validation mode for AWRA-L v4.5, WaterDyn and CABLE.

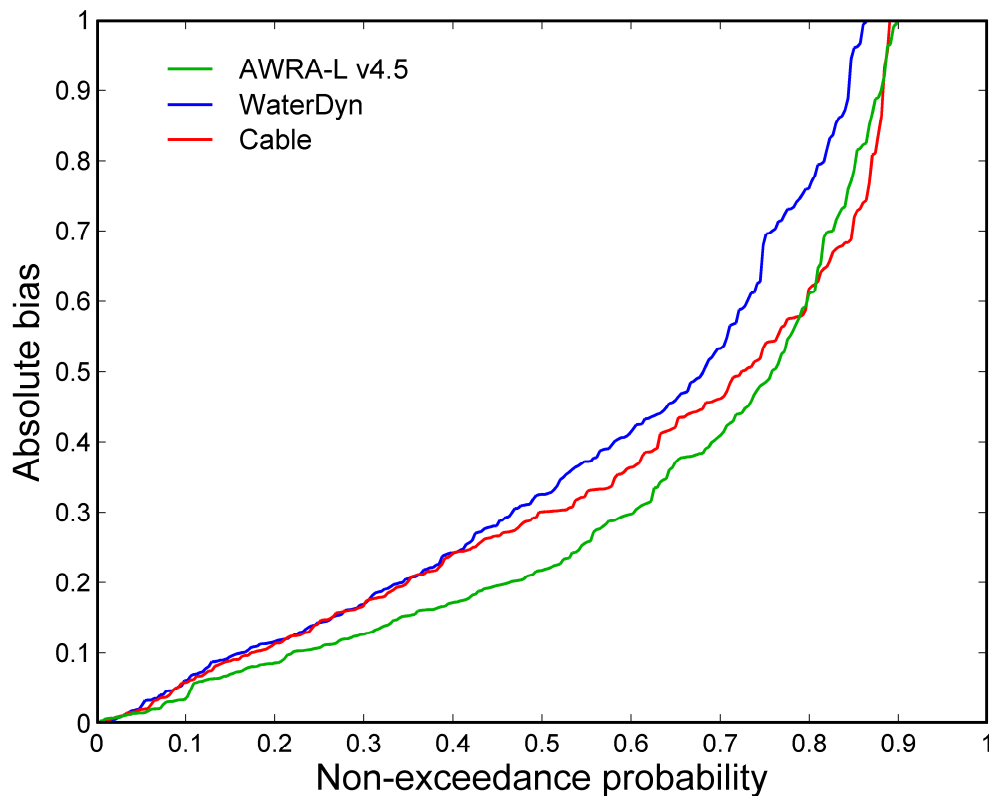


Figure 32. Cumulative distribution of absolute bias of streamflow predictions in validation mode for AWRA-L v4.5, WaterDyn and CABLE.

COMPARISON WITH AWRA-L V3.5 AND AWRA-L V4.0

Calibration performance

In this section the continentally-calibrated AWRA-L v4.5 results are compared to those from previous versions of AWRA (AWRA-L v3.5 and AWRA-L v4.0). The performances of the three versions of AWRA-L in calibration are shown in Figures Figure 33Figure 36. For daily efficiencies, AWRA-L v4.5 performs better than the two previous versions with AWRA-L v4.0 performing slightly better than AWRA-L v3.5 (Figure 33). There is little difference in the performance of the three versions of AWRA-L for monthly efficiencies with AWRA-L v4.5 performing slightly better than the other two versions for the best-modelled catchments and AWRA-L v3.5 performing slightly better for the worst-modelled catchments (Figure 34). On the bias metric, the performance of the three versions are almost identical, but with AWRA-L v3.5 performing slightly better than the other two versions for the worst-modelled catchments (Figure 35). For the F value, which is a combination of daily and monthly efficiency as well as the bias, AWRA-L v4.5 performs slightly better than AWRA-L v4.0, which, in turn, is slightly better than AWRA-L v3.5 (Figure 36).

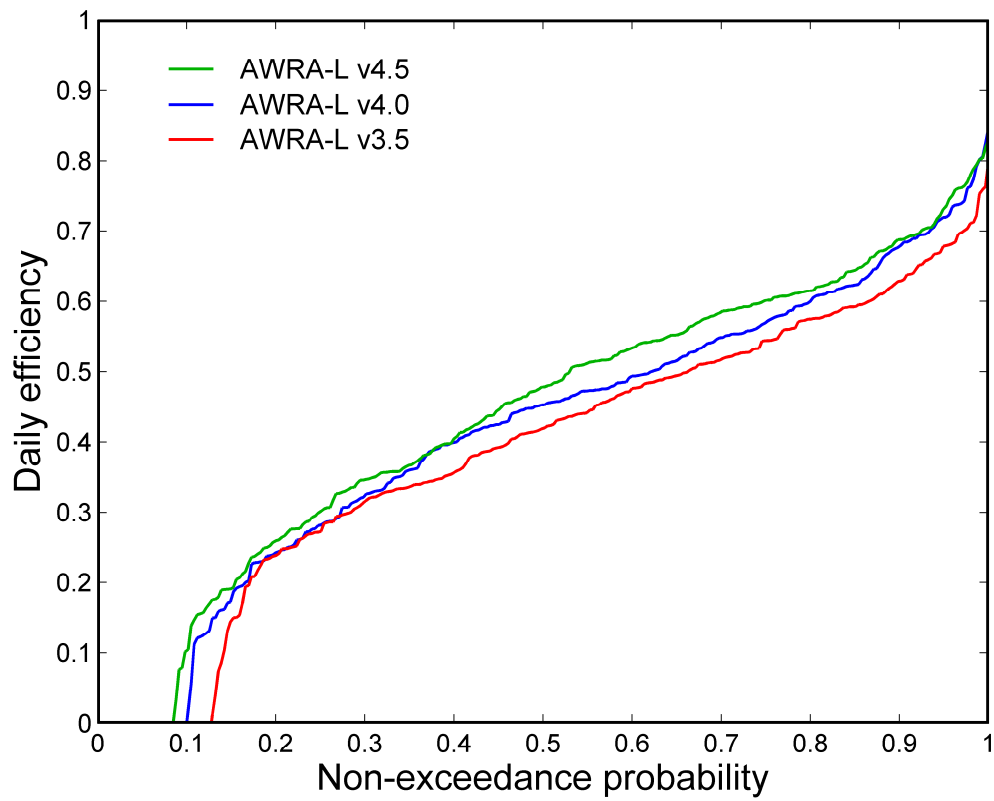


Figure 33. Cumulative distribution of daily efficiency of streamflow predictions in continental calibration mode for AWRA-L v4.5, AWRA-L v3.5 and AWRA-L v4.0.

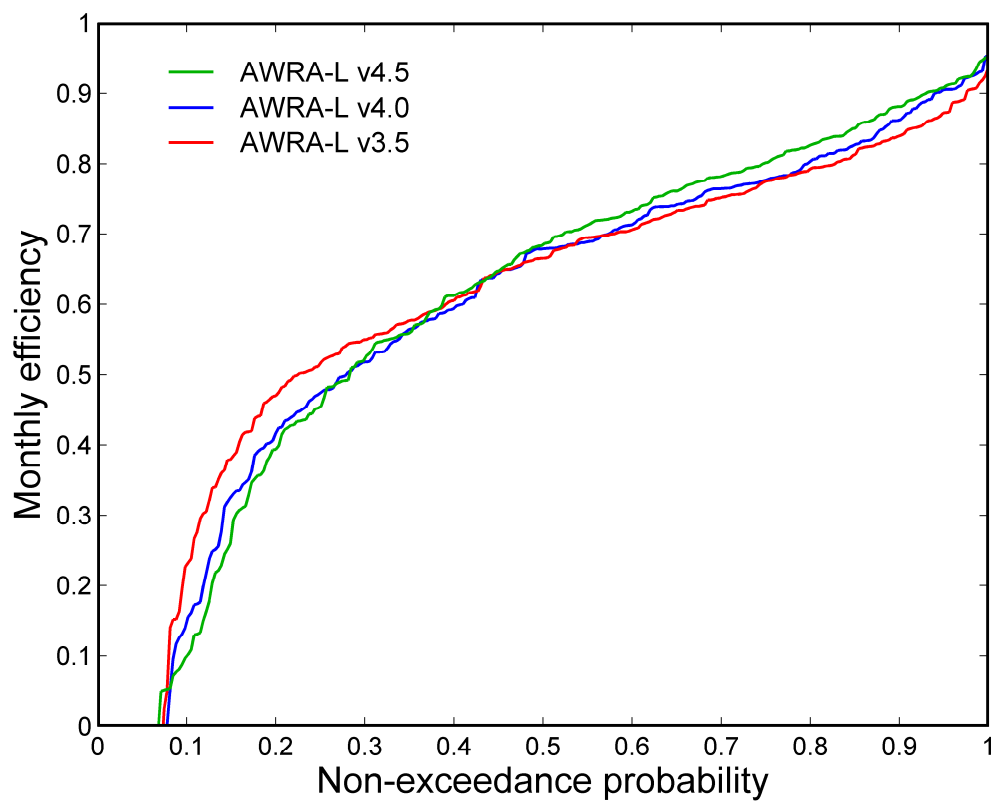


Figure 34. Cumulative distribution of monthly efficiency of streamflow predictions in continental calibration mode for AWRA-L v4.5, AWRA-L v3.5 and AWRA-L v4.0.

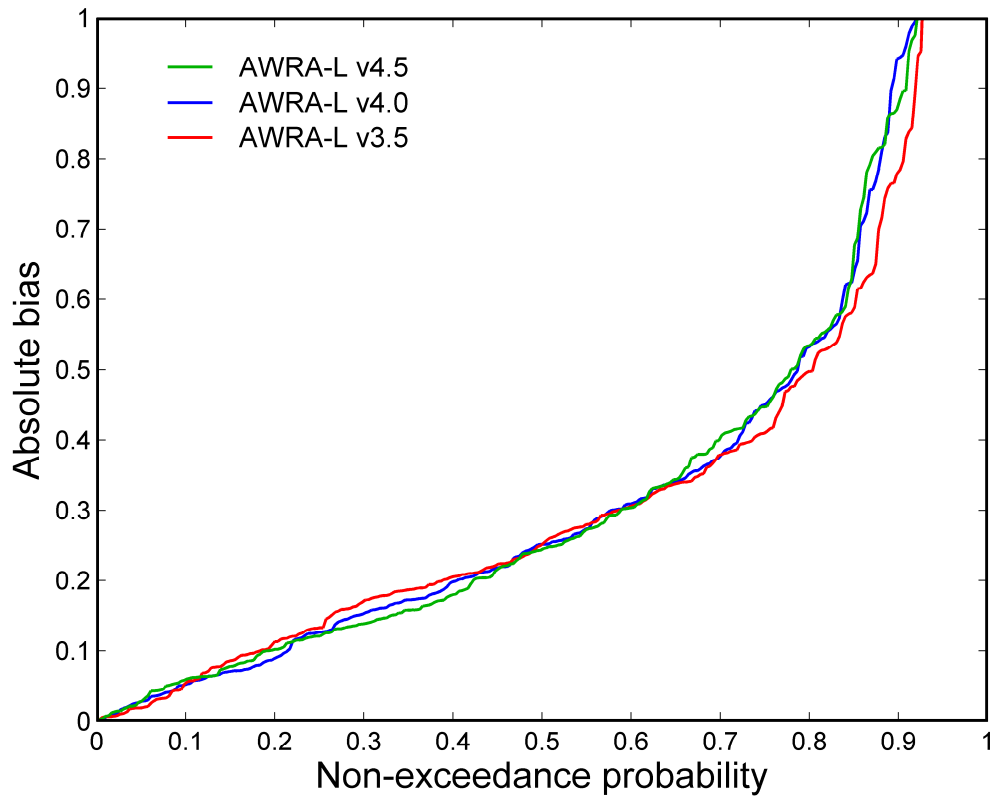


Figure 35. Cumulative distribution of absolute bias of streamflow predictions in continental calibration mode for AWRA-L v4.5, AWRA-L v3.5 and AWRA-L v4.0.

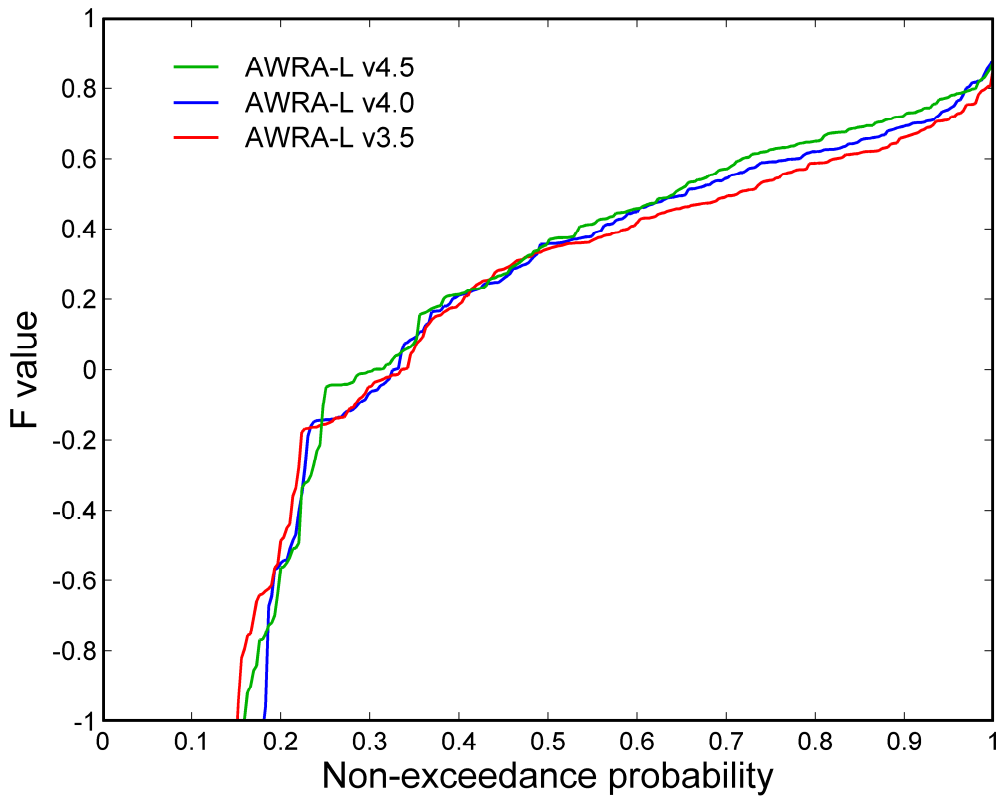


Figure 36. Cumulative distribution of F value of streamflow predictions in continental calibration mode for AWRA-L v4.5, AWRA-L v3.5 and AWRA-L v4.0.

Validation performance

The validation results for the three versions of AWRA-L are almost identical to the calibration results with AWRA-L v4.5 typically performing as well as or better than the other two versions (Figures Figure 37Figure 40).

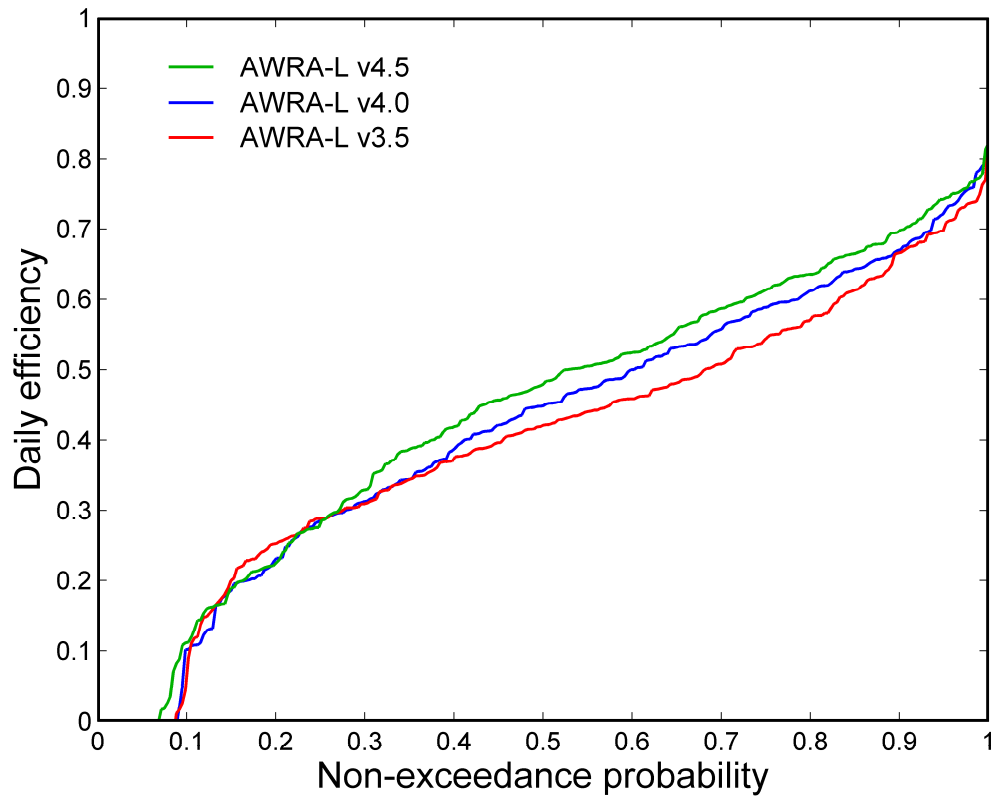


Figure 37. Cumulative distribution of daily efficiency of streamflow predictions in validation mode for AWRA-L v4.5, AWRA-L v3.5 and AWRA-L v4.0.

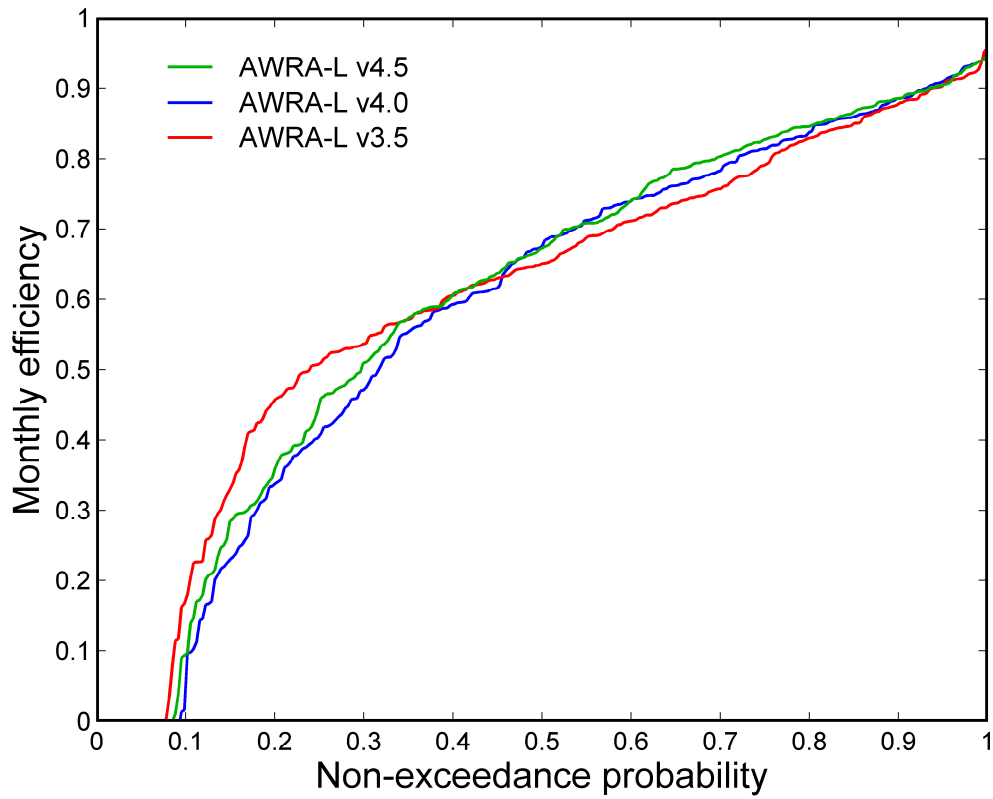


Figure 38. Cumulative distribution of monthly efficiency of streamflow predictions in validation mode for AWRA-L v4.5, AWRA-L v3.5 and AWRA-L v4.0.

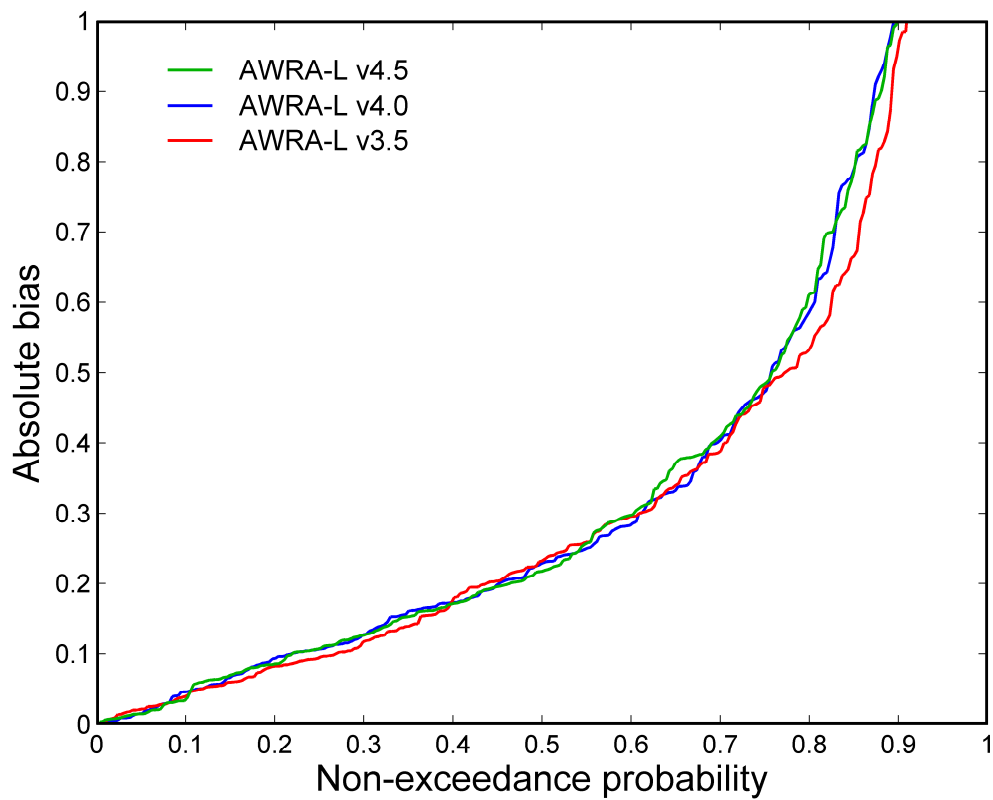


Figure 39. Cumulative distribution of absolute bias of streamflow predictions in validation mode for AWRA-L v4.5, AWRA-L v3.5 and AWRA-L v4.0.

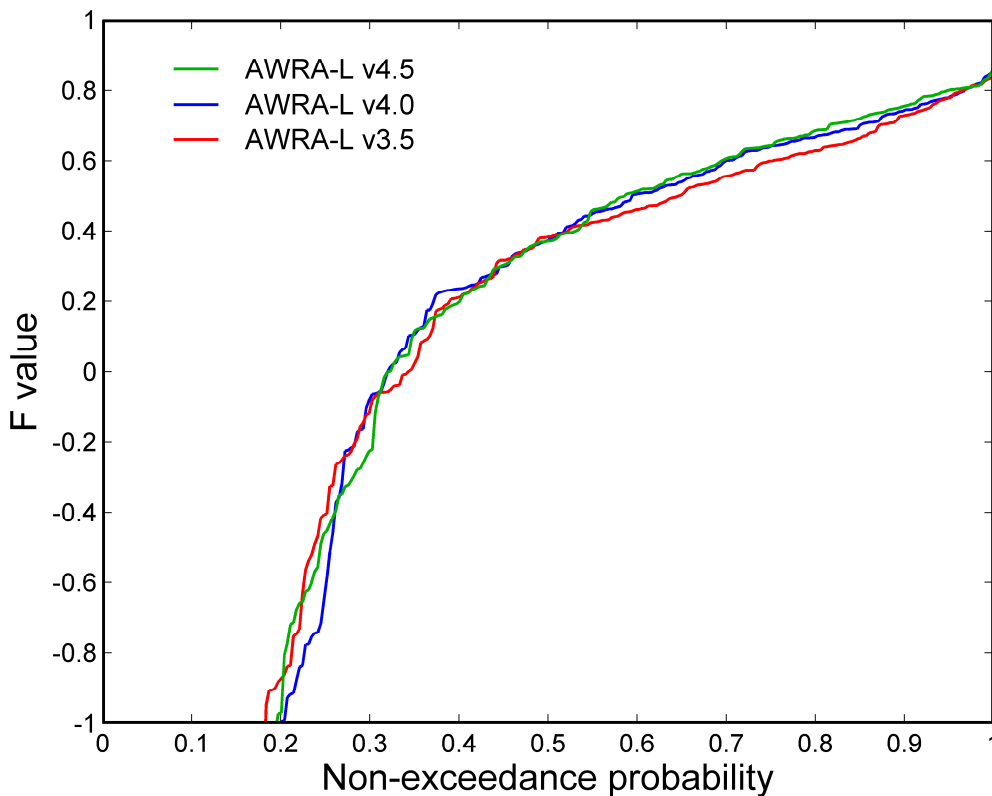


Figure 40. Cumulative distribution of F value of streamflow predictions in validation mode for AWRA-L v4.5, AWRA-L v3.5 and AWRA-L v4.0.

REGIONAL CALIBRATION OF AWRA-L V4.5 AND COMPARISON WITH CONTINENTAL CALIBRATION RESULTS

In the regional calibration of AWRA-L, Australia is divided into eight regions based on climatic conditions. The model parameters are calibrated separately for each of these eight regions. Streamflow data from all 589 catchments was used in calibration. Figure 41 shows the eight zones and the summary statistics for performance across the different regions. There is a large variability in area between the different zones and the number of catchments in the eight zones varies between 19 and 209. The regional calibration performance for AWRA-L v4.5 is best in zone 1 (the north Queensland Pacific coast) and worst in zone 2 (the largest arid area shown in red colour).

The comparison of results from continental and regional calibrations for AWRA-L v4.5 is shown in Figures Figure 42Figure 45. Here, the exceedance curves for the continental calibration show a combination of calibration and validation performance. For almost all the catchments, the performance of the model in regional calibration is better than the continental implementation with higher daily and monthly efficiencies and lower absolute bias. The F values for the regional implementation are substantially higher than those for the continental implementation. The overall median daily and monthly efficiency and F value for the continental implementation are 0.48, 0.68 and 0.37, respectively, compared to 0.52, 0.73 and 0.49 for the regional implementation. This is to be expected as all the catchments in each of the regions are more hydrologically similar and also because one separate set of model parameters are optimised for each of the region (in contrast to a single set of model parameters optimised across the whole continent in continental implementation).

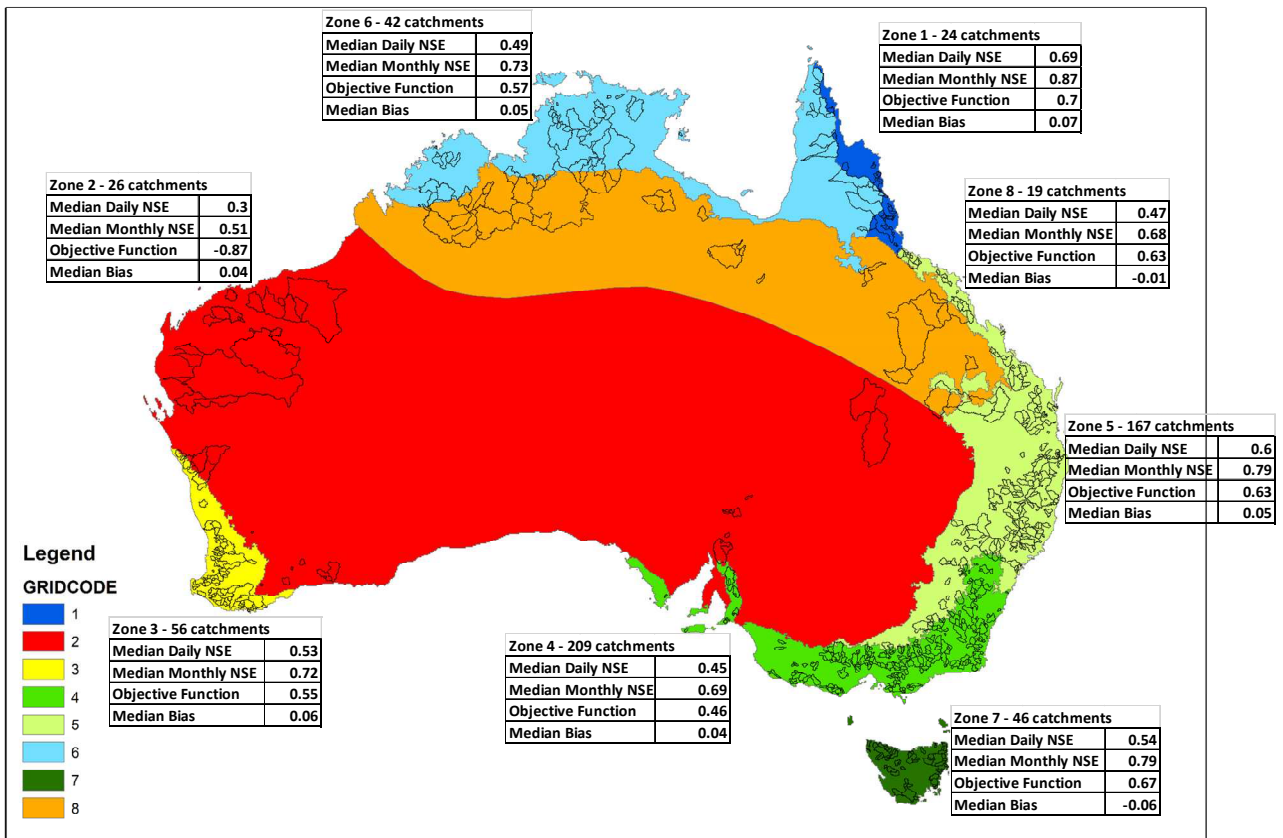


Figure 41. Regional calibration zones and summary statistics of AWRA-L v4.5 performance for each region. (The term “objective function” refers to the median of the F value. The term “median bias” refers to the median of the raw bias).

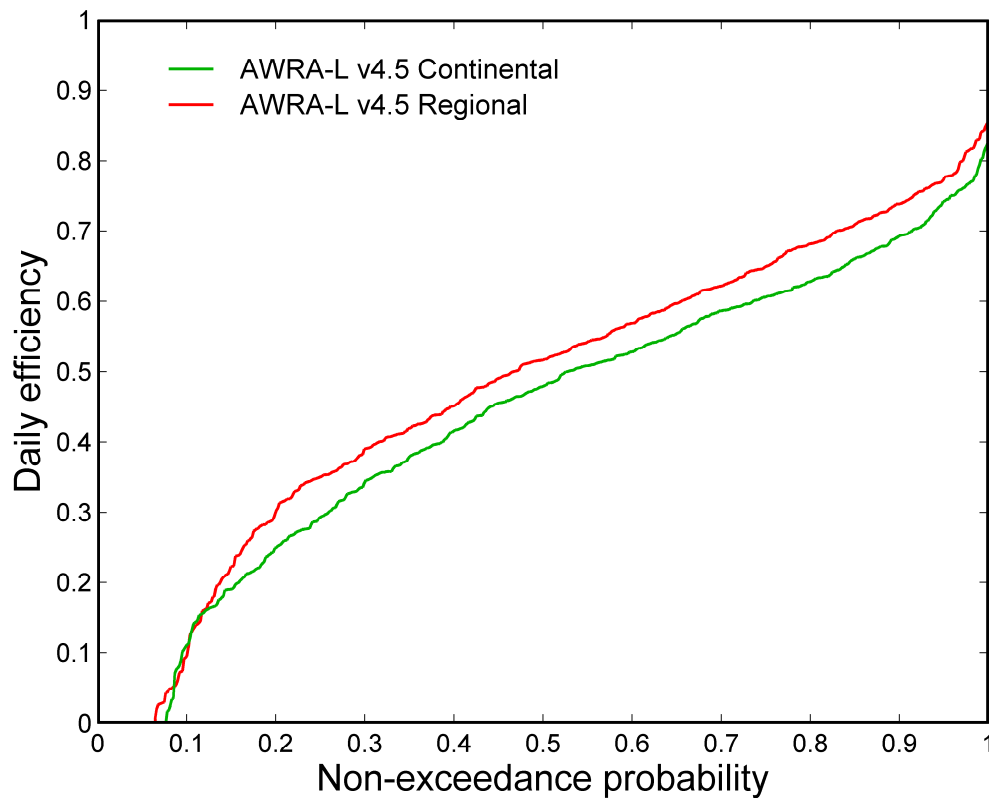


Figure 42. Cumulative distribution of daily efficiency of streamflow predictions for continental and regional implementation of AWRA-L v4.5.

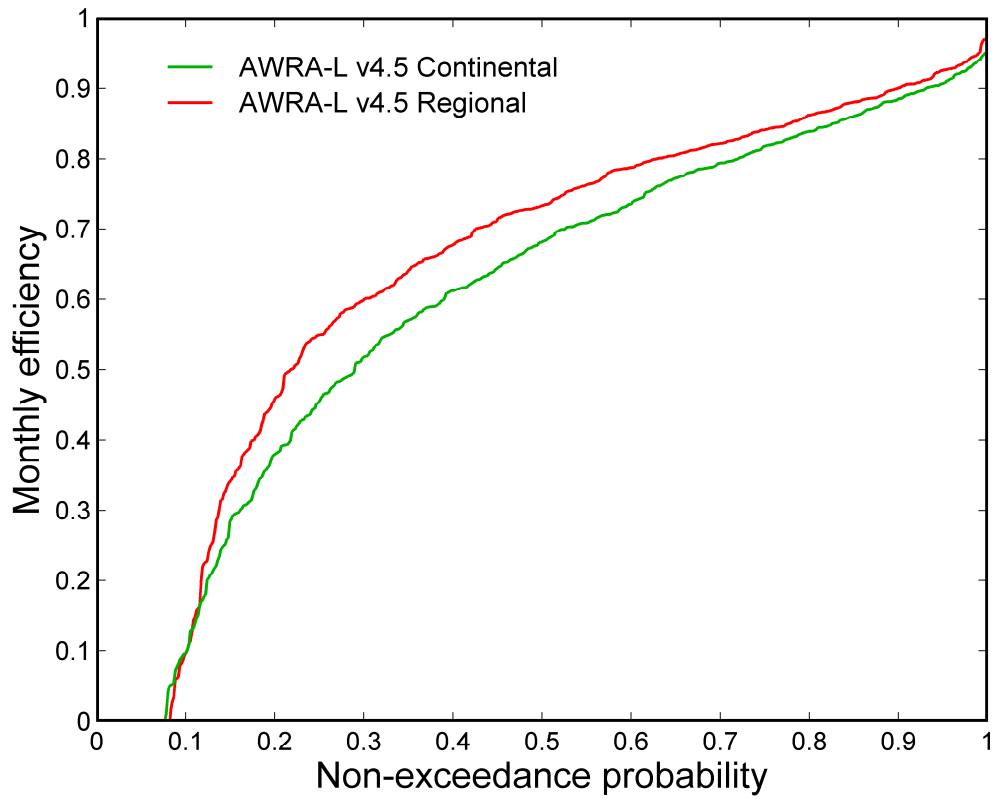


Figure 43. Cumulative distribution of monthly efficiency of streamflow predictions for continental and regional implementation of AWRA-L v4.5.

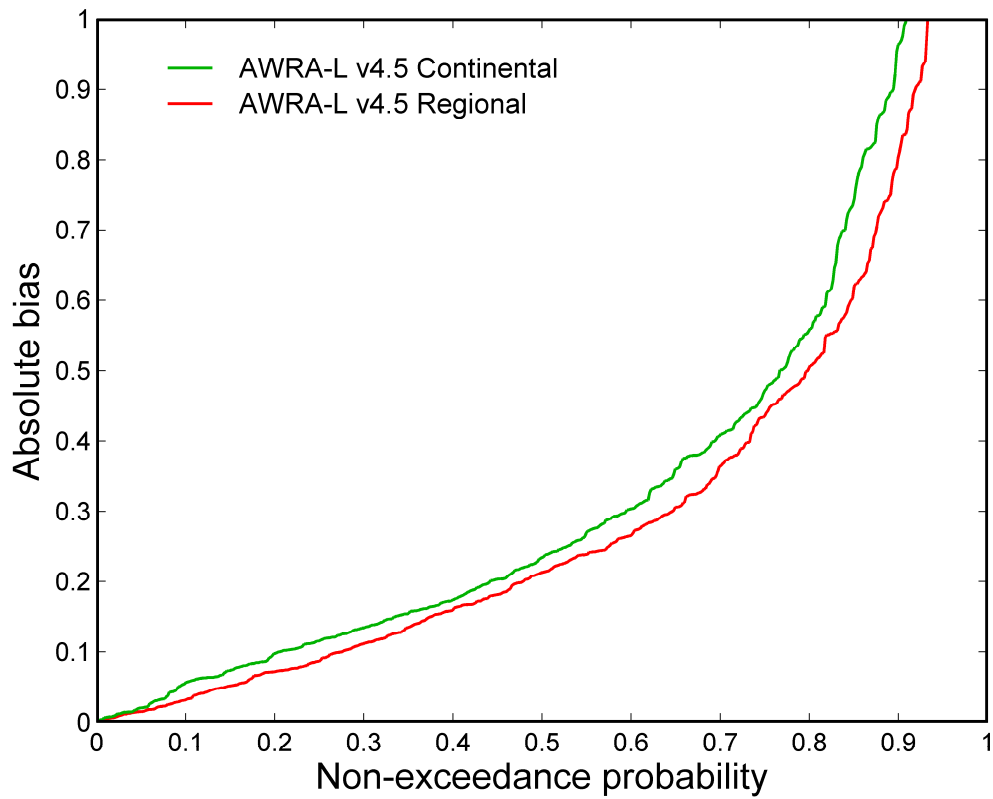


Figure 44. Cumulative distribution of absolute bias of streamflow predictions for continental and regional implementation of AWRA-L v4.5.

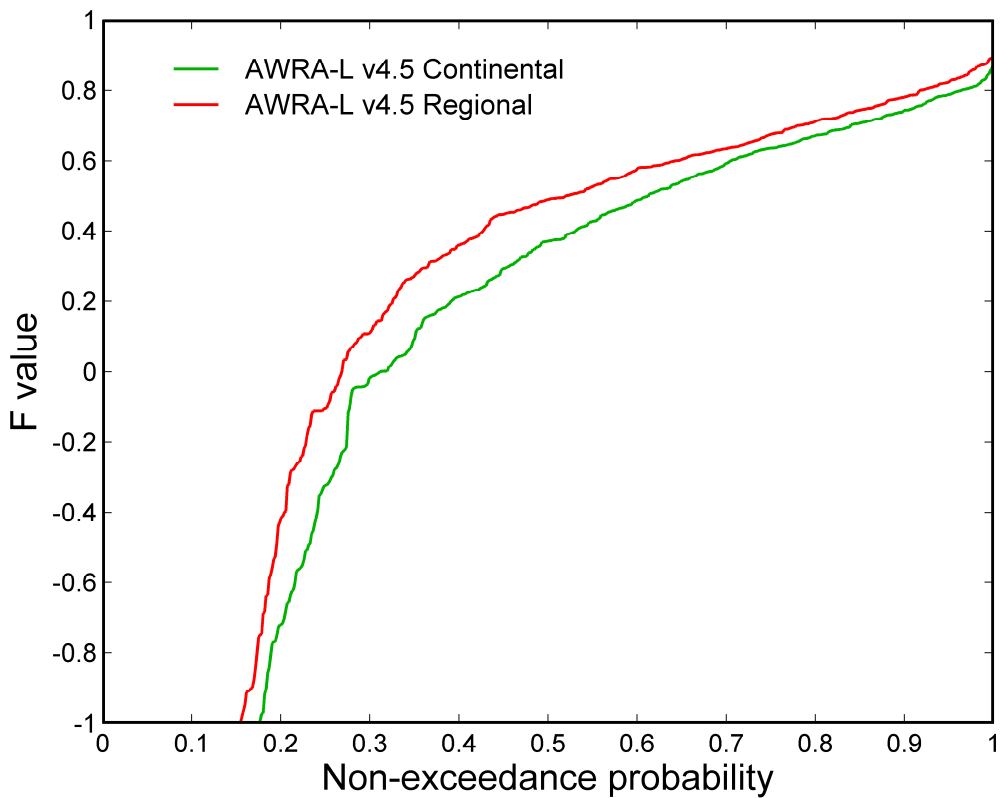


Figure 45. Cumulative distribution of F value of streamflow predictions for continental and regional implementation of AWRA-L v4.5.

SOIL MOISTURE

The point-based estimates of soil moisture are compared by monthly correlation with the weighted profile estimates (0–90 cm) of each model and the AMSR-E and ASCAT satellite based estimates (Figure 46). AWRA-L and CABLE perform best for the 90 cm profile and both are significantly better than the two satellite based estimates. There appears to be a steady improvement in performance of AWRA-L between v3.5 and v4.5. It should be noted that the total depth of the two layers of WaterDyn can vary between 100 cm and 220 cm and this can have an impact on the estimates of profile soil moisture in the top 90 cm.

As a result of ASCAT providing significantly poorer correlation with Oznet and SASMAS than AMSR-E, only the latter is used for comparison with catchment-averaged topsoil moisture (Figure 47). Evaluation is done

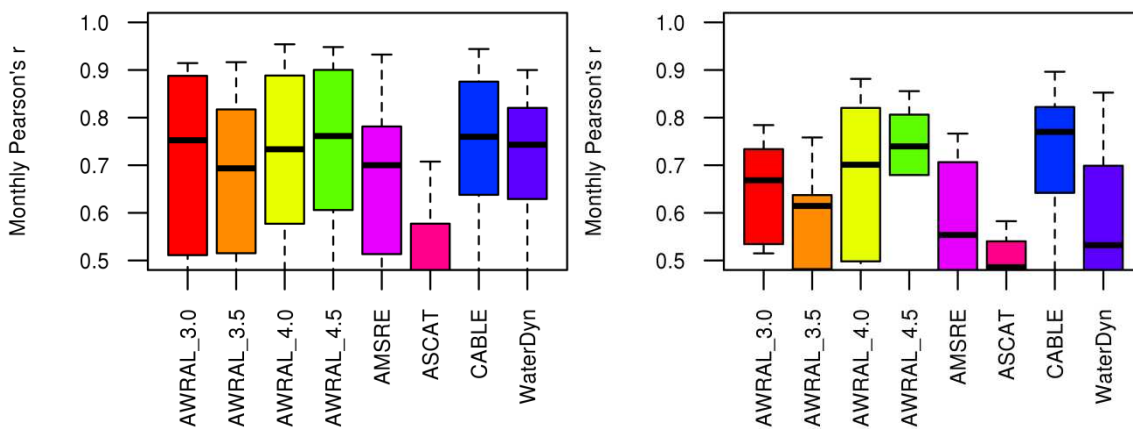


Figure 46. Correlation of monthly volumetric soil moisture predictions of models against (a) OzNet and (b) SASMAS probe data over a 90 cm profile.

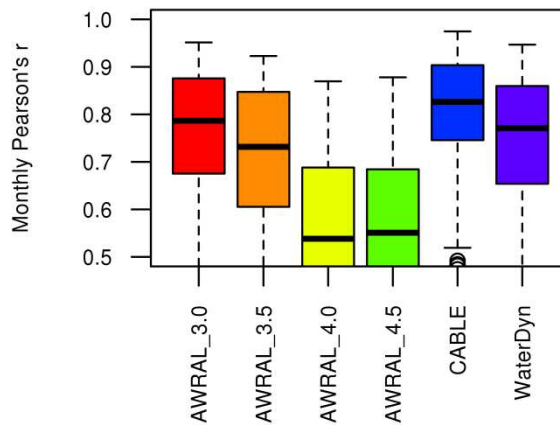


Figure 47. Correlation of model predictions of topsoil moisture content with AMSR-E observations.

using the 294 validation catchments. AWRA-L v4.5 gives poorer soil moisture correlations with AMSR-E for the top soil layer than both CABLE and WaterDyn. There also appears to be a reduction in the quality of AWRA-L's topsoil moisture prediction since v3.0. It should be noted that whereas the top soil layer depth in AWRA-L is 10 cm, it is 2.2 cm in CABLE and variable, but mostly relatively shallow, in WaterDyn. The AMSR-E soil moisture estimate represents the top 2–3 cm. It should also be noted that the soil moisture of the top 2–3 cm effectively represents the antecedent rainfall, while the profile soil moisture is important for a number of agricultural and flood inundation decisions.

EVAPOTRANSPIRATION

AWRA-L v4.0 and AWRA-L v4.5 perform at roughly the same level as CABLE and WaterDyn, respectively, according to the evaluation of catchment-averaged actual ET predictions against satellite based CMRSET data (Figure 48). It should be noted that the version of CABLE used here has been calibrated against flux tower ET whereas AWRA-L is calibrated against streamflow only. There is a slight drop in performance of AWRA-L v4.5 compared to v4.0. Until CMRSET is evaluated over more sites not used in calibration of CMRS it is unclear whether this result is robust. Evaluation over additional recently installed sites and against data recently made available by King et al. (2011) is recommended.

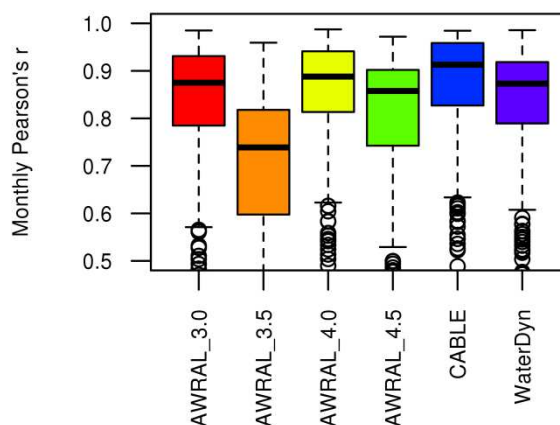


Figure 48. Correlation of monthly CMRSET observations with model predictions of ET.

SUMMARY OF MODEL PERFORMANCE

The comparisons of prediction performance between AWRA-L v4.5 and a range of continentally-calibrated peer models have shown that AWRA-L is a good choice as a modelling technology to support National

Water Accounts and Australian Water Resources Assessments. In both calibration and validation modes, AWRA-L v4.5 typically provides streamflow predictions that are as good as or better than the alternatives. In comparison to other models, AWRA-L also has other advantages such as the ability to predict many landscape properties and fluxes other than streamflow, and the fact that it has been explicitly coupled to groundwater and river routing modules. It is therefore recommended that AWRA-L continues to be used to prepare data for the National Water Accounts and Australian Water Resources Assessments.

The comparisons of prediction performance between current version of the model (AWRA-L v4.5) and older versions (AWRA-L v3.5 and AWRA-L v4.0) show that the current version performs overall better than the older versions.

The results from regional calibrations indicate that the model performs better than in continental implementation when the parameters are calibrated for hydrologically similar catchments within each region.

The profile soil moisture (0–90 cm) is represented well by AWRA-L v4.5 and CABLE. The estimates from WaterDyn are comparable to AWRA-L and CABLE when compared to OzNet point measurements but WaterDyn performs substantially poorer than AWRA-L and CABLE when compared to SASMAS probe data. According to AMSR-E satellite catchment based evaluation, AWRA-L v4.5 does not represent the top thin soil layer moisture temporal dynamics as well as WaterDyn and CABLE. There are various differences between the models in soil layer sizes, parameterisations and modelling timestep that explain these results.

The performance of AWRA-L in predicting ET varies from one version to the next depending on calibration (AWRA-L v4.5 is calibrated to streamflow only). It should be noted that the version of CABLE used here has been calibrated against flux tower ET whereas AWRA-L is only calibrated against streamflow. It is possible that calibration AWRA-L against multiple observations (streamflow, ET, soil moisture, etc) may improve AWRA-L estimates of ET and soil moisture. There are modelling experiments underway to investigate this.

CONTACT US

t 1300 363 400
+61 3 9545 2176
e enquiries@csiro.au
w www.csiro.au

YOUR CSIRO

Australia is founding its future on science and innovation. Its national science agency, CSIRO, is a powerhouse of ideas, technologies and skills for building prosperity, growth, health and sustainability. It serves governments, industries, business and communities across the nation.

FOR FURTHER INFORMATION

Land and Water Flagship
Jai Vaze
t +61 2 62465871
e jai.vaze@csiro.au
w www.csiro.au/